
Masters Theses

Student Theses and Dissertations

Spring 2022

Controlling microalloy interactions on precipitation, hot ductility, and microstructure -- Mechanical property relationships

Madhuri Varadarajan

Follow this and additional works at: https://scholarsmine.mst.edu/masters_theses



Part of the [Metallurgy Commons](#)

Department:

Recommended Citation

Varadarajan, Madhuri, "Controlling microalloy interactions on precipitation, hot ductility, and microstructure -- Mechanical property relationships" (2022). *Masters Theses*. 8101.
https://scholarsmine.mst.edu/masters_theses/8101

This thesis is brought to you by Scholars' Mine, a service of the Missouri S&T Library and Learning Resources. This work is protected by U. S. Copyright Law. Unauthorized use including reproduction for redistribution requires the permission of the copyright holder. For more information, please contact scholarsmine@mst.edu.

CONTROLLING MICROALLOY INTERACTIONS ON PRECIPITATION, HOT
DUCTILITY, AND MICROSTRUCTURE – MECHANICAL PROPERTY

RELATIONSHIPS

by

MADHURI VARADARAJAN

A THESIS

Presented to the Graduate Faculty of the

MISSOURI UNIVERSITY OF SCIENCE AND TECHNOLOGY

In Partial Fulfillment of the Requirements for the Degree

MASTER OF SCIENCE

in

METALLURGICAL ENGINEERING

2022

Approved by:

Dr. Laura Bartlett, Advisor

Dr. Ronald O'Malley

Dr. Simon Lekakh

© 2022

MADHURI VARADARAJAN

All Rights Reserved

PUBLICATION THESIS OPTION

This thesis consists of the following three articles, formatted in style used by the Missouri University of Science and Technology:

Paper I, found on pages 37–56, has been published in the proceedings of AISTech Conference, 2020.

Paper II, found on pages 57–80, has been published in the AISTech Conference proceedings in Nashville, TN, in July 2021.

Paper III, found on pages 81–105, is intended for submission to *Steel Research International*.

ABSTRACT

One of the main problems faced in the continuous casting of micro-alloy steels is the formation of transverse cracks. Transverse cracks are surface, or near-surface cracks formed perpendicular to the casting direction. The research focuses on using laboratory hot tensile tests methods to determine the low ductility ranges in high strength steel grades with different micro-alloy additions of titanium, niobium, and vanadium. The hot ductility of commercially produced as-cast slab and beam blank samples was evaluated using two experimental methods: tensile testing utilizing a servo-hydraulic load frame with a resistance furnace and thermomechanical testing using rapid Joule heating. The tests were performed at a 3×10^{-3} /s strain rate in a temperature window of 650°C - 950°C to mimic industrial unbending temperatures during the continuous casting. A ductility trough with a minimum percentage reduction in area (% RA) was observed closer to the A_{r3} transformation temperature of the alloys. The ductility drop at this temperature is likely related to the formation of a thin layer of ferrite film along the austenite grain boundaries resulting in minimum ductility and intergranular failure. Both test methods showed similar low ductility trends, but the upper and lower edges of the ductility trough temperature range differed between the two test methods. The differences are attributed to the heating and cooling rates of the two test methods. Future studies are required to perform in-situ-based deformation tests with the aim of directly observing transverse crack formation during solidification and cooling.

ACKNOWLEDGEMENTS

First, I want to thank God and my parents, Mr. K N Varadharajan, and Mrs. V V Vimala, for their constant encouragement and love throughout my life. Secondly, I would like to thank my advisors, Dr. Laura N Bartlett, Dr. Ronald J O'Malley, and Dr. Simon N Lekakh, for their support, assistance, and guidance during my research work. Besides my advisor, I am grateful to Dr. Mario Buchely for his help during the early stages of my research work and all the valuable comments and suggestions. I would like to extend my gratitude to Mr. Brian Bullock for assisting with the sample preparation for hot ductility studies and the experimental setup's fabrication. I would like to thank the undergraduate research assistant for their help with sample preparation. I would also like to thank Ms. Denise Eddings, Ms. Teneke Hill, and Ms. Emily Bullock for making sure everything happened in a smooth and organized manner.

This project has been supported by the Peaslee Steel Manufacturing Research Center (PSMRC). My heartfelt thanks to all the members of PSMRC for providing samples for the hot ductility studies and their financial support during my research work.

Finally, I would like to thank my friends Damilola Balogun, Richard Osei, Tyler Richards, Deva Prasad, Koushik Karthikeyan, who were all constant pillars of my support and gave me many cherished memories during my period in Missouri S&T.

TABLE OF CONTENTS

	Page
PUBLICATION THESIS OPTION.....	iii
ABSTRACT.....	iv
ACKNOWLEDGEMENTS.....	v
LIST OF ILLUSTRATIONS.....	xi
LIST OF TABLES.....	xvi
NOMENCLATURE	xvii
 SECTION	
1. INTRODUCTION.....	1
1.1. BACKGROUND INFORMATION	1
1.2. REGIONS OF LOW-TEMPERATURE DUCTILITY	3
1.3. ZONE I – HIGH DUCTILITY, LOW-TEMPERATURE REGION (HDL).....	4
1.4. ZONE II – REGION OF LOW DUCTILITY EMBRITTLEMENT.....	5
1.4.1. Intergranular Failure: Precipitate Free Zones.....	6
1.4.2. Intergranular Failure: Grain Boundary Sliding.....	7
1.4.3. Intergranular Failure: Thin Ferrite Films.....	8
1.5. HIGH DUCTILITY, HIGH-TEMPERATURE REGION (HDH).....	10
2. PROCESS VARIABLES INFLUENCING THE FORMATION OF TRANSVERSE CRACKS	12
2.1. MOLD OSCILLATION	12
2.2. SECONDARY COOLING AND CASTING SPEED.....	13
2.3. MOLD HEAT TRANSFER	13

3. INFLUENCE OF STEEL COMPOSITIONS ON THE HOT DUCTILITY OF STEELS	14
3.1. CARBON.....	14
3.2. NITROGEN.....	15
3.3. VANADIUM	16
3.4. NIOBIUM.....	16
3.5. TITANIUM.....	17
3.6. SULPHUR	18
3.7. ALUMINUM.....	19
3.8. PHOSPHOROUS	19
3.9. MN:S RATIO	21
4. INFLUENCE OF TEST VARIABLES ON THE HOT DUCTILITY OF STEELS.....	23
4.1. STRAIN AND STRAIN RATE	25
4.2. EFFECT OF STRAIN RATE IN HOT TENSILE TESTING.....	27
4.3. COOLING RATE.....	28
4.4. THERMAL HISTORY.....	29
4.5. EXPERIMENTAL DETERMINATION OF HOT DUCTILITY OF STEELS	32
 PAPER	
I. THE INFLUENCE OF TI, NB AND V ON THE HOT DUCTILITY OF AS CAST MICROALLOYED STEELS	37
ABSTRACT	37
1. INTRODUCTION.....	38
2. EXPERIMENTAL METHOD	40

2.1. MATERIALS AND COMPOSITION	40
2.2. EXPERIMENTAL DETERMINATION OF HOT DUCTILITY OF STEELS	42
2.3. THERMODYNAMIC MODELING AND METALLOGRAPHIC ANALYSES	44
3. RESULTS AND DISCUSSION	45
3.1. STRESS – STRAIN BEHAVIOR AND HOT DUCTILITY CURVES OF THE V MICROALLOY STEEL	45
3.2. STRESS – STRAIN BEHAVIOR AND HOT DUCTILITY CURVES OF NB -TI MICROALLOY STEEL	47
3.3. STRESS – STRAIN BEHAVIOR AND HOT DUCTILITY CURVES OF V-NB -TI MICROALLOY STEEL.....	49
3.4. WIDTH OF HOT DUCTILITY TROUGH.....	51
3.5. DEPTH OF HOT DUCTILITY TROUGH	51
3.6. AUSTENITE GRAIN SIZE	52
4. CONCLUSION	53
ACKNOWLEDGEMENT	54
REFERENCES.....	55
II. HOT DUCTILITY BEHAVIOR OF V-N MICROALLOYED STEELS.....	57
ABSTRACT	57
1. INTRODUCTION.....	57
2. EXPERIMENTAL PROCEDURE	60
3. RESULTS AND DISCUSSIONS	64
3.1. STRESS – STRAIN BEHAVIOR AND HOT DUCTILITY CURVES OF LOW V STEEL	66
3.2. STRESS – STRAIN BEHAVIOR AND HOT DUCTILITY CURVES OF HIGH V STEEL	67

3.3. FRACTOGRAPHY OF FRACTURED SURFACES	69
3.3.1. Low V Steel.....	69
3.3.2. High V Steel.	71
3.4. METALLOGRAPHY IN LONGITUDINAL CROSS SECTION.....	73
3.4.1. Low V Steel.....	73
3.4.2. High V Steel.....	75
3.5. COMPARISON OF DUCTILITY TROUGH OF LOW AND HIGH V STEEL.....	76
4. CONCLUSION	78
ACKNOWLEDGEMENT	79
REFERENCES.....	79
III. HOT DUCTILITY BEHAVIOR OF V-NB BEAM BLANK STEEL	81
ABSTRACT	81
1. INTRODUCTION.....	82
2. PROCEDURE	85
2.1. EXPERIMENTAL.....	85
2.2. THERMODYNAMIC SIMULATIONS	88
3. RESULTS.....	88
3.1. STRESS-STRAIN BEHAVIOR OF V-NB MICRO ALLOYED STEEL.....	88
3.2. EXAMINATION OF TESTED SPECIMENS.....	90
4. DISCUSSION	97
5. CONCLUSIONS.....	102
REFERENCES.....	103

SECTION

5. CONCLUSIONS AND RECOMMENDATIONS..... 106

 5.1. CONCLUSIONS 106

 5.2. RECOMMENDATIONS 108

BIBLIOGRAPHY.....110

VITA.....118

LIST OF ILLUSTRATIONS

SECTION	Page
Figure 1.1: Transverse corner cracks in a continuously cast low carbon Nb-V-Ti micro-alloy steel.....	1
Figure 1.2: Schematic of a curved mold, vertical continuous casting machine, and its characteristics stresses.....	3
Figure 1.3: Schematic diagram showing the three characteristic ductility regions on a hot ductility curve.....	4
Figure 1.4: Schematic representations of hot ductility regions relating to the embrittlement mechanisms	6
Figure 1.5: Schematic representation of the micro void coalescence mechanism due to the formation of precipitate free zones (PFZ) on either side of the austenite grain boundary.	7
Figure 1.6: Schematic showing the formation of wedge cracks by grain boundary sliding.....	8
Figure 1.7: Micrograph shows the formation of thin ferrite films on prior austenite grain boundaries for Nb steel at deformation temperature 800°C.	9
Figure 1.8: Schematic shows the micro void formation and coalescence mechanism and ferrite films at austenite grain boundaries.....	9
Figure 3.1: Effect of carbon and phosphorous content on the hot ductility of steels.	20
Figure 4.1: Different thermal cycles to determine the hot ductility of steels using tensile testing	24
Figure 4.2: Schematic diagrams showing the thermal cycles studied: slow cycle with servo-hydraulic load frame equipped with SiC furnace.	34
Figure 4.3: MTS servo hydraulic load frame.....	34
Figure 4.4: Schematic diagrams showing the thermal cycles studied: fast cycle using Joule resistive device.....	36
Figure 4.5: High temperature micro-mechanical tester.	36

PAPER I

Figure 1: Position of hot ductility samples taken from as-cast steel slab.	41
Figure 2: Schematic diagrams showing the thermal cycles studied.	44
Figure 3: Engineering stress- engineering strain curves of vanadium microalloy steel at different temperatures	46
Figure 4: a) Hot ductility curves of vanadium microalloy steel from both test methods b) Thermodynamic modeling showing precipitation of vanadium carbides from 700°C - 800°C.	46
Figure 5: Engineering stress- engineering strain curves of Nb -Ti microalloy steel at different temperatures.	48
Figure 6: a) Hot ductility curves of Nb-Ti microalloy steel from both test methods b) Thermodynamic modeling showing precipitation of TiN from the liquid just after the liquidus and (Nb,Ti)(C,N) formation after solidification from 700 -1100 °C.	48
Figure 7: Engineering stress- engineering strain curves of V- Nb -Ti microalloy steel at different temperatures.	49
Figure 8: a) Hot ductility curves of V-Nb-Ti microalloy steel from both test methods b) Thermodynamic modeling showing precipitation of TiN along with (Nb,Ti,V)(C,N) formation after solidification from 600 -1100 °C.	50
Figure 9: Prior austenite grain size analysis of as-cast a) V microalloy steel with an average grain size of 208 μm b) Nb -Ti microalloy steel with an average grain size of 36 μm and c) V-Nb-Ti microalloy with an average grain size of 28 μm.	53

PAPER II

Figure 1: Position of hot ductility samples taken from: (a) beam – blank and (b) as-cast steel slab.	61
Figure 2: Schematic diagrams showing the thermal cycles studied	63
Figure 3: Thermodynamic modeling of equilibrium phase transformations during cooling of the low V steel.	64

Figure 4: Thermodynamic modeling of equilibrium phase transformations during cooling of the high V steel.	65
Figure 5: Engineering stress – strain curves of low V steel at different deformation temperatures for: (a) slow and (b) fast cooling.	66
Figure 6: Hot ductility curves of low V steel from both test methods.	68
Figure 7: Engineering stress – strain curves of high V steel at (a) slow and (b) fast cooling tests.	68
Figure 8: Hot ductility curves of high V steel obtained from both test methods.	69
Figure 9: Fracture surfaces of low V steel tested at slow cooling rate.	70
Figure 10: Mixed mode intergranular fracture with ductile voiding at 800°C in low V steel tested with high cooling rate.	71
Figure 11: Fracture surfaces of high V steel tested at slow cooling rate.	71
Figure 12: Fracture surfaces of high V (0.09 wt.%V) steel obtained from fast cooling rate tests.	73
Figure 13: Optical micrographs of the longitudinal cross section of fracture edge of low V steel after slow cooling at (a) 650°C and (b) 850°C test temperatures.	74
Figure 14: Optical micrographs of the longitudinal cross section of fracture edge of low V steel after fast cooling at (a) 800°C and (b) 900°C test temperatures.	75
Figure 15: Optical micrographs of the longitudinal cross section of fracture edge of high V steel tested after slow cooling at (a) 750°C and (b) 900°C test temperatures.	76
Figure 16: Optical micrographs of the longitudinal cross section of fracture edge of high V fast cooled steel at (a) 700°C and (b) 850°C test temperatures.	77
Figure 17: Hot ductility curves of high V and low V steel from a) servo-hydraulic MTS load frame with low heating/cooling rates and b) Joule resistive heating method with fast heating/cooling rates.	79

PAPER III

Figure 1: Position of hot ductility samples taken from a V-Nb micro alloyed beam blank	86
Figure 2: Shows a schematic of used temperature profile for both methods.....	87
Figure 3: Engineering stress – strain curves at different deformation temperatures for: (a) slow and (b) fast cooling test schedules.....	89
Figure 4: Relationship between tensile strength and temperature for the V-Nb micro-alloyed steel for two test schedules.....	89
Figure 5: Hot ductility curves of V-Nb micro alloyed steel from two testing schedules.....	90
Figure 6: Fracture surfaces of V-Nb micro alloyed steel tested at 800°C (fast test schedule).....	91
Figure 7: Fracture surfaces of V-Nb micro alloyed steel tested at 850°C test temperatures (fast test schedule).....	91
Figure 8: Fracture surfaces of V-Nb micro alloyed steel tested at 650°C (fast test schedule).....	92
Figure 9: Fracture surfaces of V-Nb micro alloyed steel tested at 950°C (fast test schedule).....	92
Figure 10: Fracture surfaces of V-Nb micro alloyed steel tested at a slow cooling rate.....	93
Figure 11: Optical micrographs of the longitudinal cross section of fracture edge of V-Nb micro alloyed steel tested at 650°C (a), 800°C (b,c) and 850°C (d) applying fast cooling schedule.	94
Figure 12: Optical micrographs of the longitudinal cross section of fracture edge of V-Nb micro alloyed steel after slow cooling at (a) 800°C, (b) 850°C and (c) 650°C test temperatures.	95
Figure 13: SEM – EDS analysis of the longitudinal cross section of fracture edge (800°C, fast schedule)	96
Figure 14. SEM – EDS analysis of the longitudinal cross section of fracture edge (800°C, slow schedule).....	96

Figure 15: Equilibrium phase transformations during cooling of the studied V-Nb micro alloyed steel.	98
---	----

Figure 16: Continuous cooling transformation diagrams of studied V-Nb micro alloyed steel.	101
---	-----

SECTION

Figure 5.1: Solidification and testing approach of hot 3-pt bend tests.	108
--	-----

Figure 5.2: Controlled deformation test apparatus	109
---	-----

LIST OF TABLES

PAPER I	Page
Table 1: Chemistry of the slab section in wt. % as determined by optical emission arc spectroscopy and Leco combustion and inert gas fusion analysis.....	42
PAPER II	
Table 1: Chemistry of the samples as determined by optical emission arc spectroscopy and Leco combustion and inert gas fusion analysis (wt. %).	60
PAPER III	
Table 1: Chemistry of the V-Nb micro alloyed steel (wt. %).	85

NOMENCLATURE

Symbol	Description
α	ferrite
γ	austenite

1. INTRODUCTION

1.1. BACKGROUND INFORMATION

Micro alloy steels are used in many applications such as construction, oil and gas extraction, pressure vessels, and transportation. One of the main problems faced in the continuous casting of micro-alloy steels is the formation of transverse cracks. Transverse cracks are surface or near-surface cracks formed perpendicular to the casting direction, as shown in Figure 1.1. These cracks are often associated with oscillation marks, and they can penetrate to a depth of 5-8mm or more below the slab's surface.

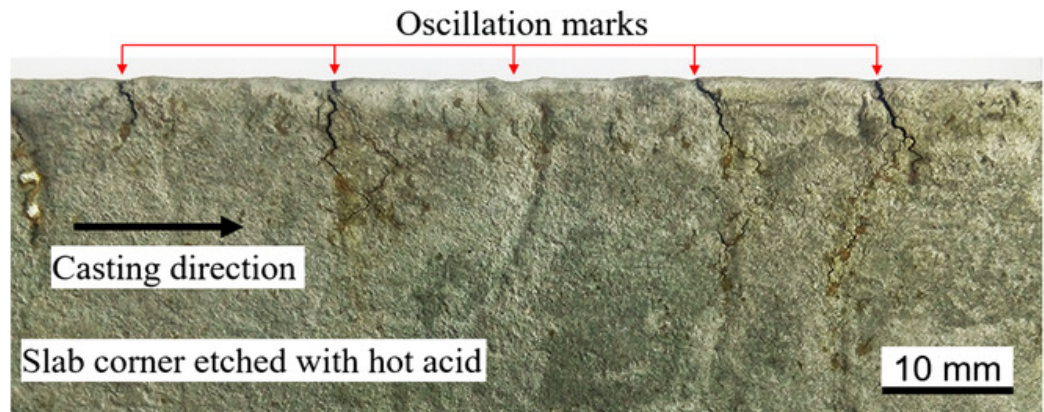


Figure 1.1: Transverse corner cracks in a continuously cast low carbon Nb-V-Ti micro-alloy steel [1].

The continuous casting process and the characteristic stresses are shown in Figure 1.2 [2]. In the continuous casting process, the molten steel is poured from a ladle to a tundish and then exists through a refractory tube known as a submerged entry nozzle (SEN) into a water-cooled copper mold. The liquid steel begins to solidify in the mold, forming a thin solid shell continuously removed from the bottom of the mold by drive rolls [3]. So,

the solidified shell must be strong to support the molten metal, which prevents catastrophic failure such as “breakouts” where the molten metal escape through the solidified skin to drain over the bottom of the casting machine [4].

Mold oscillation is necessary to prevent sticking, but it is responsible for producing oscillation marks or transverse ripples on the strand’s surface. Beneath the copper mold, in the secondary cooling zone, water and air mists impinge on the strand surface to ensure the strand is cooled evenly from all sides to avoid differences in the cooling rates [3].

It is essential to understand the sources of stress during continuous casting of steel which can be due to various factors. These include friction between the strand and the mold, bulging of the strand caused by the ferrostatic pressure, phase transformation effects, thermal effects (variable heat transfer within the mold, different temperature gradients within the slabs, and contact with the rollers), mechanical effects due to the misalignment of the casting machine, mold distortion, nonconcentric roll cage and straightening strains [5] as shown in Figure 1.2. Under certain conditions, cracks may form along with the oscillation marks on the top surfaces and edges of the strand. When the vertically cast strand is straightened, the top surface and the edges of the strand are put under tension, and transverse cracking can occur. The straightening operation is carried out when the strand is completely solidified [3] in the temperature range of 1100-700°C at a low strain rate of $10^{-3} - 10^{-4}$ /s. This temperature range coincides with the interval in which steel exhibits a ductility trough in laboratory hot tensile tests [2].

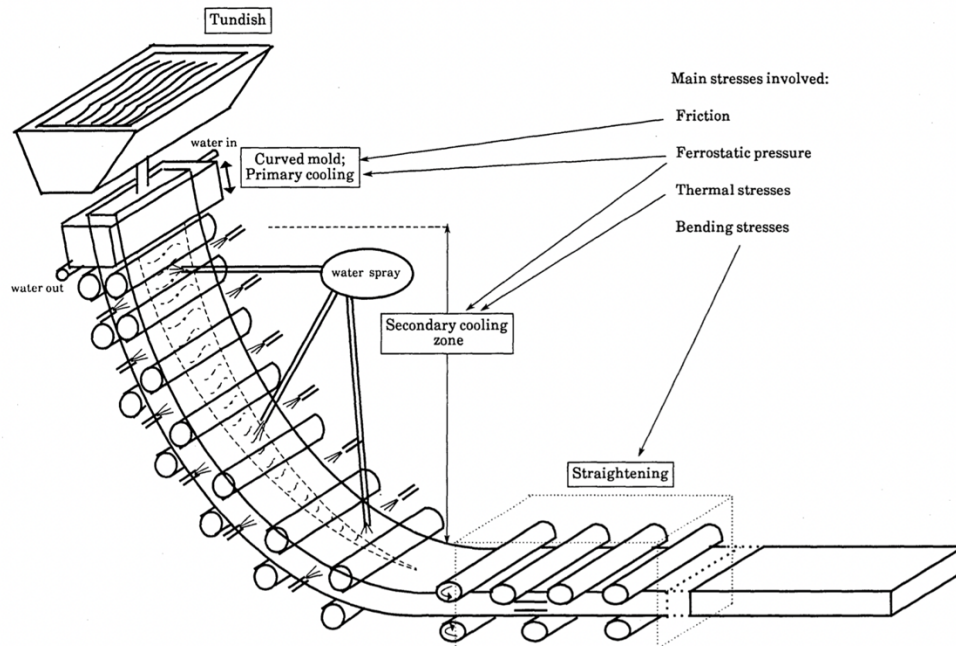


Figure 1.2: Schematic of a curved mold, vertical continuous casting machine, and its characteristics stresses.

1.2. REGIONS OF LOW-TEMPERATURE DUCTILITY

It has been found that the hot ductility behavior of steel can be used as an indication of cracking susceptibility in continuous casting, mainly for transverse cracking. Of all the laboratory testing methods, the tensile test has been the most popular method for studying transverse cracking. Continuously cast carbon steels generally exhibit three regions of low ductility, as shown in Figure 1.3. The depth and width of the hot ductility trough are influenced by the chemistry process variables such as the primary and secondary cooling conditions [2]. The hot ductility curves contain three regions, namely

- I. High ductility, the low-temperature region
- II. Region of embrittlement
- III. High ductility, the high-temperature region

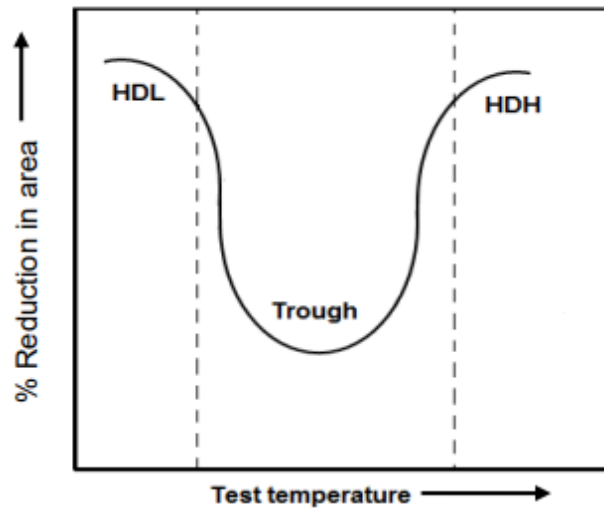


Figure 1.3: Schematic diagram showing the three characteristic ductility regions on a hot ductility curve.

1.3. ZONE I – HIGH DUCTILITY, LOW-TEMPERATURE REGION (HDL)

Embrittlement in steels can be prevented by reducing the amount of strain at the prior austenite grain boundaries. The strain concentrations at the austenite grain boundary in the HDL region can be reduced by increasing the volume fraction of ferrite. The strength difference between the ferrite and austenite decreases with decreasing temperature, increasing the plastic strain in the austenite, thereby decreasing the ferrite's strain [5]. The strain concentration at the grain boundaries is reduced, and the amount of ferrite present leads to recovery of ductility at the low-temperature end of the trough. Ferrite has a high stacking fault energy, and therefore, dynamic recovery, a softening process that operates at all strains, can readily occur [2,6]. The ductility recovery is due to the high-volume fraction of ferrite (α) (>45%) present during deformation or α forming in large amounts during deformation close to the Ae_3 temperatures. Before the Ar_3 transformation

temperatures, a large volume fraction of ferrite is present before the test allowing the strain to be dispersed. The ductility recovers fully 20-30°C below the undeformed A_{r3} , which is ~ 745°C for 0.10% C and ~710°C for 0.16% C in plain carbon steels[2]. The fully ferritic structure shows an increase in ductility because recovery in the ferrite occurs readily, subgrain is large, and the flow stress is low [8-15].

1.4. ZONE II – REGION OF LOW DUCTILITY EMBRITTLEMENT

The embrittlement region is the most important and is associated with the intergranular cracks at the austenite grain boundaries. The intergranular failure occurs in the austenite grain boundaries by grain boundary sliding or transformation-controlled intergranular failure. In the former case, the mechanism predominantly takes place in the austenite phase field, and grain boundary sliding followed by austenite grain edge or corner cracking is the dominant mechanism. In the latter case, the intergranular failure is associated with intergranular micovoid coalescence in thin ferrite films at prior austenite grain boundaries [2,8]. The major temperature regions of embrittlement are shown in Figure 1.4. The first range exists in the liquidus and solidus two-phase region, where the liquid is still present in between growing columnar dendrites [13]. The primary cause of embrittlement is the presence of liquid film in the interdendritic region that does not freeze until the temperatures are well below the solidus temperature of the alloy. The ductility is independent of strain rate and is mainly affected by chemical composition microsegregation of elements such as carbon, sulfur, and phosphorus [9].

The major dominating mechanism and the microstructural features associated with the brittle embrittlement regions are grain boundary sliding, thin ferrite films, and grain boundary sliding.

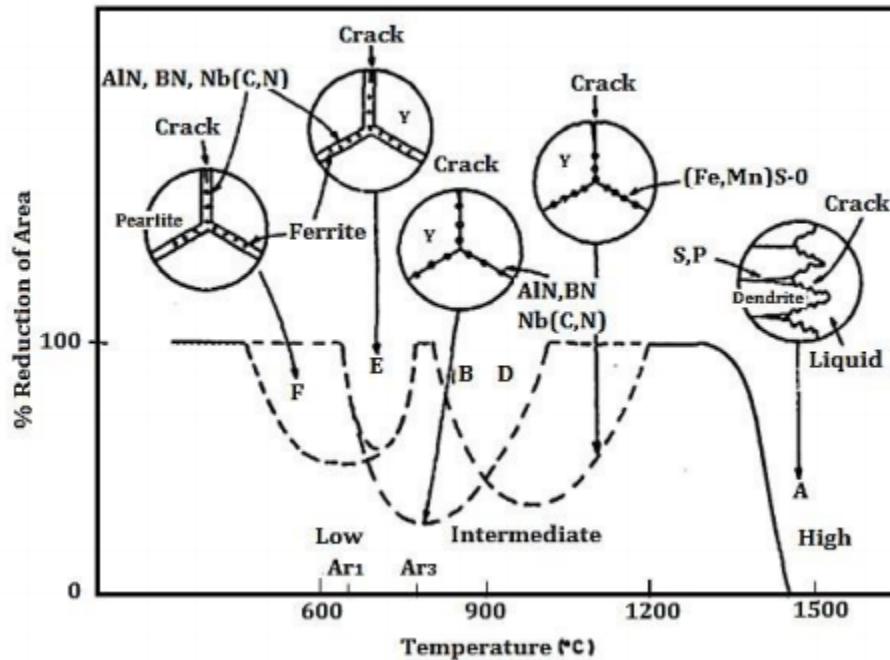


Figure 1.4: Schematic representations of hot ductility regions relating to the embrittlement mechanisms [11].

1.4.1. Intergranular Failure: Precipitate Free Zones. Precipitate free zones (PFZ) are narrow bands without any precipitates adjacent to the initial austenite grain boundaries. The common reason for forming the precipitates is that precipitates nucleate heterogeneously on vacancies. The grain boundary is a sink for vacancies. The region closer to the grain boundaries cannot nucleate the precipitates even though the matrix may be supersaturated with solute. The grain boundary itself acts as heterogeneous nucleation sites. The particles first nucleate at these boundaries, removing solute from the matrix. The solute

depleted region adjacent to the boundary remains precipitate free [2,8,16]. During deformation, the strain is concentrated in weaker PFZs leading to intergranular failure by microvoid nucleation and coalescence [12]. Micro voids form around the grain boundary precipitates such as Nb(C, N), AlN, or V(C, N), leading to intergranular fracture via the micro void coalescence mechanism as shown in Figure 1.5. This fracture mechanism is mainly linked to fine precipitates on the grain boundaries.

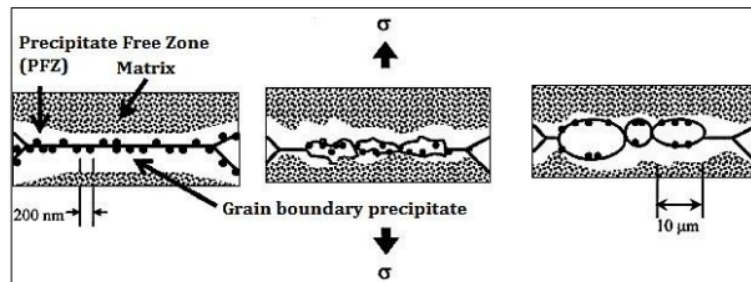


Figure 1.5: Schematic representation of the micro void coalescence mechanism due to the formation of precipitate free zones (PFZ) on either side of the austenite grain boundary [12].

1.4.2. Intergranular Failure: Grain Boundary Sliding. Grain boundary sliding occurs in a fully austenitic region from A_{r3} - 1200°C, but the mechanism dominates at high temperatures in a completely austenitic phase field. Due to the limited dynamic recovery of the austenite, grain boundary sliding can easily cause intergranular cracking. The little dynamic recovery of austenite encourages work hardening allowing high stresses to build up at grain boundary triple points, grain corners, edges, or grain boundary particles leading to intergranular failure by the nucleation of grain boundary cracks. This fracture mechanism can also be associated with creep occurring at strain rates below $1 \times 10^{-4}/s$ [8]. Intergranular failure initiated by grain boundary sliding occurs at higher strain rates $1 \times 10^{-3}/s$ generally

used in hot tensile testing. A schematic diagram showing the formation of wedge cracks by grain boundary sliding is shown in Figure 1.6. This model shows that the grain boundary crack formation by the grain boundary sliding can occur even without fine particles or inclusions on the grain boundaries [13]. However, some researchers [14,15] have shown that the cavity nucleated by grain boundary sliding can grow when fine particles are present along the grain boundary. Fine precipitates such as oxides, nitrides, sulfides, carbides, or carbonitrides along the austenite grain boundaries can act as stress raisers favoring intergranular crack formation[2].

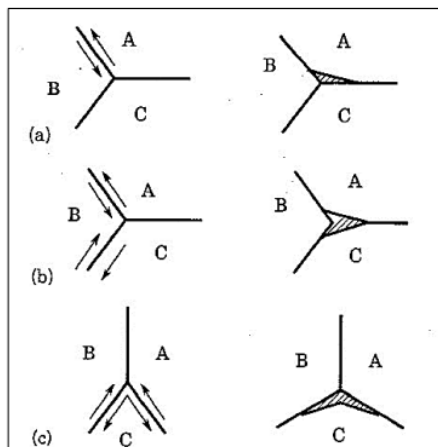


Figure 1.6: Schematic showing the formation of wedge cracks by grain boundary sliding. The arrows indicate grain boundary sliding and sense of translation [8].

1.4.3. Intergranular Failure: Thin Ferrite Films. Intergranular failure also occurs by forming thin films of ferrite on prior austenite grain boundaries. Ferrite is a softer phase and is more ductile than austenite, and is only detrimental when a thin layer of ferrite (5-20 μm) is present along the austenite grain boundary, as shown in Figure 1.7. Ferrite has lower flow stress than austenite and is softer than austenite at elevated temperatures due to a high dynamic recovery rate [2,17-18]. This allows the strain to concentrate in the ferrite film,

encouraging voiding around precipitates or inclusions present in the grain boundary [14], as shown in Figure 1.8. These voids link up to failure by micro void coalescence, resulting in intergranular cracking along the ferrite films. The ferrite thin films play a similar role as PFZ's.

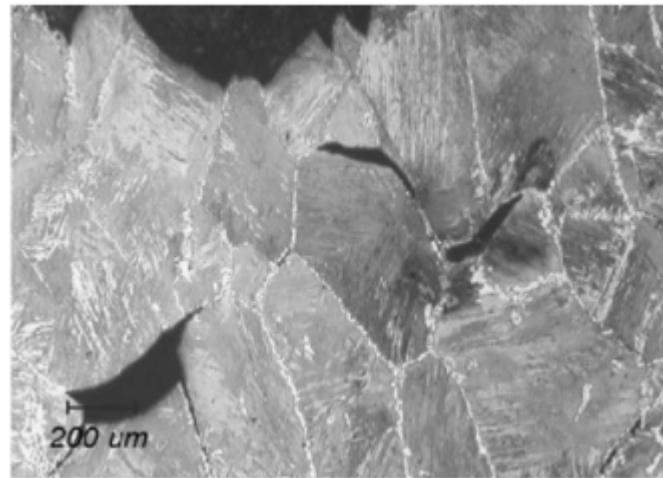


Figure 1.7: Micrograph shows the formation of thin ferrite films on prior austenite grain boundaries for Nb steel at deformation temperature 800°C [14].

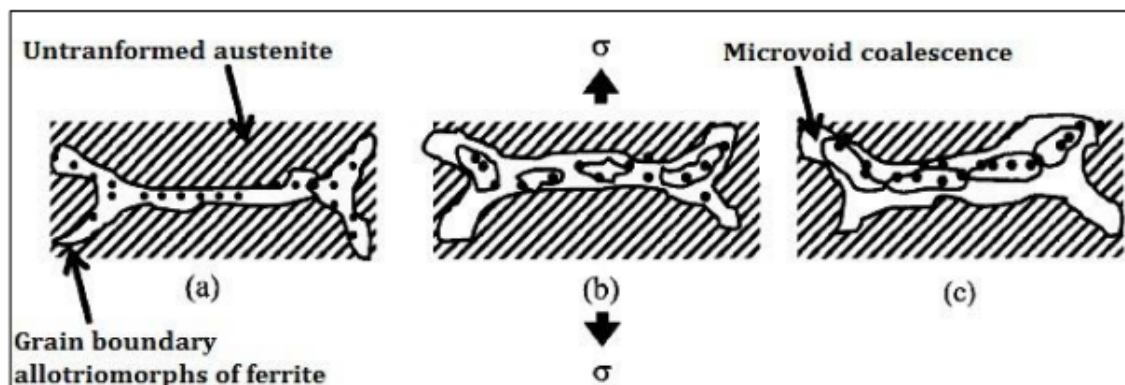


Figure 1.8: Schematic shows the micro void formation and coalescence mechanism and ferrite films at austenite grain boundaries [2].

Below the A_{r3} temperature, the number of ferrite increases, and ductility increases. In addition, the solubility of carbides, nitrides, and carbonitrides is lower in ferrite than in austenite, promoting precipitation in the ferrite film. Thus, the cause of the ductility trough in this temperature range is a combination of ferrite films on grain boundaries and micro-alloy carbide, nitride, and complex carbonitride precipitates.

1.5. HIGH DUCTILITY, HIGH-TEMPERATURE REGION (HDH)

Above 1200°C , ductility is high due to dynamic recrystallization unaffected by steel composition and processing parameters [2]. The mechanism that restores the steel's ductility involves the grain boundary movement. The cracks formed because of grain boundary sliding or stress concentrations due to PFZ's are stopped due to grain boundary moving away from the crack. The ductility of the steels will recover because the growth and coalescence of cavities cannot be achieved away from the grain boundary area[2,8]. This is evident from the large voids from the fractured surface tested in the HDH region that are not associated with the second phase particles. These voids grow from the intergranular cracks formed during the early stages of deformation, which gets isolated within the grains due to grain boundary migration. The original cracks get distorted into large voids until the final fracture occurs by necking between these voids. High temperatures ($> 1200^{\circ}\text{C}$) lead to less precipitation in the matrix and at the grain boundaries promoting dynamic recrystallization and hence the higher the ductility of the steels. Increasing temperatures also leads to lower flow stress and increased dynamic recovery, which helps in reducing the stress concentrations at the crack nucleation sites. However,

dynamic recrystallization will not occur during continuous casting due to coarse grain size and low strain (<2%) during the straightening operation [19-22].

Therefore, care must be taken while evaluating the susceptibility of steel to transverse cracking with the tensile data obtained from the high ductility, high-temperature region (HDH) of the ductility trough.

2. PROCESS VARIABLES INFLUENCING THE FORMATION OF TRANSVERSE CRACKS

The formation of transverse cracking on the surface of the strand is influenced by the composition of the steel grade, temperature of the solidified shell, and thermal and mechanical origins. The process variables affecting the formation of transverse surface cracking are discussed below.

2.1. MOLD OSCILLATION

The oscillation of the mold is essential in continuous casting as it prevents the strand shell from sticking to the mold wall. Mold oscillation produces transverse ripples called oscillation marks on the strand surface. Deep oscillation marks also increase the local variation in the heat transfer in the mold. The severity of transverse cracks depends on the depth of oscillation marks which increase the segregation of P, S, and Mn, paving a preferred path for the crack formation [23]. Transverse crack can initiate along the oscillation mark on the top surface and edges of the strand. The crack propagates during straightening when the top surface and the edges are in tension [24]. The depth of the oscillation mark can be reduced by proper choice of mold flux with low surface tension, reducing the negative strip time by increasing mold oscillation frequency or reducing the stroke length, by avoiding the peritectic carbon range, optimizing taper on the narrow face of the mold, maintaining the uniform temperature of the liquid metal in the mold and minimizing fluctuations in the mold liquid level [25-27].

2.2. SECONDARY COOLING AND CASTING SPEED

The secondary cooling strategy can be adopted to avoid transverse cracking once the hot ductility trough is defined by laboratory testing. This can be done by adjusting the casting speed and adopting different cooling practices in the caster [28]. Two different cooling practices, soft and hard cooling, are used. The soft cooling method uses little water, often as air-water mist spray resulting in temperatures higher than the ductility trough temperatures in the straightening region of the caster. In contrast, hard cooling uses maximum water to decrease the strand temperature below 700°C to reduce transverse cracking [23,29].

Maximum casting speeds are usually used to ensure that the steel shell coming from the mold is thick enough to withstand the ferrostatic pressure, preventing breakouts. A slight increase in the casting speed can significantly increase the surface temperature of the whole strand. This can be beneficial by reducing the amount of micro-alloy precipitation, thereby reducing the occurrence of transverse cracking if the straightening operation is carried out in the high ductility, high-temperature region (above 1200°C) [8].

2.3. MOLD HEAT TRANSFER

The strand surface structure and thermal stresses in the continuous caster can vary with heat transfer [21]. The coarse-grained columnar structure closer to the strand surface caused by non-uniform solidification in the mold increases the risk of transverse cracking. The mold heat transfer can be controlled by reducing mold turbulence, consistent powder feeding, maintaining stable mold level control, and optimizing mold taper to ensure good contact between the slag layer and the mold [16].

3. INFLUENCE OF STEEL COMPOSITIONS ON THE HOT DUCTILITY OF STEELS

Various elements significantly impact the hot ductility of steels, particularly the interactions of Ti, Nb, and V with varying levels of Al, C, and N. The effect of precipitate formation depends on the size, morphology, and distribution. The chemical composition of the steel thermomechanical cycle governs these characteristics. Therefore, it is important to understand the influence of steel composition on the hot ductility of steel.

3.1. CARBON

The carbon content in the steel has an important effect on the position of the hot ductility trough, especially in plain C-Mn and C-Mn-Al steels. As the carbon content in the steel increases, the ductility trough moves to lower temperatures as it lowers the $\gamma \rightarrow \alpha$ transformation temperature. This is because the ductility is controlled by the formation of thin films of ferrite on the austenite grain boundaries. Recovery of ductility on the lower temperature side of the ductility trough (Region III) can take place when sufficient volume fraction of ferrite is present and recovery on the higher side of the ductility trough can happen when ferrite films are no longer present and dynamic recrystallization is possible [18,23]. Peritectic steels (0.10 – 0.15 % C) are highly susceptible to transverse cracking because of the shrinkage of the strand shell caused by the transformation [24]. The coarser as-cast austenite grain structure that forms in peritectic steels is detrimental to hot ductility leading to intergranular fracture [2,8]. For steels with carbon greater than 0.28%, the position of the ductility trough shifts 100K higher approximately, and a distinct change is observed in the fracture mode. The intergranular fracture occurs in the austenite because

of grain boundary sliding rather than at thin ferrite films on prior austenite boundaries. This is because increasing the carbon content increases the activation energy for dynamic recrystallization thereby increasing the critical strain for dynamic recrystallization [23].

3.2. NITROGEN

The nitrogen content in the steel plays an important role in controlling the extent of transverse cracking in micro-alloy and Al killed steels. The ductility trough is widened and deepened with increasing nitrogen levels. The ductility is impaired when nitrogen is paired with aluminum due to the formation of nitrides or carbo-nitrides which can adversely affect the hot ductility of steels [32]. Increasing the nitrogen to 0.01% causes a drop in the ductility of steel. Micro-alloyed steels with low nitrogen levels (<0.005%) and carbon levels in the peritectic range (0.08 – 0.17%) do not cause transverse cracking as long as the aluminum level is below 0.04%. The nitrides precipitates are stable at high temperatures and are formed first before the carbides in Nb containing steels [34,35]. Higher nitrogen levels encourage the precipitation of Nb(C, N) in the austenite instead of NbC as the composition of the precipitates favors nitride formation rather than carbides. In Ti micro-alloyed steels, Ti preferentially combines with N forming TiN precipitates and the remaining N combines with any available aluminum forming AlN. The amount of nitrogen must be low, to obtain a high Ti/N ratio which favors precipitates coarsening and improves the ductility of steels. It is therefore the influence of nitrogen on the precipitation with alloying elements that determine the hot ductility[35,36]. Cracking in the steels is more prevalent with nitrogen levels ranging from 120-150 ppm and the cracks are minimized with nitrogen below 40 ppm [33].

3.3. VANADIUM

Vanadium micro-alloy steels are reported to be more sensitive to nitrogen concentration than Nb micro-alloy steels, which exhibit different carbonitride thermodynamic stability and precipitation kinetics [37,38]. Vanadium steels with high nitrogen levels (90-120 ppm) have been reported to cause transverse cracking; however, below 50 ppm, transverse cracking was not observed [17]. High nitrogen levels favor the precipitation of V(C, N) or VN which can significantly reduce the ductility of steels. The combination of high vanadium levels ($>0.07\%$) and high nitrogen (90-120 ppm) has also been reported to be highly susceptible to transverse cracking [34]. However, vanadium levels of less than 0.07% were reported to inhibit the drop in ductility. At lower controlled nitrogen contents, vanadium steels are reported to have better ductility than Nb steels because the VN particles are less detrimental to hot ductility than fine Nb(C, N) precipitates that form at the austenite grain boundaries that prevent dynamic recrystallization. The former precipitation encourages grain boundary sliding leading to low ductility intergranular failure [39]. For steels that are solutionized during reheating before hot deformation, Nb can be more effective than V at reducing grain growth to improve ductility, but it can also extend the ductility trough to higher temperatures than vanadium. It has also been noted that the vanadium precipitates in both a more coarse and random manner than Nb precipitates, which again favors higher ductility [26].

3.4. NIOBIUM

Niobium is more detrimental to hot ductility than other microalloying elements because Nb(C, N) precipitates out rapidly during deformation in the temperature

corresponding to the low ductility region. In niobium microalloyed steels, the loss in ductility of the steel is associated with intergranular failure caused either by suppression of dynamic recrystallization or the formation of precipitate free zones[2,8,10,40]. Nb may precipitate as fine Nb(C, N) particles in the austenite resulting in deepening and widening of the hot ductility trough. The fine precipitation of Nb(C, N) leads to matrix strengthening and raises the stress in the grain boundary regions. In Nb containing steels, the strain gets concentrated in the precipitate free zones in the grain boundary regions which are relatively weaker. The grain boundary precipitation encourages voiding around precipitates of Nb(C, N) and the extension of cracks formed by grain boundary sliding[2,8]. Niobium delays the onset of dynamic recrystallization to higher temperatures and delays the recovery of ductility to higher temperatures. Nb additions from 0.017% up to 0.074% were shown to have an effect on ductility [2, 40-42]. Al additions to Nb containing steels were also shown to deepen and widen the ductility trough [2, 43].

3.5. TITANIUM

The addition of titanium could be beneficial in reducing the transverse cracking susceptibility, but it is dependent on many factors. The interaction between other microalloying elements such as Nb, V with varying amounts of nitrogen, austenite grain size with the pinning effect of TiN plays an important role. However, the addition of Ti can also improve ductility from its ability to combine preferentially with nitrogen. This in turn will reduce the amount of nitrogen available for precipitation as either AlN or Nb(C, N), both of these precipitates can reduce the ductility of the steels[2,8]. The addition of Ti improves the ductility of the steels under solution treatment conditions. High-temperature

precipitant TiN or Ti-rich precipitates usually below the liquidus or just above the solidus temperature of the alloy. These precipitates do not completely dissolve under the solution treatment temperatures and so they can pin the austenite grain boundaries and prevent grain growth [44]. Therefore, in solution treatment conditions, the improvement in ductility is mainly due to grain refinement rather than by compositional effects. The research data available on the influence of Ti additions on the formation of transverse cracking indicate that small Ti additions have a beneficial effect. However, laboratory hot tensile testing, do not predict the true behavior of Ti on the problem of transverse cracking. It is important that the reader takes care while interpreting hot ductility data on the Ti containing steels.

3.6. SULPHUR

Sulfur can reduce the hot ductility of steels by weakening the grain boundary area for the following reasons: (i) sulfur segregation to the boundary, (ii) formation of low melting Fe-S compounds [45] and the (iii) combined effect of Mn and sulfides on the formation of cavities, which links up to produce low ductility intergranular failure [19]. The effect of sulfur on the hot ductility usually depends on the test conditions. For steels that are solution treated at 1330°C, the amount of sulfur that will dissolve and precipitate as fine sulfides at the grain boundaries is important for controlling the ductility [46-48]. The amount of sulfur that redissolves depends on the Mn content. For steel with 1.4% Mn, the amount of sulphur sulfur redissolved is $>0.001\%$ S. At the solution treatment temperature, once the sulfur level reaches the maximum dissolvable amount, an increase in the sulfur content will show no change in the hot ductility behavior [49,50].

Sulfur levels are kept to a minimum to avoid transverse cracking. Reducing the sulfur levels reduces the volume fraction of sulfides available for precipitation. Calcium treatment has been shown to improve the hot ductility of steels by modifying the sulfides as well as reducing the total sulfur in the steels. These modified sulfides can dissolve at 1330°C which reduces the sulfides available for precipitation in the interdendritic regions as well as on the austenite grain boundaries [47,51,52].

3.7. ALUMINUM

Aluminum is added to steels during steelmaking to remove oxygen from the solution by forming alumina inclusions. In the presence of nitrogen, aluminum precipitates as AlN. The precipitation of AlN is very sluggish in austenite unless the precipitation is enhanced by thermal or mechanical treatments [41,53]. Increasing the total Al levels above 0.035% increases cracking by widening the low ductility region by extending the ductility trough to higher temperatures. At low strain rates, the fine AlN precipitates at the grain boundaries act as an initiation site for void nucleation that hinders grain boundary mobility[2]. The cavities that nucleate continue to grow at the pinned grain boundaries leading to void coalescence and finally leading to intragranular failure. Al levels of more than 0.035% can be used if the nitrogen level in the steel is below 40 ppm[53].

3.8. PHOSPHOROUS

Phosphorous tend to segregate at the grain boundaries in both ferrite and austenite, weakening the boundary and lowering the ductility of the steels producing brittle intergranular failure [54-57]. Suzuki et al [55] studied the influence of phosphorous on the

hot ductility of plain carbon steel. They have shown that the detrimental effect of phosphorous depends on the carbon content for plain carbon steel and the phosphorous should not possess a problem if the carbon content is less than 0.2 wt.% C. Figure 3.1. shows the effect of phosphorous and carbon content on the hot ductility of steels. This was explained in terms of the solidification process which produces a ferrite structure in the steels with carbon lesser than 0.2 wt.% C. The samples were melted and strained at a strain rate of 5 s^{-1} . A good ductility is defined as a region with a % RA greater than 60 % in the temperature range from 1200°C - 900°C .

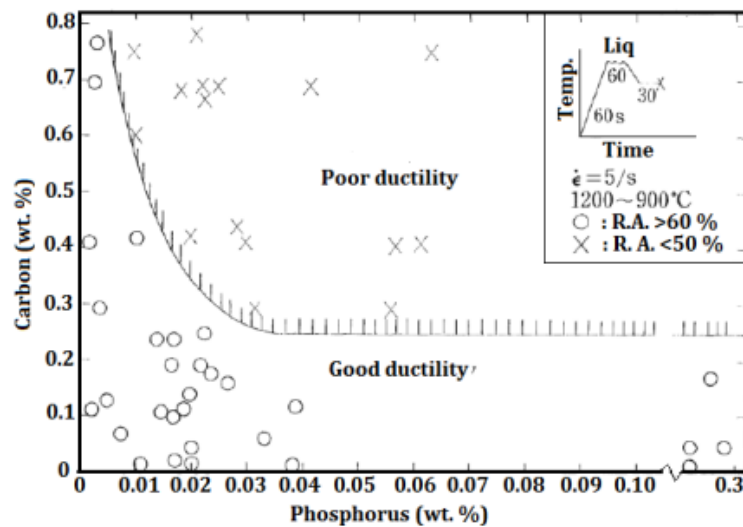


Figure 3.1: Effect of carbon and phosphorous content on the hot ductility of steels [55].

Previous research [12,41,58] has shown that the phosphorous content recovers the ductility of steels in the temperature range from 1200°C - 700°C to improve the hot ductility of steels. This occurs when the phosphorous content is in the range of 0.005-0.015% and the carbon content of the steel is less than 0.25%.

3.9. MN:S RATIO

The effect of manganese and sulfur content on the hot ductility of the steels was studied previously and it was reported that the hot ductility improves when the manganese content increases, and the sulfur content decreases. In plain carbon steels, manganese sulfides are usually associated with intergranular failure in the low-temperature austenitic region where the sulfur content is above 30 ppm [59-63]. The ratio of manganese to sulfur must be excess of 30 ppm to prevent embrittlement with Mn content above 0.1wt%. De Toledo et al [64] studied the influence of sulfur and Mn:S ratio on the crack susceptibility and hot ductility of steels. In a low sulphur steel (0.03% S), the critical $(Mn:S)_c = 40$ and for high sulphur steel (0.3% S), the critical $(Mn:S)_c = 3.5$. Based on the experimental data, Toledo et al derived an equation for the Mn:S ratio as,

$$(Mn:S)_c = 1.345 S^{-0.7934} \quad (1)$$

where S is the weight % of sulfur in the steel.

The Mn:S ratio lower than 30 causes sulfides (Fe, Mn) S to precipitate along the austenite grain boundaries thereby reducing the strength of the grain boundary. Cardosa et al [59] studied the influence of MnS on the hot ductility of plain carbon steel and found that the manganese sulfides have a strong influence on the hot ductility of the steel. The ductility loss was mainly attributed to the formation of thin grain boundary films of ferrite and during deformations, strain gets concentrated at the MnS inclusions in the ferrite network. The higher the number of MnS inclusions at the austenite grain boundaries easier the microvoids to coalesce and grow leading to intergranular failure. For microalloyed steels, steels cooled directly to the test temperature ranging from 1100°C - 700°C, Mintz et al [65] reported that increasing Mn content at a constant S level improved the hot ductility

of steels. This is because an increase in the manganese content leads to grain refinement which reduces the critical strain required for dynamic recrystallization. Increasing sulfur content is also accompanied by grain refinement but any improvement in hot ductility has a negative effect of having higher volume fraction of manganese sulfide inclusion at austenite grain boundaries which promotes intergranular failure.

4. INFLUENCE OF TEST VARIABLES ON THE HOT DUCTILITY OF STEELS

Over the last 40 years, researchers have worked on different experimental methods to determine the hot cracking susceptibility under continuous casting conditions. Hot ductility is the most assessed parameter to determine the cracking susceptibility using an elevated temperature tensile test. There is no standardized test and different experimental procedures have been adopted by different researchers. Among all the laboratory tests, the most popular for the study of transverse cracking is the simple hot tensile test. The ideal test condition involves prior melting of the sample, followed by controlled cooling to the test temperatures and deformation at low strain rates. However, the use of prior heat treatment of samples close to the solidus temperature of the alloy has proved to get similar results compared to the melting of the samples. Many investigations have been carried out in the solution treatment temperature range of 1300-1350°C and cooling to the test temperature. Two broad categories of tensile testing have been used to determine the hot ductility of steels: (i) Servo hydraulic load frames namely MTS or Instron tensile testing machines equipped with induction coil or furnace and (ii) The Gleeble apparatus. The most used thermal and deformation cycle in the tensile test is shown in Figure 4.1.

In-situ melted and solidified: The tensile specimen is heated to 15-30°C above the liquidus temperature in a quartz tube and cooled to the test temperature at a specified cooling rate and then deformed to failure. This method provides the most accurate simulations of the continuous casting conditions as it includes the effect of solidification behavior, segregation of elements, and cooling zone.

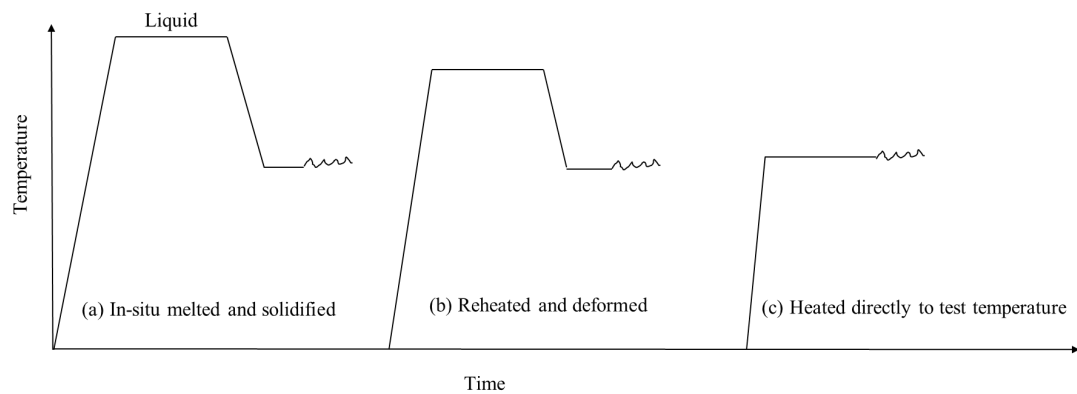


Figure 4.1: Different thermal cycles to determine the hot ductility of steels using tensile testing.

This method ensures the complete dissolution of TiN particles, MnS inclusions and allows segregation in the interdendritic boundaries. However, it is difficult to simulate the surface chill zone and columnar structure of a continuous cast strand in a laboratory tensile test. The length of the columnar grains presented in a continuously cast strand cannot be replicated in a laboratory hot tensile test.

In the *reheated and deformed method*, the tensile specimen is heated above the precipitate dissolution temperature. This is to dissolve the precipitates and produce a coarse grain structure which is similar to the cast structure before the straightening operation. It is then soaked at the dissolution temperature and cooled to the test temperature at a specified cooling rate. This method is reliable and an easily controlled process. The main disadvantage is that the microstructure is not the same as in the continuous casting condition as the cooling does not begin from above the liquidus temperature. High-temperature micro-alloy precipitants such as TiN and MnS can precipitate from the liquid or just below the solidus. Reheating the specimen will not dissolve these nitrides. Figure

4.1(c) shows the tensile specimen is directly heated to the tensile test temperature, stabilized for a short time, and then deformed to failure under suitable strain rate conditions. This method is the least accurate representation of the continuous casting conditions. In the straightening region of the caster, the temperature range extends from below and above the phase transformation regions (austenite to ferrite transformations, precipitate regions). The tests performed below and above the transformation temperature region do not have the initial conditioning of the microstructure. In a directly heated sample, thin films of ferrite at the austenite grain boundaries do not form. This method does not allow for the influence of cooling on transformation and precipitation behavior. The influence of test variables on the hot ductility of steels are discussed below.

4.1. STRAIN AND STRAIN RATE

Schrewe [66] showed that the strand support involves the non-movement of the solidifying liquid form which consists of the shell of the solid steel and the molten liquid metalcore. During bending, the inner radius of the solidifying solid shell is subjected to compression while the outer radius is in tension. On the contrary, during straightening the inner radius is under tension while the outer radius is subjected to compression. Excessive strain may lead to strand defects and failure. Strain values up to 1.5% on the outer strand surface are accepted because the solidified steel has sufficient compressive strength to accommodate the strand [67].

Lankford [7] first proposed the surface strain during straightening which is given by

$$\varepsilon = \frac{t}{2R} \quad (2)$$

where t is the thickness of the strand, R is the radius of the strand's curvature and ε is the approximate strain on the surface of the strand.

The strain rate depends on the design of the unbending system. The minimum strain rate is given by,

$$\dot{\varepsilon} = \frac{t}{2R} \times \frac{v}{l} \quad (3)$$

where t is the thickness of the strand, R is the radius of the strand's curvature, v is the casting speed and l is the gauge length to develop the full bending strain.

Lankford assumed the bending strain develops between the smallest and largest gauge length of the following such as the distance from the tangent point to the first bending roll, the thickness of the slab or the shell thickness (in case of straightening with a liquid core). However, Irvine [68] and Deisinger [69] et al defined l as the length of the unbending zone. The strain rates during straightening process are around $1 \times 10^{-4}/s$ in continuous casting of slabs, $5 \times 10^{-3}/s$ in billet casting and $1 \times 10^{-3}/s$ in thin slab casting.

Increasing the strain rate of the straightening region and refining the grain size (typically below $200 \mu m$) can both improve the ductility, and a narrow trough is observed [70-72]. Increasing the strain rate will reduce the amount of grain boundary sliding [73] and the refined grain size will make it more difficult for the cracks to propagate along the grain boundaries. Higher strain rates improve the ductility by reducing the time for strain induced precipitation [13], reduces the time for the formation and diffusion-controlled

growth of voids adjacent to the precipitates at the grain boundaries [74]. Increasing the strain rate has the ability to work harden the grain boundary ferrite films. This hardens the ferrite film and reduces strain localization as strain now accumulates into the surrounding austenite, resulting in a more uniform strain distribution [41].

4.2. EFFECT OF STRAIN RATE IN HOT TENSILE TESTING

Bailey et al [75] showed that in laboratory hot tensile tests, the strain rate decreases as the specimen elongates which is given by,

$$\dot{\varepsilon} = \frac{d\varepsilon}{dt} = \frac{1}{L} \times \frac{dL}{dt} \quad (4)$$

where $\dot{\varepsilon}$ is the true strain rate, ε is the true strain, L is the specimen gauge length in mm, $\frac{dL}{dt}$ is the machine cross head speed in mm/s. The strain rate is at a maximum for a constant crosshead speed, at the beginning of the test. The strain rate decreases until the onset of necking after which it increases and gradually decreases to the point of fracture. The calculated elastic strain rates will be slightly higher than the actual elastic strain rates as some of the elastic strain will occur outside the gauge length. This equation is valid for estimating the plastic strain rate once the maximum load has been reached where the plastic deformation occurs uniformly throughout the gauge length. Laboratory tensile tests are usually conducted in the same order of magnitude strain rate ranges that match with the industrial conditions. Bailey et al [75] proposed the mean strain rate in the hot tensile tests can be calculated as,

$$\ddot{\varepsilon} = \frac{1}{\Delta t} \times \ln \left(\frac{d_0}{d_f} \right)^2 \quad (5)$$

where Δt is the time during which the specimen was under stress, d_0 is the initial diameter of the specimen, d_f is the final diameter of the specimen at fracture.

4.3. COOLING RATE

Abushosha et al [29] found that increasing cooling rate to the test temperature after solution treatment temperatures from 1400-1200°C lowered the ductility of steels by deepening the ductility trough. The deepening of the hot ductility trough was related to the formation of finer particle size or finer inclusion distribution at the austenite grain boundaries due to the fast-cooling rate. The higher the cooling rate, larger the undercooling and the higher the Gibbs free energy for more particles to nucleate. These fine particles distributed along the austenite grain boundaries acts as stress raisers which encourage cavitation eventually leading to brittle intergranular failure during deformation. The faster primary cooling and slower secondary cooling patterns are used in industrial process. The cooling rate from the primary cooling to the secondary cooling zone usually ranges 1-2°C/s for a thick slab casting of 200-250 mm and 3-5°C/s for thin slab casting of 60-80 mm [67]. The cooling rate in the secondary cooling zone is in the order of 0.1-0.3°C/s [64]. The slow cooling rate allows time for segregation and growth of the precipitates or inclusions to take place. Kang [74] suggested that the cooling rate in the order of 0.2-0.3°C/s can be used because it correlates well with the cooling rate of secondary cooling zone of the continuous casting process. The slow cooling rate of 0.2-0.3°C/s will be difficult to compare with the earlier research because most of the researchers have used an average cooling rate of 1°C/s or higher.

In low carbon C-Mn steels, Abushosha et al [29] found that decreasing the cooling rate causes the ductility to increase because the slow cooling rate allows the ferrite layer at the grain boundaries to increase in thickness and leads to coarser MnS precipitation. Therefore, larger the particles or inclusions, the larger the interparticle spacing and more difficult for the cavities to connect leading to higher ductility. The increase in thickness of the ferrite film at the austenite grain boundaries reduces the strain concentration; favoring transgranular failure and increase in ductility of the steels. Slow cooling is favorable as it provides sufficient time for the particles to coarsen at the austenite grain boundaries giving better ductility. Therefore, the cooling rate is important as it decides both the size of the precipitates and inclusions. It also must be noted, however that the volume fraction of the precipitates is governed by the chemical composition.

4.4. THERMAL HISTORY

The other major variable affecting the hot ductility of steels is the thermal history. The thermal oscillation patterns experienced at the surface of the slab during the continuous casting process is very complex and difficult to simulate in a laboratory hot tensile test. During the continuous casting process, the surface of the slab is in contact with the water sprays and the guide rolls which produces thermal oscillations [2,7,8]. The rate of cooling in the primary cooling zone is faster than in the secondary cooling zone. Furthermore, the cooling rate at the strand's corner is always higher both in the board as well as in the mid-surface of the slab. The high cooling rate in the primary cooling zone causes the strand temperature to drop to a minimum (T_{\min}) followed by rapid surface reheating to (T_{\max}) due to the strand's hot interior. The minimum surface temperature of the strand (T_{\min}) can be

as low as 500-600°C mainly at the corner of the strand. This is then caused by the thermal fluctuations as the temperature in the strand rises by passing through the guide rolls and decreases as it leaves and the continuous spray of water on the surface of the strand to maintain cooling [76].

Mintz et al [80], Cardosa et al [76], El-wazri et al [77] studied the effect of thermal history on the hot ductility of plain carbon steels and niobium microalloy steels and their finding showed that the minimum surface temperature of the strand (T_{\min}) has an impact on the hot ductility of the steels. Their research showed that if the surface temperature of the strand falls below the straightening temperature, a high volume fraction of precipitates occurred both in the matrix and along the austenite grain boundaries which results in poor ductility. Moreover, when the surface temperature of the strand falls below the A_{r3} temperature, proeutectoid ferrite forms at the austenite grain boundaries, the precipitation of second phase particles will further be enhanced in the ferrite. The precipitates containing nitride forming elements are less soluble in ferrite compared to austenite which makes the ductility of the steels to deteriorate.

Walker and Marshall's et al [77,78] studied the effect of AlN precipitation on the hot ductility of C-Mn-Al-N steels. The steels were soaked at 1300°C for one minute and then rapidly cooled to a temperature between 500°C - 750°C before reheating to 1000°C, which is a typical strand straightening temperature. They found that when the temperature drops below the A_{r3} temperature and then reheating to 1000°C resulted in a significant increase in the volume fraction of aluminum nitride precipitates with the corresponding drop in the size of the austenite grains. They also studied that the high volume fraction of AlN precipitates does not occur if the temperature falls above the A_{r3} temperature. Walker

and Marshall suggested during the α to γ reaction, small grains are formed just above the A_{c3} temperature. The aluminum and nitrogen can diffuse rapidly over short distance to the grain boundaries because of the formation of small size austenite grains, preventing grain growth. The failing to fall below the A_{r3} temperature during reheating will not produce small size austenite grains which makes aluminum and nitrogen to diffuse further to the distant grain boundaries and not much AlN will form. However, Gladman and Pickering insisted that the AlN precipitation does not take place until the onset of γ to α phase transformation. It was also mentioned that the during the cooling of steel, AlN will not precipitate in unstrained austenite at the cooling rate which is normally applied in steel processing.

Luo et al [79] investigated the effects of undercooling on C-Mn-Al-Nb and C-Mn-Nb-Al-Ti steels. The samples were melted and cooled at 4°C/s to 100°C below the deformation temperature. The samples were held for 60 sec, reheated again at 4°C/s and deformed using a strain rate of $5 \times 10^{-4}/\text{s}$. Their results showed that the undercooling decreased the ductility for both grades of steel at 800°C . However, no major change was observed in the ductility when the deformation was above 900°C . Cardoso et al [76] also studied the effect of undercooling on the hot ductility of C-Mn-Al steels. In this study, the samples were solution treated at 1350°C and undercooling by 100°C encourages AlN precipitation in the austenite which raised the temperature for the onset of dynamic recrystallization and a wider ductility trough was observed. At lower temperature, undercooling by 100°C , resulted in early formation of ferrite that increased the ductility trough by $50\text{-}100^{\circ}\text{C}$. The pronounced effect of undercooling was observed in the low (0.026%) Al steel than the high (0.085%) Al steel because AlN precipitation were already

enhanced in the high Al steels. Their results shows that the undercooling as found in continuous casting process can lower the ductility in low Al containing steels and the conventional hot ductility tests may not be able to reveal this effect.

4.5. EXPERIMENTAL DETERMINATION OF HOT DUCTILITY OF STEELS

Several different experimental techniques are being considered to measure the hot ductility of steels in the low temperature ductility range during continuous casting. The methods involve either reheating of as-received slab sections provided from industry in the low ductility temperature range and producing a controlled amount of deformation while measuring load and displacement. The two experimental methods used were: (1) a tensile testing apparatus utilizing a MTS servo-hydraulic load frame with a slow heating/cooling rate resistance furnace with SiC elements (referred in this article to as the “Slow cooling test”) and (2) a custom built thermomechanical testing apparatus that employs rapid internal Joule heating system coupled with an electro-mechanically controlled tensioning system (referred to as the “Fast cooling test”).

Servo-hydraulic MTS load frame - Subsize #3 round (diameter 6 mm), specimens with a gauge length of 25 mm were prepared according to the ASTM E8-16a standard were used in slow cooling tests. The main features of the testing apparatus include a resistance furnace capable of temperatures up to 1400°C, maximum strain-rate of 10/s and a maximum load capacity of 11kip. For this test, the thermomechanical cycle was as follows: the specimens were heated at 1°C/s to 1200°C in argon atmosphere and then were held for 2 min for dissolution of precipitates. Subsequently, the samples were cooled to the test temperature in the range of 650°C-950°C at a cooling rate of 1°C/s. Samples were held at

the test temperature for 2 min. They were then strained to failure at a constant strain rate of $3 \times 10^{-3}/s$ which was selected to approximately match the strain rate during the straightening operation of the continuous casting process. After failure, the samples were allowed to cool to room temperature inside the furnace. Figure 4.2 shows a schematic temperature profile for the slow cooling test. The image showing testing equipment is shown in Figure 4.3.

Advantages

- High precision
- Already set up to perform high temperature testing

Disadvantages

- Possible specimen oxidation
- Needs inert gas protection
- No way to re-melt specimen
- Slow heating to the testing temperature
- Difficult to measure strain in a gage length

Applications

- Determination of tensile stress and strain at different test temperatures

A custom-built thermomechanical testing apparatus that employs rapid internal Joule heating system coupled with an electro-mechanically controlled tensioning system. The fast-cooling test utilized a Joule heating system with an attached mechanical loading assembly for tensile testing of a flat specimen using an inline drive (10 kN max), a load cell (0.5N resolution) and laser displacement sensor ($\pm 1 \mu m$ resolution).

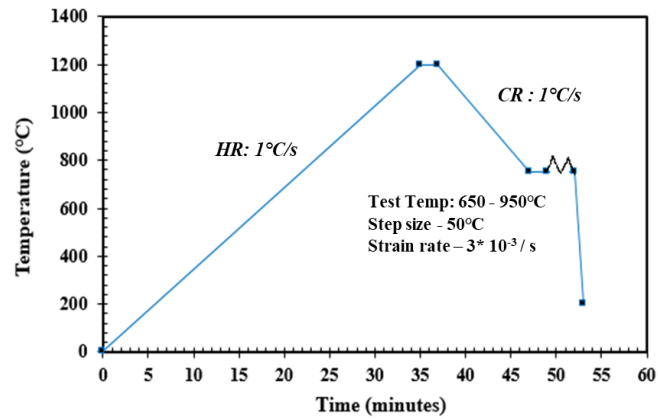


Figure 4.2: Schematic diagrams showing the thermal cycles studied: slow cycle with servo-hydraulic load frame equipped with SiC furnace.

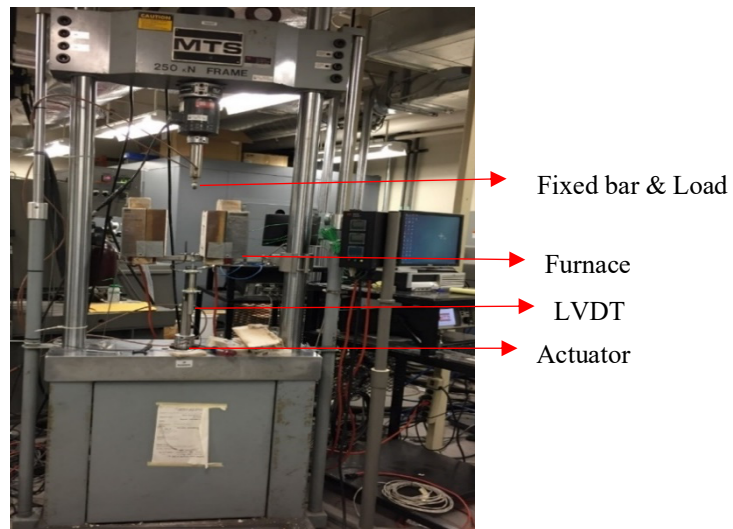


Figure 4.3: MTS servo hydraulic load frame.

For this test, the sample was placed inside a chamber with a continuous flow of argon throughout the test cycle to avoid oxidation of the samples. The samples are flat specimens, typically 97 mm (long) x 23 mm (width) in cross section with a thickness of 3mm. A 400-amp DC joule heater was used to heat the samples and a pyrometer (1 mm spot size, ± 1 °C) monitored the temperature of the sample. The system employed LabVIEW software to

monitor and control the test and the temperature profile using feedback control. Figure 5.3 shows a schematic temperature profile for the fast hot tensile test using Joule heating. The samples were heated at 5°C/s up to 1200°C and then soaked for 2 min. The samples were then cooled to the test temperature in the range of 650°C -950°C at a cooling rate of 4°C/s. The samples were soaked in the test temperature for 2 min and then strained to failure using a constant strain rate of 3×10^{-3} /s. After failure, the sample was cooled rapidly to the room temperature. Both test methods employed the same strain rate and testing temperatures but with different heating and cooling rates. Figure 4.4 shows a schematic temperature profile for the fast cooling test. The image showing testing equipment is shown in Figure 4.5.

Advantages

- Uses resistance heating and computer control to achieve fast heating and cooling rates
- Multiple controlled heating and cooling profiles possible
- Specimen size is small and allows targeted areas to be tested
- Inert atmosphere possible using flowing argon

Disadvantages

- Non-uniform temperature distribution
- The specimen cannot be re-melted and solidified
- Some initial challenges in measuring %RA

Applications

- Determination of tensile stress and strain at different test temperatures

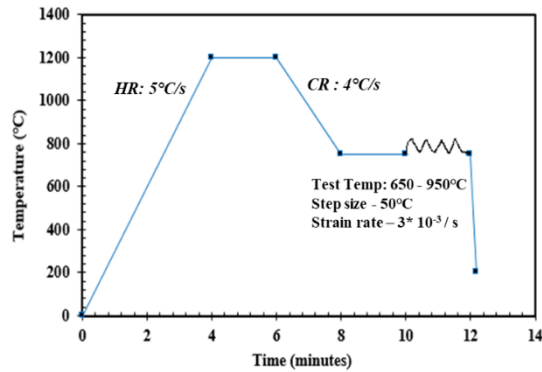


Figure 4.4: Schematic diagrams showing the thermal cycles studied: fast cycle using Joule resistive device.

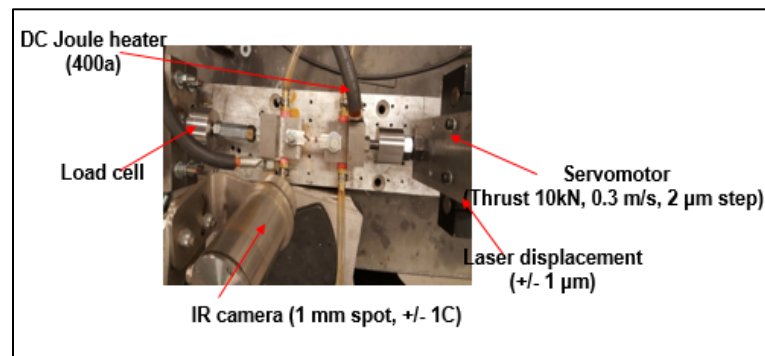


Figure 4.5: High temperature micro-mechanical tester.

This research work focuses on the use of two laboratory hot tensile test methods, one using a servo hydraulic load frame equipped with resistive heating furnace and one using a custom-built joule heating apparatus equipped with an electro-mechanical tensioning cylinder. Tensile samples taken from the as-cast steel slabs and beam blank samples were reheated, soaked, cooled to temperature, and tested to failure to determine the reduction of area (%RA) of the specimen. The two test methods are compared and factors influencing the ductility of these steels are discussed.

PAPER**I. THE INFLUENCE OF TI, NB AND V ON THE HOT DUCTILITY OF AS CAST MICROALLOYED STEELS**

Madhuri Varadarajan, Laura N. Bartlett, Ronald J. O'Malley, Simon N. Lekakh

Peaslee Steel Manufacturing Research Center, Missouri University of Science and
Technology,

1400 North Bishop Avenue, Missouri, United States, 65409-0340

Phone: 573-341-4711

Email: lnmkvf@mst.edu

ABSTRACT

Microalloying with Ti, Nb, and V, both individually and in combination, is a common method for producing steels with high strength and toughness. However, interaction with other elements and impurities can lead to cracking during continuous casting and rolling. The hot ductility of commercially cast V, Nb and Nb-V-Ti steels has been investigated using two experimental methods: tensile testing utilizing a servo-hydraulic load frame with a resistance furnace and thermomechanical testing using rapid joule heating. The temperature dependent ductility of these steels is compared for both test methods. Factors that influence the ductility of these steels are discussed.

1. INTRODUCTION

One of the main problems faced in continuous casting is the formation of transverse cracks. Transverse cracks are surface or near surface cracks in the cast slab that are oriented perpendicular to the direction of casting. These cracks are often associated with oscillation marks and they can penetrate to a depth of 5-8mm or more below the surface of the slab. The cracks often originate in the straightening region of the caster on the top surface of the slab when unbending occurs at temperatures of 700-1000°C where the steel is known to exhibit low ductility. This “ductility trough” can be observed in hot tensile tests by measuring the % reduction of area (%RA) at specimen failure. Carbon steels generally exhibit three regions of low ductility. A high temperature ductility trough exists at temperatures near the solidus temperature where liquid is still present. In the high temperature low ductility range, ductility depends on segregation of alloying elements and impurities that produce a low melting point liquid that is associated with hot tearing. The second ductility trough exists in a temperature range from 900 to 1200°C in austenite. In this temperature range oxides, sulphides, carbonitrides, and other fine precipitates formed at austenite grain boundaries can reduce ductility. Precipitation on austenite grain boundaries can lead to precipitate free zones adjacent to the grain boundary that create localized weakening in this area, producing low ductility intergranular failure [1]. The third ductility trough exists in the temperature range from 600-900°C near the A_{r3} temperature. In this region ferrite films are formed at austenite grain boundaries. Below the A_{r3} temperature, the amount of ferrite increases, and ductility increases. In addition, the solubility of carbides, nitrides and carbonitrides is lower in ferrite than in austenite,

promoting precipitation in the ferrite film. Thus, the cause of the ductility trough in this temperature range is a combination of ferrite films on grain boundaries as well as microalloy carbide, nitride and complex carbonitride precipitates [2, 3].

To avoid high production costs and yield losses on finished products, it is important that defects in continuous cast slabs are minimized. The hot ductility of steel is highly dependent on the presence of microalloying elements such as Nb, V and Ti [4]. Optimal use of microalloying elements, such as Ti, Nb, and V, can produce steels that exhibit high strength and toughness when appropriate thermomechanical processing is employed [5-7]. Unfortunately, these elements can sometimes lead to increased susceptibility to transverse cracking.

Niobium has been shown to have a strong effect on the hot ductility of steels, deepening the “ductility trough” and extending the low ductility region to higher temperatures. Mintz, et. al., and Sricharoenchai, et. al., suggest that this is mainly due to the formation of Nb(C, N) precipitates which can retard recrystallization and form precipitates on austenite grain boundaries. Nb additions from 0.017% up to 0.074% were shown to have an effect on ductility [2, 10-12]. Al additions to Nb containing steels were also shown to deepen and widen the ductility trough [2, 13].

Vanadium and titanium have also been shown to affect transverse crack sensitivity. At high nitrogen levels (90-120ppm), vanadium has been reported to cause transverse cracking but below 50 ppm, transverse cracking was not observed [8]. High nitrogen levels favor the precipitation of V(C, N) or VN, but vanadium levels below 0.07% have been reported to inhibit the drop in ductility [9]. Ti additions of 0.015-0.04% Ti have also been reported to decrease crack sensitivity by forming coarse TiN, thereby reducing the

formation of fine AlN and Nb(C,N) precipitates [14,15]. Mintz, et. al., reported that Ti additions can maintain a fine austenite grain size during heat treatment due to the grain boundary pinning effects by TiN precipitates which are stable at high temperatures [16]. However, the benefits were not evident in the continuously cast steels.

The objective of the present research is to investigate the influences of Ti, Nb and V on the hot ductility of three as-cast microalloyed steel slabs received from industry. This paper focuses on the use of two laboratory hot tensile test methods, one using a servo hydraulic load frame equipped with resistive heating furnace and one using a custom built joule heating apparatus equipped with an electro-mechanical tensioning cylinder. Tensile samples taken from the as-cast steel slabs were reheated, soaked, cooled to temperature, and tested to failure to determine the reduction of area (%RA) of the specimen. The two test methods are compared and factors influencing the ductility of these steels are discussed. In future work, these testing methods will also be compared to a proposed new hot bending test method that will be capable of directly observing crack initiation on an as-solidified and cooled specimen.

2. EXPERIMENTAL METHOD

2.1. MATERIALS AND COMPOSITION

Steel slab samples with compositions shown in Table 1 were supplied by United States Steel Corporation. Samples for hot tensile testing were cut from 203mm thick, as-cast slab samples from the locations shown in Figure 1. The hot ductility samples were prepared so that the tensile specimen orientation was perpendicular to the columnar grain

structure of the as-cast slab to ensure that testing was performed perpendicular to the direction of solidification in the slab. Care was taken when cutting of the samples to avoid centerline segregation, internal crack sites, and the narrow face edges of the as-cast slab. The heat affected regions from the oxy-acetylene torch cuts were avoided during preparation of the tensile samples.

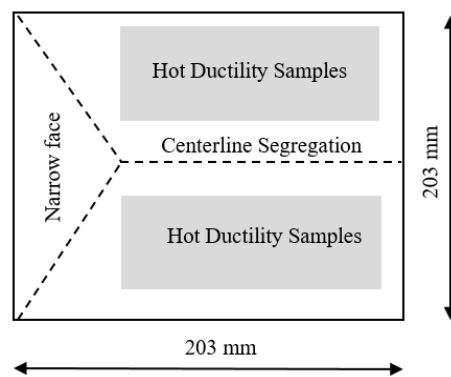


Figure 1: Position of hot ductility samples taken from as-cast steel slab.

Optical emission arc spectroscopy analysis was performed along the length of the slab and the average chemical composition of the steels, reported in wt. %, are given in Table 1. Leco combustion and inert gas fusion analysis were used to determine the composition of carbon, sulphur and nitrogen levels in the steels. The three steels studied are aluminum deoxidized steels with varying levels of carbon ranging from low to medium carbon content range with varying amounts of microalloying elements of V, Nb and Ti.

Table 1: Chemistry of the slab section in wt. % as determined by optical emission arc spectroscopy and Leco combustion and inert gas fusion analysis.

	C*	Si	Mn	P	S*	Al	V	Nb	Ti	N** (ppm)
V Steel	0.175	0.03	0.64	0.02	0.007	0.046	0.061	-	0.002	42
Nb-Ti Steel	0.102	0.03	1.11	0.02	0.017	0.037	-	0.026	0.018	76
V-Nb-Ti Steel	0.090	0.21	1.20	0.02	0.011	0.031	0.045	0.040	0.023	60

* - Leco CS600 Analyzer, ** - TC 500 N/O Analyzer

The V steel had a somewhat higher carbon content than the Nb-Ti and V-Nb-Ti steel with 0.06%V and a residual Ti of 0.002%. The Nb-Ti steel had a higher Mn and S content than the V steel and contained 0.026% Nb and 0.018% Ti. The V-Nb-Ti steel had similar Mn and S levels to the Nb-Ti steel, but contained 0.023% Ti and 0.04% Nb and V. All three steels studied had nitrogen levels that ranged from 42 to 76 ppm.

2.2. EXPERIMENTAL DETERMINATION OF HOT DUCTILITY OF STEELS

Several different experimental techniques are being applied in this research for measuring the hot ductility of steels in the temperature range associated with transverse crack formation during continuous casting. The methods being reported here involve the reheating of as-cast slab samples to re-dissolve the microalloy precipitates (where possible) and then cooling to the desired test temperature and applying a controlled displacement at a controlled strain rate while measuring the load to failure. A test procedure that directly tests the as-solidified and cooled steel is planned in future work. In this paper, the hot ductility of commercially cast V, Nb-Ti and V-Nb-Ti steels has been investigated using two experimental methods: (1) tensile testing utilizing a servo-hydraulic load frame with a resistance furnace and (2) custom built thermomechanical testing apparatus that uses rapid

joule heating with a electro-mechanically controlled tensioning system. Figure 2 (a) shows a schematic temperature profile used for the hot tensile tests, which were performed using the servo-hydraulic load frame with the resistance furnace. The samples were prepared according to the ASTM E8-16a standard. Small round sub-size specimens were used. The thermomechanical cycle used in this study was as follows: the specimens were heated at $1^{\circ}\text{C}/\text{s}$ to 1200°C in argon atmosphere using a resistance furnace and then were held for 2 min for dissolution of precipitates. Subsequently, the samples were cooled to the test temperature in the range of $650\text{-}900^{\circ}\text{C}$ at a cooling rate of $1^{\circ}\text{C}/\text{s}$. Samples were held at the test temperature for 2 min. They were strained to failure at a constant strain rate of $3 \times 10^{-3}/\text{s}$ which was selected to approximately match the strain rate during the straightening operation of the continuous casting process. After failure, the samples were allowed to cool to room temperature.

The rapid joule heating system uses a mechanical loading assembly with an inline drive (10 kN max), a load cell (0.5N resolution) and laser displacement sensor ($\pm 1 \mu\text{m}$ resolution). A 400 amp DC joule heater is used to heat the samples and an IR camera (1 mm spot size, $\pm 1^{\circ}\text{C}$) monitors the temperature of the sample. The system uses LabView software to monitor and control tests and temperature cycles by appropriate feedback control. Figure 2 (b) shows a schematic temperature profile for the hot tensile tests using joule heating. The samples are flat specimens, typically 96×23 mm in cross section. The samples were heated at $5^{\circ}\text{C}/\text{s}$ up to 1200°C using a DC joule heater and then soaked for 2 min. The sample is placed inside a chamber with a continuous flow of argon throughout the test cycle to avoid oxidation of the samples. The samples are cooled to the test temperature in the range of $650\text{-}900^{\circ}\text{C}$ at a cooling rate of $4^{\circ}\text{C}/\text{s}$. The samples were soaked

in the test temperature for 2 min and then strained to failure using a constant strain rate of $3 \times 10^{-3}/s$ and after failure the samples were cooled rapidly to the room temperature. Both test methods employ the same testing parameters except for the heating and cooling rates differences. The effect of the different thermal cycles from the two testing methods, particularly the effects of fast vs. slow heating and cooling, on the hot ductility results are presented and discussed.

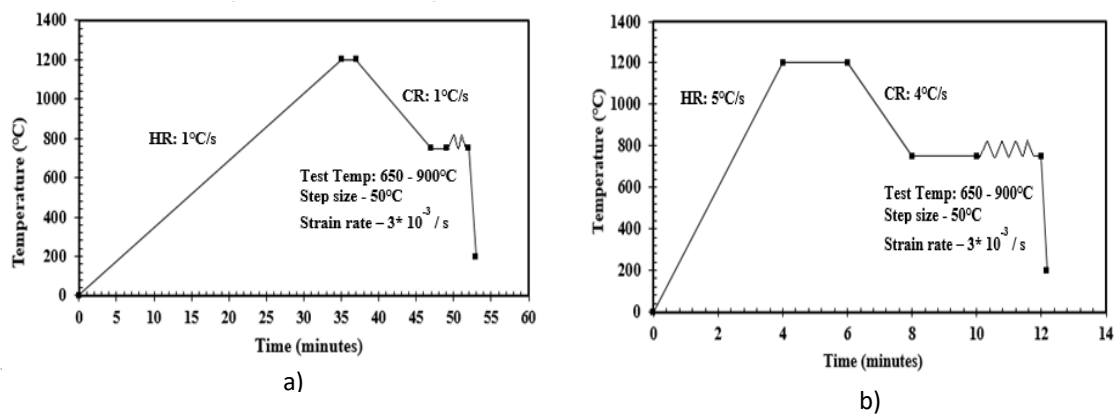


Figure 2: Schematic diagrams showing the thermal cycles studied. (a) Servo-hydraulic load frame with a resistance furnace (b) Joule resistive heating.

2.3. THERMODYNAMIC MODELING AND METALLOGRAPHIC ANALYSES

Thermodynamic modeling was performed using FactSage v7.2 to better understand the sequence of phase transformations and precipitation that is expected to occur during solidification and cooling. A prior austenite grain size analysis was also performed to investigate the effect of this variable on the hot ductility of the steels. Samples for grain size analysis were sectioned perpendicular to the columnar grain structure and they were soaked at different times in the γ - α region based on the predicted ferrite-austenite transformation temperature and then rapidly quenched to facilitate austenite grain size

measurement. Grain size measurements were performed using the linear intercept method of optical microscopy.

3. RESULTS AND DISCUSSION

3.1. STRESS – STRAIN BEHAVIOR AND HOT DUCTILITY CURVES OF THE V MICROALLOY STEEL

Figure 3 a) shows the engineering stress – engineering strain curves of the vanadium, V, microalloy steel obtained from the servo - hydraulic load frame (MTS load frame) equipped with electric furnace and Figure 3 b) shows the engineering stress – engineering strain curves from the joule heating experiment. As expected, in both tests the strength decreases with an increase in temperature. There is an abrupt drop in the stress-strain curves from MTS load frame observed at temperatures of 850°C and 900°C (indicated by arrows) which may be evidence of dynamic recrystallization. After 850°C, the curve from both test methods displayed increasing ductility as indicated by larger plastic deformation seen in the stress-strain curve.

Figure 4 a) shows the %RA as function of temperature for V microalloy steels from both test methods. The % RA varied from 37% - 97% for the temperatures from 650°C - 900°C and a ductility trough was obtained from the MTS load frame. In joule resistive heating, the %RA varied from 42% - 97%. A minimum drop in ductility was observed from temperature ranges of 700°C - 800 °C.

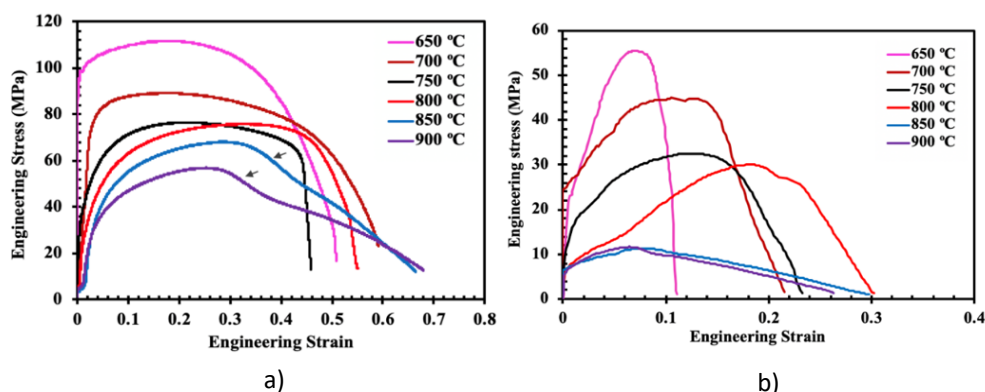


Figure 3: Engineering stress- engineering strain curves of vanadium microalloy steel at different temperatures a) MTS load frame b) Joule resistive heating.

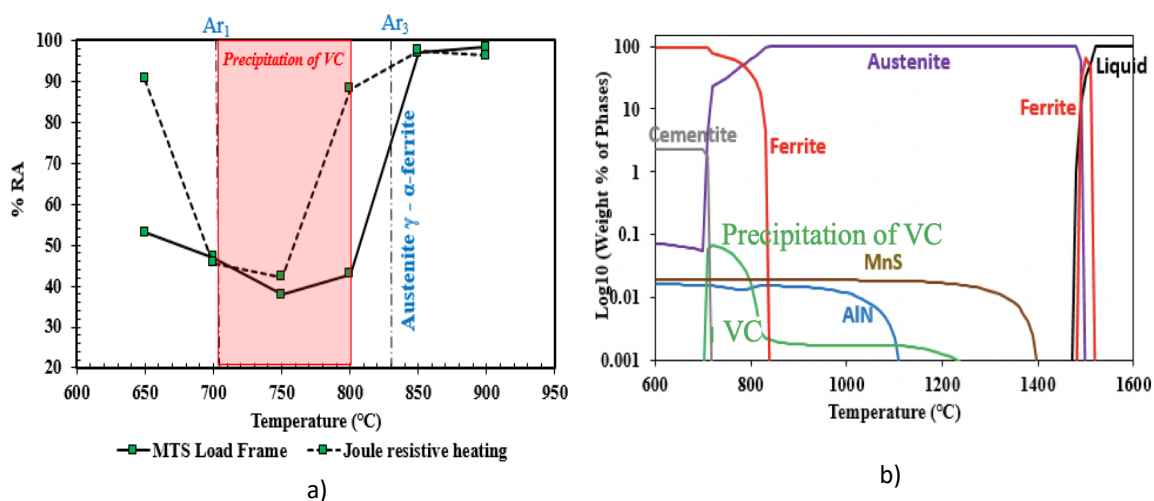


Figure 4: a) Hot ductility curves of vanadium microalloy steel from both test methods b) Thermodynamic modeling showing precipitation of vanadium carbides from 700°C - 800°C.

Comparing ductility troughs from two test methods, the minimum ductility for both methods was observed at 750°C with an %RA of around 37% for the MTS load frame test and 42% for the Joule resistive heating test. The 800°C - 700°C temperature range where low ductility is observed closely match the temperature for the formation of ferrite and

corresponding increased precipitation of vanadium carbide in ferrite predicted by thermodynamic modeling, as shown in Figure 4 b). The ductility drop of the steel is likely related to the intergranular failure along the austenite grain boundaries due to the formation of thin films of ferrite below A_{r3} that allows strain concentrations to build up along the austenite grain boundaries, promoting void formation. Carbide precipitates also form in the ferrite, further reducing the ductility of the steel.

3.2. STRESS – STRAIN BEHAVIOR AND HOT DUCTILITY CURVES OF NB - TI MICROALLOY STEEL

Figure 5 shows the engineering stress – engineering strain curves obtained from a) the MTS load frame and b) joule resistive heating tests. Both the test methods showed that with increase in temperature there was a drop in the strength of the steels as expected. The % RA varied from 55% - 98% for temperature ranges from 650°C - 900°C in MTS load frame test while in joule resistive heating test, the % RA varied from 59%-98% as shown in Figure 6(a). Both the test methods showed a minimum in ductility at 800°C with %RA around 55% (MTS load frame) and 59% (Joule resistive heating) which again was close to the austenite to ferrite transformation temperature predicted by thermodynamic modeling.

Figure 6 (b) shows the equilibrium solidification and cooling predictions for this alloy. Equilibrium modeling showed that TiN precipitates form just below the liquidus and during solidification, starting from 1490°C. On the other hand, (Nb,Ti)(C,N) was shown to precipitate in the temperature range from 1100°C-700°C and AlN precipitation was predicted below 980°C as shown in Figure 8(b). The temperature at which the ductility starts to drop corresponds closely with the A_{r3} transformation temperature of the alloy.

The predicted formation of (Nb,Ti)(C,N) at higher temperatures, shown in Figure 6(a), does not appear to negatively impact the ductility of the alloy.

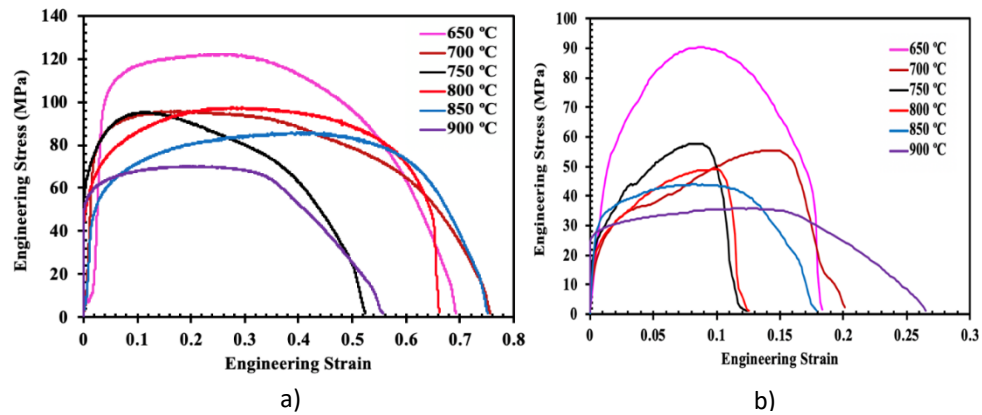


Figure 5: Engineering stress- engineering strain curves of Nb -Ti microalloy steel at different temperatures a) MTS load frame b) Joule resistive heating.

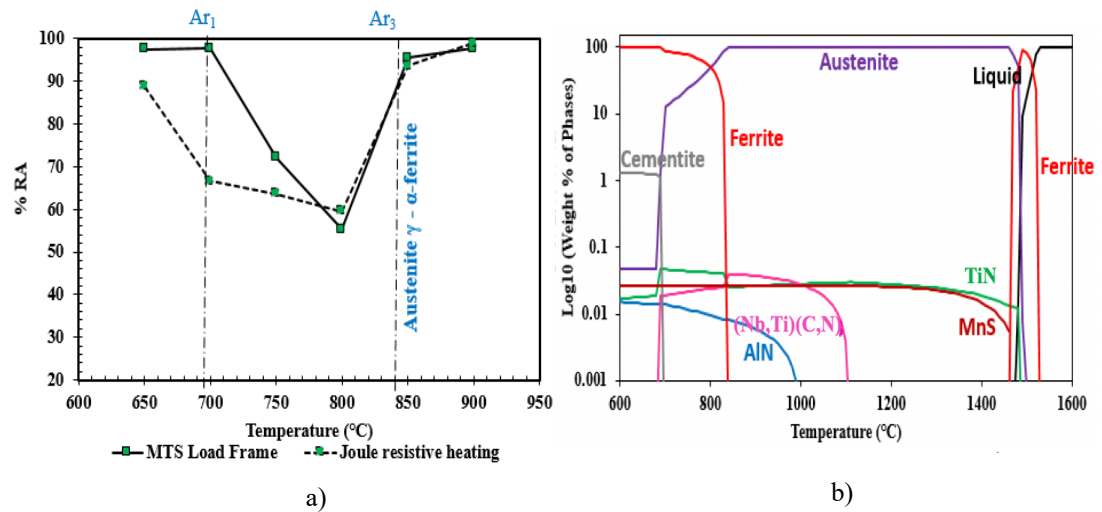


Figure 6: a) Hot ductility curves of Nb-Ti microalloy steel from both test methods b) Thermodynamic modeling showing precipitation of TiN from the liquid just after the liquidus and (Nb,Ti)(C,N) formation after solidification from 700 -1100 °C.

3.3. STRESS – STRAIN BEHAVIOR AND HOT DUCTILITY CURVES OF V-NB -TI MICROALLOY STEEL

Figure 7 shows the engineering stress – engineering strain curves obtained from a) MTS load frame test and b) joule resistive heating test. Both the test methods showed that with increase in temperature there was a drop in the strength of the steels. The % RA varied from 60% - 98% for temperature ranges from 650°C - 900°C in MTS load frame while in joule resistive heating, the % RA varied from 69%-95% as shown in Figure 8(a). The ductility drop was observed at 800°C with %RA around 60% in MTS load frame while in joule resistive heating, ductility drop was observed at 750°C with % RA around 69%.

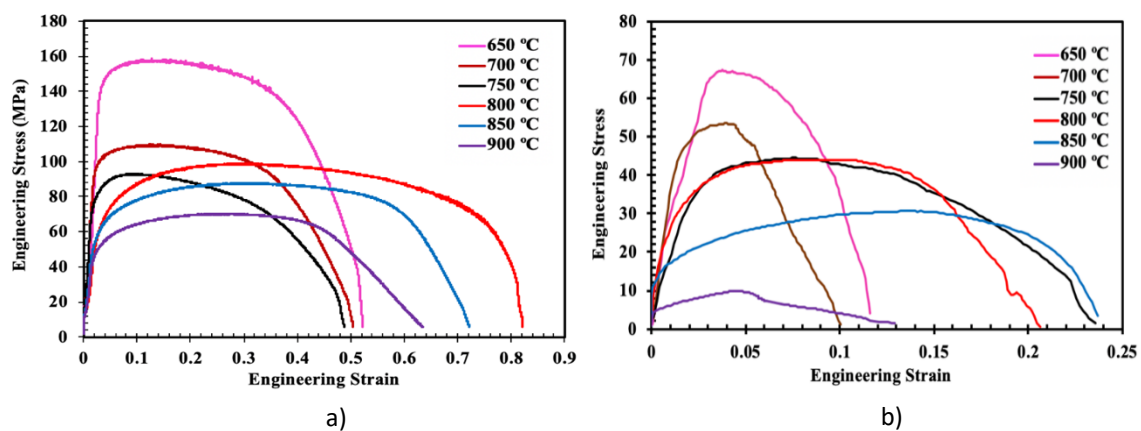


Figure 7: Engineering stress- engineering strain curves of V- Nb -Ti microalloy steel at different temperatures a) MTS load frame b) Joule resistive heating.

Figure 8 (b) shows the equilibrium solidification and cooling predictions for this alloy. Equilibrium modeling predicts that TiN precipitates below the liquidus temperature during solidification, starting below 1500°C. The addition of Ti appears to result in an improvement of the hot ductility of this steel under the conditions of this test. Since the steels were solution treated at 1200°C, TiN or Ti rich precipitates which form from the

liquidus are not completely dissolved at the solution treating temperatures. However, their presence does not appear to negatively impact the hot ductility of the steel at high temperatures. The ductility drop, as observed between 750°C-800°C is closer to the Ar₃ transformation temperature of the alloy.

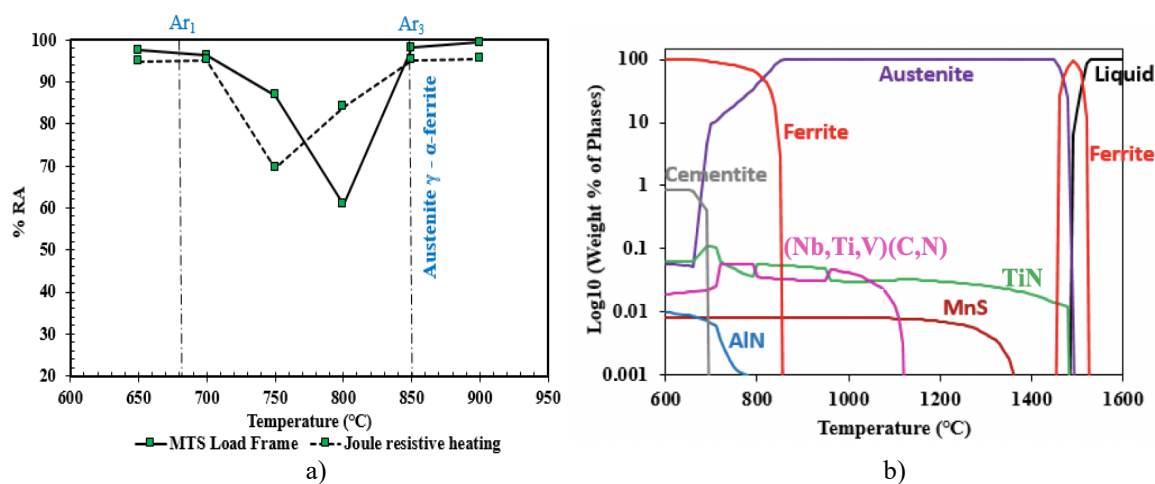


Figure 8: a) Hot ductility curves of V-Nb-Ti microalloy steel from both test methods b) Thermodynamic modeling showing precipitation of TiN along with (Nb,Ti,V)(C,N) formation after solidification from 600 -1100 °C.

TiN precipitates may pin the austenite grain boundaries, possibly preventing grain growth and improving ductility of the alloy comparing the other two steels [20]. However, TiN can also reduce the availability of nitrogen to form precipitates of AlN or Nb(C,N), which can be beneficial to the hot ductility of steel [19]. The reader should be reminded that the two test methods employed in these tests rely on the re-solutioning of precipitates during the sample soaking period prior to cooling to the test temperature. This treatment path cannot re-dissolve all of the expected depositions, such as TiN and MnS, which can form at temperatures above our soaking temperature capabilities. In the proposed future

in-situ bend tests, we hope to be able overcome this limitation and evaluate the importance of this difference on hot ductility test results.

3.4. WIDTH OF HOT DUCTILITY TROUGH

The position of the low temperature end of the ductility trough is closely related to the carbon content of the alloy. Among the three steels examined, V microalloy steel had the highest carbon content of 0.175 wt. %. They are increasing the carbon level of the alloy shifts the $\gamma \rightarrow \alpha$ phase transformation temperature (A_{r3}) to lower temperatures. At still lower temperatures, all three steels exhibited higher ductility as the ferrite volume fraction increased. Mintz, et. al. reported that the main reason for the ductility improvement is a more even distribution of strain with increasing volume fractions of ferrite [15, 21]. At temperatures greater than 850°C, the three steels all showed an increase in ductility, with %RA's of around 98% in austenite. At the high temperature end of the ductility trough, the increased cooling rate used with the joule heating experiment also tended to measure a lower temperature for the top side of the ductility trough compared to the slower cooling rate MTS frame test. This difference is likely because that cooling rate has on temperature that ferrite nucleates. Ferrite nucleation occurs at lower temperatures as cooling rate increases.

3.5. DEPTH OF HOT DUCTILITY TROUGH

The hot ductility troughs from two testing methods for V microalloy steels are deeper and broader compared to other steels. This may be due to the formation of vanadium carbide precipitates in the ferrite films that form at 700-850°C as predicted by the

thermodynamic modeling as shown in Figure 4(b) or the higher carbon content of this steel. In the Nb-Ti steel, the trough from the MTS load frame is narrower than joule heating, which appears to be wider. The difference in the shape of the trough from the two methods is likely caused by the difference in cooling rates of the test methods. The joule heating test was operated at a higher cooling rate than MTS load frame. The trough of the V-Nb-Ti microalloy steels from both test methods are narrower and shallower compared to the other steels. This may be due to the formation of TiN precipitates which restricts grain growth and results in a finer grain size or from the scavenging of nitrogen. Metallographic and TEM analyses are planned in future work to investigate these observed differences in ductility.

3.6. AUSTENITE GRAIN SIZE

Comparing the three steels in this study, Figure 9, the V microalloyed steel had a substantially larger average prior austenite grain size (208 μm) than the Nb -Ti and V-Nb-Ti steels (36 μm and 28 μm , respectively). The Ti added grades both exhibited a finer austenite grain size than the V microalloyed steel. When the temperature of the sample is decreased below the A_{r3} temperature, the austenite grain boundaries become covered with thin films of ferrite and fine prior austenite grains. planned in future work to investigate the mechanisms of fracture for these steels. The ferrite distributes more uniformly, resulting in a more refined microstructure [18].

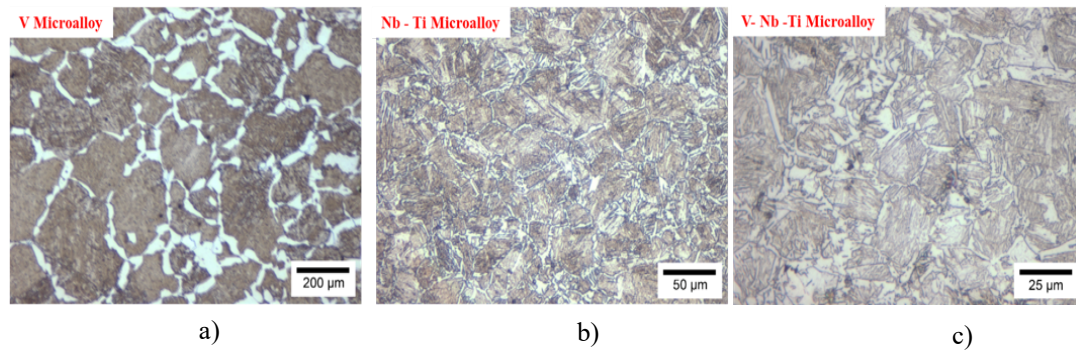


Figure 9: Prior austenite grain size analysis of as-cast a) V microalloy steel with an average grain size of $208\ \mu\text{m}$ b) Nb -Ti microalloy steel with an average grain size of $36\ \mu\text{m}$ and c) V-Nb-Ti microalloy with an average grain size of $28\ \mu\text{m}$. These steels were heat treated to form ferrite on the prior austenite grain boundaries to facilitate the austenite grain size measurements.

The V microalloyed steel has the coarsest grain size and also had the deepest and widest ductility trough along with the lowest %RA when compared to the other microalloyed steels. Steels with a finer the grain size are generally more resistant to crack propagation. With finer grain size, the crack's aspect ratio, which controls the stress concentration at the crack tip, is reduced, making it difficult for crack propagation [17]. Metallographic analysis and fractography investigations are.

4. CONCLUSION

Hot ductility curves were obtained using two high temperature test methods: (1) a tensile test utilizing a servo-hydraulic load frame with a resistance furnace and (2) a thermomechanical testing apparatus using rapid joule heating combined with an electro-mechanically controlled tensioning system. Both test methods showed similar low ductility trends, but the upper and lower edges of the ductility trough differed somewhat between

the two test methods. The differences are attributed to the two test methods' heating and cooling rate. The V micro alloyed steel slab sample had significantly lower ductility (40% RA) compared to the other two steels tested. The Nb-Ti and V-Nb-Ti microalloy steels displayed similar ductility minimums, and the temperature at which the minimum ductility was observed varied between 750-800°C. Both the Nb-Ti and V-Nb-Ti steels had improved ductility compared to V microalloy steels. V microalloy steel had the widest and deepest trough compared to other steels, but it also had the highest carbon content (0.17%C). The increased carbon shifts the ductility trough shifts to lower temperatures (750°C) due to the decrease in the $\gamma \rightarrow \alpha$ phase transformation temperature. Ductility loss in these steels may be largely controlled by the formation of thin films of ferrite at low temperatures, given that the measured low ductility temperature regions correlate well with the thermodynamically predicted $\gamma \rightarrow \alpha$ transformation temperatures. In future work, a test procedure that directly tests the as solidified and cooled steel is planned to examine the importance of high temperature precipitates, such as TiN.

ACKNOWLEDGEMENT

The authors would like to thank United States Steel Cooperation for providing as-cast slab samples for hot ductility studies. Additionally, the authors would also like to acknowledge undergraduate research assistant Aileen Martinez for her contribution on the sample preparation. This project was supported by Peaslee Steel Manufacturing Research Center (PSMRC) at Missouri University of Science and Technology (Missouri S&T),

thanks to all the faculties and industry mentoring committee of PSMRC for their help and guidance.

REFERENCES

1. H G Suzuki, S Nishimura, and S Yamaguchi, “Embrittlement of Steels Occurring in the Temperature Range from 1000-600 °C”, *Trans ISIJ*, Vol. 24, 1984, pp 169-174.
2. B Mintz, and J M Arrowsmith, “Hot ductility behavior of C-Mn-Nb-Al steels and its relationship to crack propagation during the straightening of continuously cast strand”, *Metals Technology*, Vol. 6, 1979, pp 24-32.
3. M. A. Matveev, “Causes of High Temperature Ductility Trough of Microalloyed Steels”, *Trans Indian Inst Met*, Vol. 70, No.8, 2017, pp 2193-2204.
4. K R Carpenter, R Dippenaar and C R Killmore, “Hot Ductility of Nb- and Ti-Bearing Microalloyed Steels and the Influence of Thermal History”, *Metallurgical and Materials Transactions A*, Vol. 40A, 2009, pp 573 – 580.
5. T Gladman: *The Physical Metallurgy of Microalloyed Steels*, Maney, London, 2002.
6. M P Rao, V S Sarma and S Sankaran, “Development of high strength and ductile ultrafine grained dual phase steel with nano sized carbide precipitates in a V–Nb microalloyed steel”, *Materials Science & Engineering A*, Vol. 568, 2013, pp 171-75.
7. E Peroloma ,I Timokina, K Russell and M Miller, “Characterization of clusters and ultrafine precipitates in Nb-containing C–Mn–Si steels”, *Scripta Materialia*, Vol.54, 2006, pp 471–476.
8. B Patrick and V Ludlow, “Development of Casting Practices to Minimise Transverse Cracking in Microalloyed Steels”, *Revue de Metallurgie*, Vol. 91, 1994, pp 1081-1089.
9. Yue Liu, Lin-Xiu Du, Hong Yan Wu and R Devesh Kumar Misra, “Hot ductility and Fracture Phenomena of Low-Carbon V-N-Cr Microalloyed Steels”, *Steel Research International*, Vol. 91, 2020, pp 1- 11.
10. J R Wilcox and R W K Honeycombe, “Hot Ductility of Nb and Al Microalloyed Steels Following High Temperature Solution Treatment”, *Metals Technology*, Vol. 11, 1984, pp 217-225.

11. C Ouchi and K Matsumoto, "Hot Ductility in Nb-bearing High Strength Low-alloy Steels", *Trans ISIJ*, Vol. 22, 1982, pp 181-189.
12. L Zhen, Z Hongtao, W Baorong, "Effect of Niobium on Hot Ductility of Low C-Mn Steel Under continuous Casting Simulation Conditions", *Steel Research*, Vol. 61, 1990, pp 620- 623.
13. P Sricharoenchai, C Nagasaki and J Kihara, "Hot Ductility of High Purity Steels Containing Niobium", *ISIJ International*, Vol. 32, 1992, pp 1102-1109.
14. B Mintz, "Hot Ductility of Steels and its Relationship to the Problem of Transverse cracking during continuous Casting", *International Materials Review*, Vol. 36, No.5, 1991, pp 187-217.
15. B Mintz, "The Influence of Composition on the Hot Ductility of Steels and to the Problem of Transverse Cracking" *ISIJ International*, Vol.39, 1999, pp 833-855.
16. B Mintz and J M Arrowsmith, "Influence of Microalloying Additions on Hot Ductility of Steels", in "Hot Working and Forming Processes", *The Metals Society*, 1980, pp 99-103.
17. D N Crowther and B Mintz, "Influence of grain size on hot ductility of plain C-Mn steels", *Materials Science and Technology*, Vol. 2 No. 9, 1986, pp 951-955.
18. U H Lee, T E park, K S Son, M S Kang, Y M Won, C H Yim, S K Lee, I Kim and D Kim, "Assessment of hot ductility with various thermal histories as an alternative method of in situ solidification, *ISIJ International*, Vol. 50, No. 4, pp.540-545.
19. K R Carpenter, "The influence of microalloying elements on the hot ductility of thin slab cast steel", *University of Wollonglong*, PhD Thesis, 2004
20. R Abushosha, O Comineli and B Mintz, "Influence of Ti on hot ductility of C-Mn-Al steels", *Material Science and Technology*, Vol.15, 1999, pp 278 – 286.
21. A Cowley, R Abushosha and B Mintz, "The influence of Ar₃ and Ae₃ temperatures on the hot ductility of steels", *Material Science and Technology*, Vol. 15, 1998, pp 1145-1153.

II. HOT DUCTILITY BEHAVIOR OF V-N MICROALLOYED STEELS

Madhuri Varadarajan, Laura N. Bartlett, Ronald J. O'Malley, Simon N. Lekakh, Mario F. Buchely

Peaslee Steel Manufacturing Research Center, Missouri University of Science and Technology,

1400 North Bishop Avenue, Missouri, United States, 65409-0340

Phone: 573-341-4711

Email: mvhb5@mst.edu

ABSTRACT

The hot ductility of commercially cast 0.07 wt. % C steels containing 0.04 and 0.09 wt. % V was investigated using two experimental methods. This included utilizing a load frame equipped with resistance heating and a thermomechanical simulator. The ductility loss in the low vanadium steel was observed from 700-850°C, below Ar_3 temperature. In comparison, ductility loss for the 0.09 wt.% V alloy occurred above the Ar_3 temperature. Both methods showed similarity in the position of the low ductility trough. The depth of the trough was related to heating/cooling rate during the tensile test. Factors influencing steel ductility are discussed.

1. INTRODUCTION

Micro alloy steels account for a significant part to the annual world steel production of 162.9 million tones [1]. They have yield strength values in the range of 350 – 800 MPa

[2], with a potential to exceed 1000 MPa [3], elongations of 22-25% and toughness of 250-300 J [2]. This advancement was made possible by the combination of improved steelmaking, microalloying technology, and better rolling and cooling practices [4]. Hot rolled microalloy steels are used in many applications such as construction, oil and gas extraction, pressure vessels and transportation where stringent surface quality is required. Therefore, transverse cracking is an important problem in continuous cast steels. Such defects are located at surface or near surface in the cast slab and form perpendicular to the casting direction. These cracks often originate in the straightening region of the caster on the top surface of the slab when unbending occurs at temperatures of 700-1000°C where the steel is known to exhibit low ductility [5]. This “ductility trough” can be observed in hot tensile tests by measuring the % reduction in area (%RA) at specimen failure at various temperatures.

One of the causes for low ductility in this temperature range is due to steels containing microalloying elements of Nb, V and Ti that form carbides, nitrides, and complex carbonitride precipitates. Such precipitates, in combination with ferrite films formed during cooling on grain boundaries, dramatically decrease steel ductility. [6,7]. To avoid increase in production costs and yield loss on finished products, it is important to understand the effect of multi-component microalloy additions of Nb, Ti and V on the steel's susceptibility to transverse cracking.

Among the strong nitride or carbide forming microalloying elements, both vanadium and niobium have been reported to significantly affect transverse crack sensitivity. In particular, vanadium micro alloy steels are reported to be more sensitive to nitrogen concentration than Nb micro alloy steels, which exhibits different carbonitride

thermodynamic stability and precipitation kinetics[8,9]. Vanadium steels with high nitrogen levels (90-120 ppm), have been reported to cause transverse cracking; however, below 50 ppm, transverse cracking was not observed [10]. High nitrogen levels favor the precipitation of V(C,N) or VN that can significantly reduce the ductility of steels. The combination of high vanadium levels (>0.07%) and high nitrogen (90-120 ppm) has also been reported to be highly susceptible to transverse cracking [11]. However, vanadium levels less than 0.07% were reported to inhibit the drop in ductility. At lower controlled nitrogen contents, vanadium steels are reported to have better ductility than Nb steels because the VN particles are less detrimental to hot ductility than fine Nb(C,N) precipitates that forms at the austenite grain boundaries that prevent dynamic recrystallization. The former precipitation encourages grain boundary sliding leading to low ductility intergranular failure [12].

For steels that are solutionized during reheating prior to hot deformation, Nb can be more effective than V at reducing grain growth to improve ductility, but it can also extend the ductility trough to higher temperatures than vanadium. It has also been noted that the vanadium precipitates in both a more coarse and random manner than Nb precipitates, which again favors higher ductility [13]. Therefore, it is important to understand the effect of varying levels of vanadium and nitrogen on the hot ductility of industrial continuously cast microalloy steels and its susceptibility to transverse cracking which was the objective of this study.

In this paper, hot ductility of two commercial as-cast low carbon (0.073 wt.% and 0.086 wt.% C) steels was investigated, containing two different levels of V: 0.04 wt.% and 0.09 wt.% and nitrogen in the order of 100 ppm. Hot ductility was determined by

measuring the reduction of area in representative tensile samples using two different experimental tensile tests: i) An MTS frame equipped with a resistance furnace, and ii) a thermomechanical simulator with rapid Joule heating. The hot ductility was evaluated in 650-900°C temperature range, applying a constant strain rate of $3 \times 10^{-3}/s$.

2. EXPERIMENTAL PROCEDURE

The chemical compositions of commercially produced steels used in this study are listed in Table 1. Optical emission arc spectroscopy was used to determine the wt. % of elements present in the steel samples. Leco combustion and inert gas fusion analysis was used to determine the composition of carbon, sulfur, and nitrogen levels. Two types of steel samples were analyzed: i) a beam blank sample that was silicon killed steel containing 0.07 wt. % C and 0.04 wt. % V (designated as “Low V”) and (ii) an as-cast slab that was aluminum-silicon deoxidized and contained 0.09 wt. % C and 0.09 wt. % V (designated as “High V”). Both steels had nitrogen contents, varying between 108 and 116 ppm.

Table 1: Chemistry of the samples as determined by optical emission arc spectroscopy and Leco combustion and inert gas fusion analysis (wt. %).

Steel	C*	Mn	Si	P	S*	Al	V	N**	Sample type
Low V	0.07	1.20	0.25	0.011	0.029	0.001	0.04	108 ppm	Beam Blank
High V	0.09	1.32	0.30	0.018	0.003	0.03	0.09	116 ppm	As-cast slab

* - Leco CS600 Analyzer, ** - TC 500 N/O Analyzer

The samples for hot tensile testing were cut from 203mm thick, as-cast slab and 345mm long beam blank samples from the locations shown in Figure 1. The hot ductility samples were prepared so that the tensile specimen orientation was perpendicular to the columnar grain structure of the steel samples to ensure that testing was performed perpendicular to the direction of solidification. Care was taken when cutting of the samples to avoid narrow face edges of the as-cast slab, centerline segregation and internal crack sites. The heat affected regions from the oxy-acetylene torch cuts were avoided during preparation of the tensile samples.

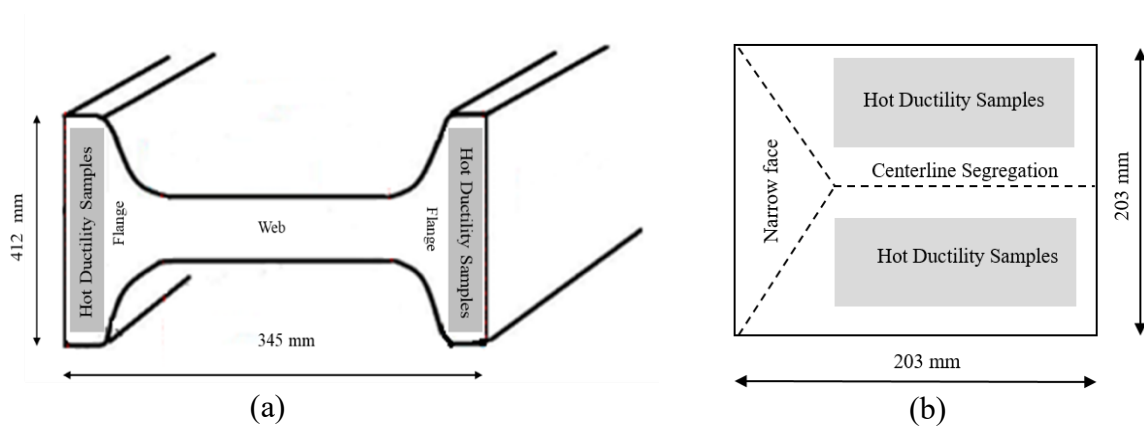


Figure 1: Position of hot ductility samples taken from: (a) beam – blank and (b) as-cast steel slab.

The temperatures and strain rates applied in this research to measure the hot ductility were chosen based on known ranges for transverse crack formation during continuous casting. Two experimental techniques with different preheating and cooling cycles were performed during the tensile tests. Both methods involved the reheating of the samples to re-dissolve the microalloy precipitates (where possible) and then cooling to the desired test temperature and applying a controlled displacement at a controlled strain rate

while measuring the load to failure. Two experimental methods used were: (1) a tensile testing apparatus utilizing a MTS servo-hydraulic load frame with a slow heating/cooling resistance furnace with SiC elements (referred in this article to as the “Slow cooling test”) and (2) a custom built thermomechanical testing apparatus that employs rapid Joule heating with an electro-mechanically controlled tensioning system (referred to as the “Fast cooling test”).

Figure 2(a) shows a schematic temperature profile for the slow cooling test. Small round (diameter 9 mm), sub-size specimens with a gauge length of 25 mm were prepared according to the ASTM E8-16a standard were used in slow cooling tests. For this test, the thermomechanical cycle was as follows: the specimens were heated at 1°C/s to 1200°C in argon atmosphere and then were held for 2 min for dissolution of precipitates. Subsequently, the samples were cooled to the test temperature in the range of 650-900°C at a cooling rate of 1°C/s. Samples were held at the test temperature for 2 min. They were then strained to failure at a constant strain rate of 3×10^{-3} /s which was selected to approximately match the strain rate during the straightening operation of the continuous casting process. After failure, the samples were allowed to cool to room temperature inside furnace.

The fast cooling test utilized a Joule heating system with an attached mechanical loading assembly for tensile testing of a flat specimen using an inline drive (10 kN max), a load cell (0.5N resolution) and laser displacement sensor ($\pm 1 \mu\text{m}$ resolution).

For this test, the sample is placed inside a chamber with a continuous flow of argon throughout the test cycle to avoid oxidation of the samples. The samples are flat specimens, typically 96 x 23 mm in cross section. A 400-amp DC joule heater was used to heat the

samples and a pyrometer (1 mm spot size, ± 1 °C) monitored the temperature of the sample. The system employed LabVIEW software to monitor and control the test and the temperature profile using feedback control. Figure 2 (b) shows a schematic temperature profile for the fast hot tensile test using Joule heating. The samples were heated at $5^{\circ}\text{C}/\text{s}$ up to 1200°C and then soaked for 2 min. The samples were then cooled to the test temperature in the range of $650\text{-}900^{\circ}\text{C}$ at a cooling rate of $4^{\circ}\text{C}/\text{s}$. The samples were soaked in the test temperature for 2 min and then strained to failure using a constant strain rate of $3 \times 10^{-3}/\text{s}$. After failure, the sample was cooled rapidly to the room temperature. Both test methods employ the same strain rate and testing temperatures but employed different heating and cooling rates.

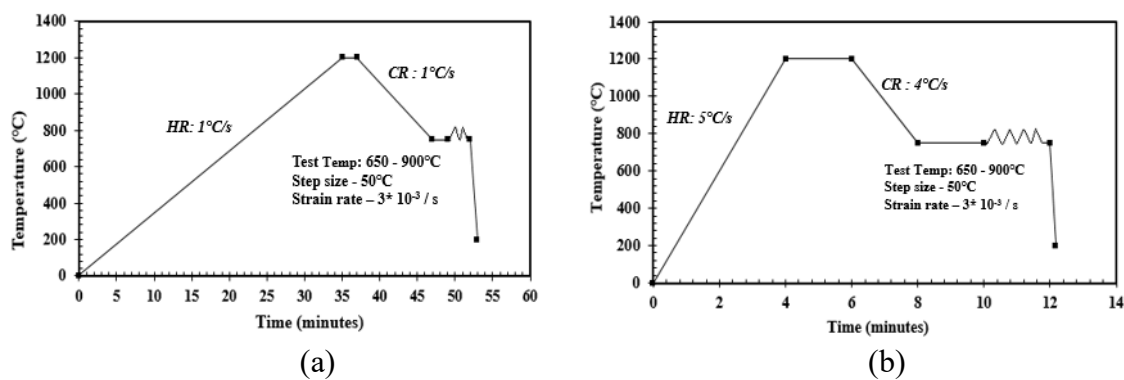


Figure 2: Schematic diagrams showing the thermal cycles studied: (a) slow cycle with servo-hydraulic load frame equipped with SiC furnace and (b) fast cycle using Joule resistive device.

Representative fractured surface samples from two test methods were examined using a scanning electron microscope (TESCAN-VEGA). Sections parallel to the tensile axis were prepared for optical metallography using standard metallographic techniques in order to better understand microstructure/mechanical property relationships and the origin

of failure during testing. Thermodynamic modeling was performed using FactSage v7.2 with FactPS, FToxid, FTmisc and FSstel databases to understand the phase transformation and precipitation sequence for the two steels during solidification and cooling.

3. RESULTS AND DISCUSSIONS

The calculated equilibrium phase diagrams for the low V (Figure 3) and high V (Figure 4) steels show the predicted temperature ranges for stability of liquid, austenite, ferrite, and various secondary phases. Both steels exhibited peritectic solidification behavior. Figure 3(a) shows the equilibrium transformation and precipitation formed upon cooling for the low V steel, where the temperature at which the austenite transforms to ferrite (A_{r3}) was around 840°C and the ferrite completion temperature was 650°C. The major vanadium precipitate bearing phases are VN stable below 1290°C and V(C,N) below 749°C. The transitional composition of vanadium phases is shown in Figure 3(b).

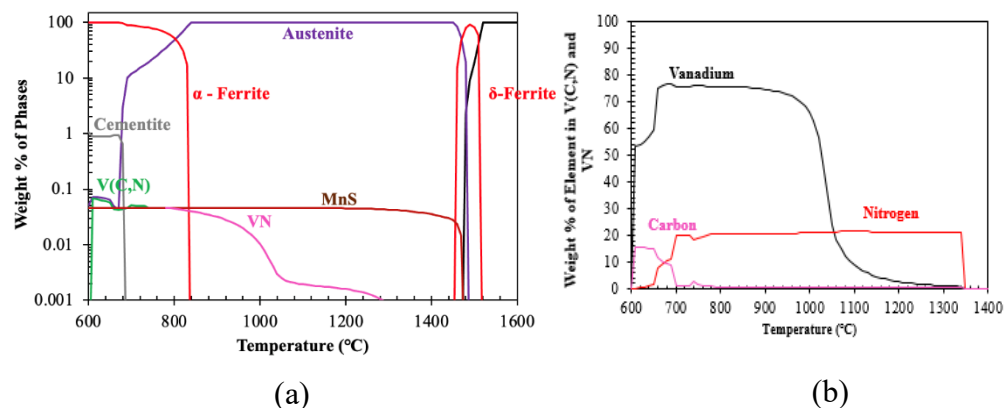


Figure 3: Thermodynamic modeling of equilibrium phase transformations during cooling of the low V steel: (a) phase diagram and (b) distribution of elements in precipitated V(C,N) and VN phases.

In the high V steel, the temperature at which the austenite transforms to ferrite (Ar3) was around 853°C and the ferrite completion temperature was 610°C. The precipitated phases in high V steel included MnS, AlN, VN and V(C,N). The AlN precipitation could be seen below 1140°C, but because the AlN precipitation may be sluggish during transformation and therefore may not be present in the studied steel. Accordingly, a higher level of aluminum (> 0.03wt%.) and nitrogen (90-120 ppm) may be required to allow AlN precipitation which could reduce ductility [14]. MnS is shown to be stable below 1400°C, while in the low V steel, MnS is stable at 1480°C as shown in Figure 3 (a). This is because of the higher sulfur content in the low V steel, which results in roughly five times the amount of MnS. The VN precipitated at 1090°C with volume fraction increase during cooling and subsequent complex V(C,N) could be precipitated at lower temperature. Figure 4(b) shows the distribution of elements between VN and V(C,N) phases.

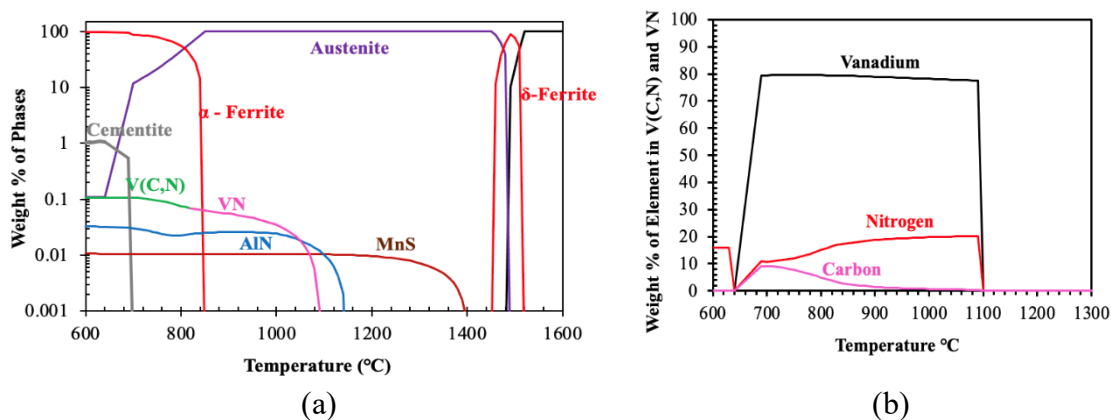


Figure 4: Thermodynamic modeling of equilibrium phase transformations during cooling of the high V steel: (a) phase diagram and (b) distribution of elements in precipitated V(C,N) and VN phases.

3.1. STRESS – STRAIN BEHAVIOR AND HOT DUCTILITY CURVES OF LOW V STEEL

The effect of deformation temperature on the engineering stress–strain curves of the low V steel was shown in Figure 5(a) for slow cooling and Figure 5(b) for fast cooling. For the slow cooling rate, the strength level at 850°C was observed to be higher than at 800°C. Similar behavior is observed in the fast-cooling test, where the strength level at 800°C was higher than at 750°C. This phenomenon could be due to dynamic strain aging caused by the interactions between the solute atoms of carbon and nitrogen with the dislocations. The movement of these solute atoms to the dislocations produces a solute rich atmosphere around the dislocations which increases the force necessary to cause the dislocation to slip. A greater force is required to deform the steel, increasing its strength, and lowering the ductility. An abrupt drop (indicated by arrows) is observed in the engineering stress – strain curves at a temperature 900°C for the fast cooling test, suggesting the onset of dynamic recrystallization. Below 850°C, the curve from fast cooling tests displayed increasing ductility.

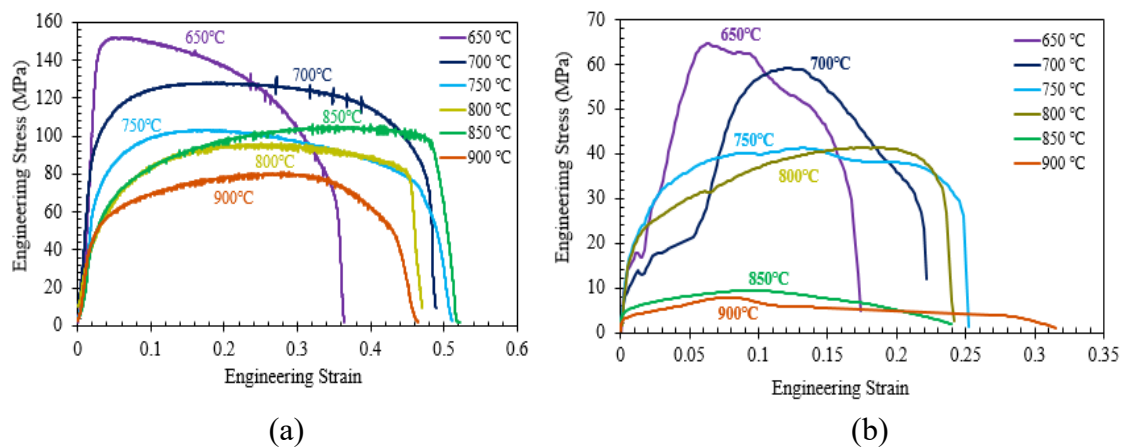


Figure 5: Engineering stress – strain curves of low V steel at different deformation temperatures for: (a) slow and (b) fast cooling.

Figure 6 shows the % reduction in area as a function of deformation temperatures for low V steel from both test methods. For the slow cooling test, the % RA varied from 46% to 66%, a ductility trough was also observed with minimum drop in ductility between 700°C - 850°C, and the lowest drop in ductility took place at 850°C. During fast cooling tests, the % RA varies from 40% to 98% and a minimum ductility drop was observed between 700°C - 800°C. In both test methods, the minimum ductility trough is observed just below the Ar_3 transformation temperature of the alloy.

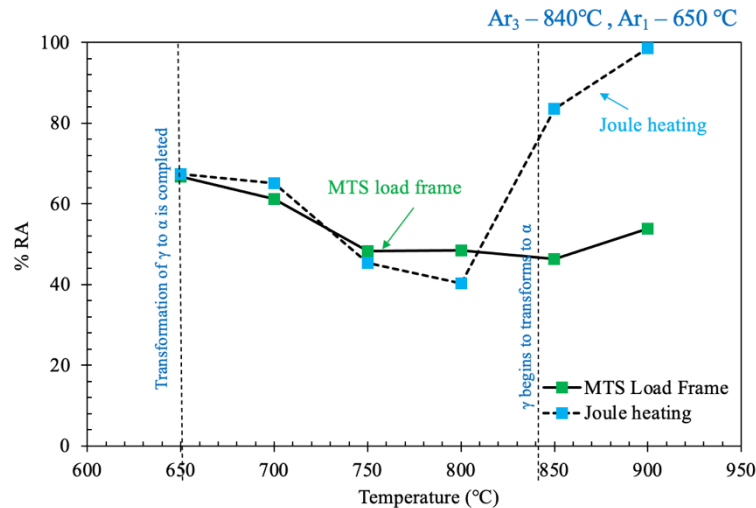


Figure 6: Hot ductility curves of low V steel from both test methods.

3.2. STRESS – STRAIN BEHAVIOR AND HOT DUCTILITY CURVES OF HIGH V STEEL

Figure 7(a) shows the effect of deformation temperature on the engineering stress – strain curves of the high V steel obtained using the servo hydraulic MTS load frame for the slow cooling test and Figure 7(b) shows the engineering stress – strain behavior obtained from the Joule fast cooling test. For the fast-cooling test, the strength decreased with increasing test temperature from 650°C-750°C. Also, during both the fast and slow

cooling tests, the strength levels at 850°C and 900°C were higher than at 800°C. This suggests that dynamic strain aging may also be occurring in the high V steel. An abrupt drop (indicated by arrow) is observed in the engineering stress – strain curves at a temperature of 1000°C for the slow cooling test and at a temperature of 950°C for the fast cooling test, suggesting the onset of dynamic recrystallization.

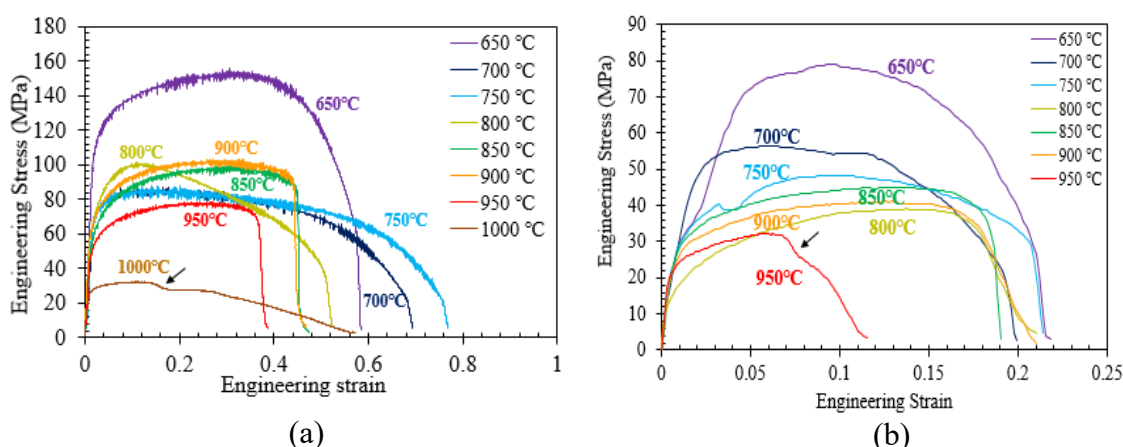


Figure 7: Engineering stress – strain curves of high V steel at (a) slow and (b) fast cooling tests.

Figure 8 shows the % reduction in area as a function of deformation temperatures for the high V steel obtained from both test methods. The % RA varied from 31% - 99% for the slow cooling test. A decrease in the ductility was observed at from 800°C - 950°C and the lowest ductility was observed in the fully austenitic region at 900°C. When the fast cooling method was used, the % RA varied from 35% - 86% and a decrease in ductility was observed at between 750°C and 900°C. The lowest ductility for the fast cooling test was observed at 850°C, which corresponds with the A_{r3} transformation temperature of the alloy. For the slow cooling test condition, the ductility minimum occurs above the

transformation temperature of the alloy, which suggests that some work hardening may be taking place in the austenitic region, increasing strength and lowering ductility. In fast cooling test, the ductility is lowest in a two-phase region of ferrite and austenite. This may be due to the differences in the cooling cycles between the test methods and the temperature range from 850°C-750°C indicates the formation of ferrite films and the possible VN or V(C,N) precipitation predicted by FactSage leading to intergranular failure along the austenite grain boundaries.

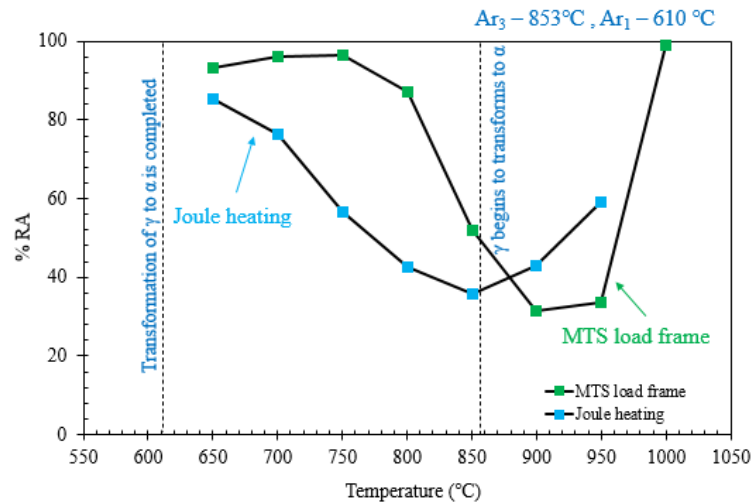


Figure 8: Hot ductility curves of high V steel obtained from both test methods.

3.3. FRACTOGRAPHY OF FRACTURED SURFACES

3.3.1. Low V Steel. The fracture surfaces for slow cooling rate test method at deformation temperatures of 850°C and 900°C are shown Figure 9. The deformation temperature at 850°C exhibited the lowest ductility of 46% RA. The fracture surface is entirely ductile, with micro void coalescence as shown in Figure 9(a,b). These micro voids nucleate at strain discontinuity such as MnS inclusions or second phase particles such as

VN. The fracture surface for the deformation temperature at 900°C is entirely ductile with a large number of small dimple like features as shown in Figure 9(c,d). The large number of small dimples are present where there are a large number of nucleation sites and the adjacent micro voids coalesce, limiting the size of the dimples. The small ductile dimples lead to higher ductility at 900°C.

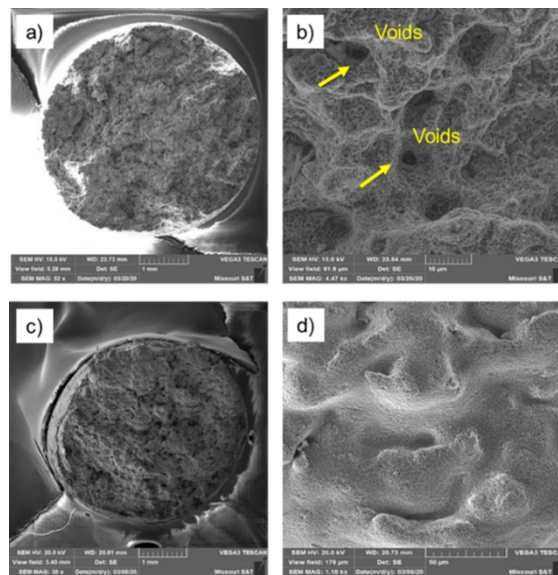


Figure 9: Fracture surfaces of low V steel tested at slow cooling rate : (a, b) at 850°C and (c, d) at 900°C test temperatures.

Further observations are difficult for the slow cooling rate test conditions because the surface is covered with an oxide film. The fracture surfaces of low V steel after fast cooling and tested at 800°C is shown in Figure 10. For this test condition, oxidation of the fracture surface is minimal. The fracture surface at 800°C exhibits mixed mode intergranular failure along with ductile voiding as shown in Figure 10(a,b). The inclusions

or precipitates that adsorb at the grain boundaries promotes dimpled intergranular fracture leading to lower ductility at 800°C.

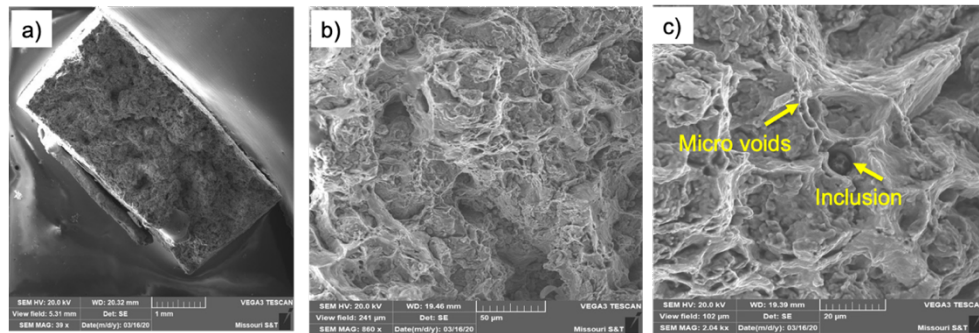


Figure 10: Mixed mode intergranular fracture with ductile voiding at 800°C in low V steel tested with high cooling rate: (a) low, (b) medium, and (c) at high magnification.

3.3.2. High V Steel. The fracture surfaces at deformation temperatures of 750°C and 900°C from slow cooling rate tests are shown in Figure 11.

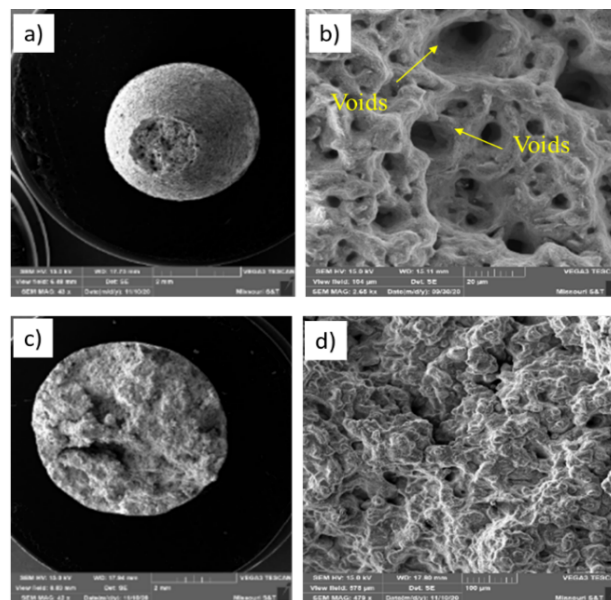


Figure 11: Fracture surfaces of high V steel tested at slow cooling rate: (a, b) at 750°C and (c, d) at 900 °C test temperatures.

Recovery of the ductility occurred at 750°C and the fracture surface consists predominantly of ductile micro voids as shown in Figure 11(a,b). But the fracture surface tested at 900°C exhibits a brittle behavior with intergranular fracture surfaces. However, it was covered with a layer of oxide film because of oxidation during the slow cooling test, Figure 11(c,d).

The fracture surfaces of high V steel at deformation temperatures of 650°C and 850°C from fast cooling tests is shown in Figure 12. The fracture surface at 650°C exhibits mixed mode intergranular fracture with ductile voiding. The distribution and location of potential micro void nucleation sites such as MnS, VN, V(C,N) or AlN precipitates can affect the fracture surface appearance. The non-uniform distribution of nucleating particles and the nucleation and growth of isolated micro voids in the loading cycle produce a fracture surface with various dimple sizes [15]. In some regions of the fracture surface, intergranular ductile rupture is also seen as shown in Figure 12(b).

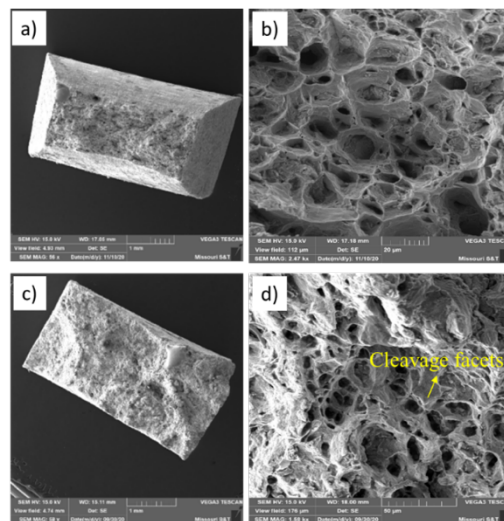


Figure 12: Fracture surfaces of high V (0.09 wt.%V) steel obtained from fast cooling rate tests: (a, b) at 650 °C and (c,d) at 850°C test temperatures.

The fracture morphologies at 850°C reveal many dimple-like features nested together as shown in Figure 12(d). During deformation in austenite, the predicted precipitate formation of VN can occur on austenite grain boundaries along with the formation of precipitate free zones on either side of the grain boundary. The strain may concentrate in the weaker precipitate free zones and micro voids may form around these precipitates on grain boundaries leading to fracture by micro void coalescence. In some areas of the fracture surface, cleavage facets are also seen leading to lower ductility.

3.4. METALLOGRAPHY IN LONGITUDINAL CROSS SECTION

3.4.1. Low V Steel. The optical micrograph of the longitudinal cross section of the fracture edge of the low V steel at deformation temperatures of 650°C and 850°C after slow cooling is shown in Figure 13. The cross section consists of voids near the fracture edge (Figure 13(a)).

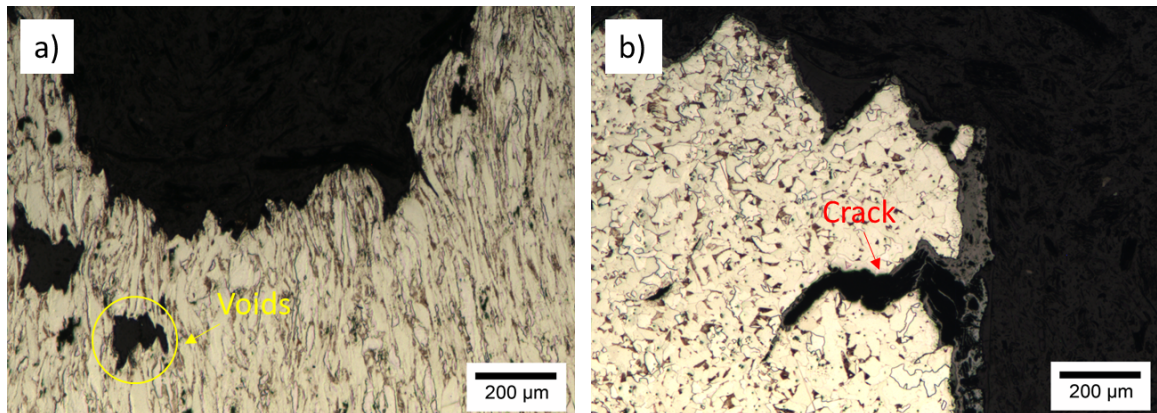


Figure 13: Optical micrographs of the longitudinal cross section of fracture edge of low V steel after slow cooling at (a) 650°C and (b) 850°C test temperatures.

The voids were mainly concentrated close to the fracture edge leading to a % RA of 66%. The deformation temperature at 850°C which exhibited the lowest % RA of 46% consists of cracks on the sides of the fracture edge (Figure 13(b)). The cracks were observed on the sides of the fracture edge, and they were formed perpendicular to the loading direction.

The optical micrograph of the longitudinal cross section of the fracture edge of the low V steel at deformation temperatures of 800°C and 900°C from fast cooling tests is shown in Figure 14. The cross section of the fracture edge at 800°C consists of micro voids and cracks closer to the fracture edge (Figure. 14(a)) and these voids tend to expand along the loading direction. Along with the micro voids, some cracks were seen perpendicular to the loading direction. The deformation temperature at 900°C which exhibited the highest % RA of 98% consists of cracks closer to the fracture edge (Figure 14(b)). The population of these voids and cracks at 900°C is lower when compared to the deformation temperature at 800°C leading to higher ductility.

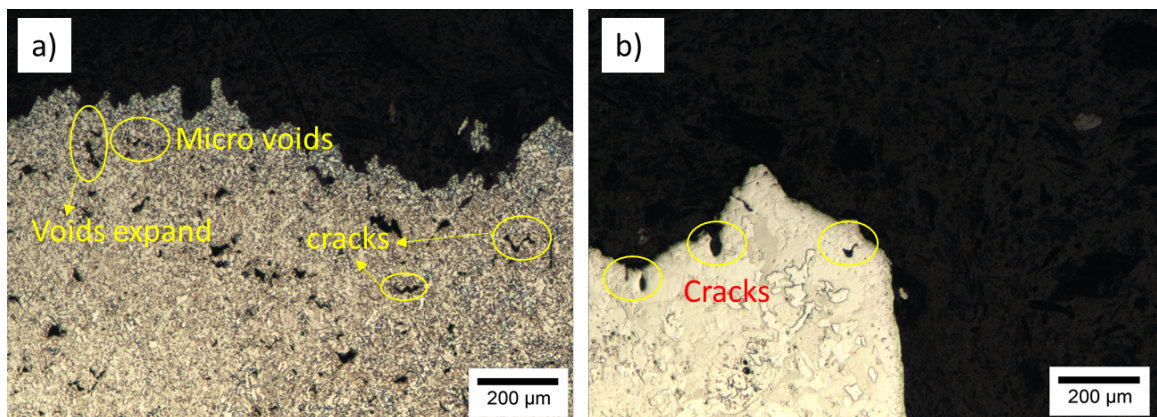


Figure 14: Optical micrographs of the longitudinal cross section of fracture edge of low V steel after fast cooling at (a) 800°C and (b) 900°C test temperatures.

3.4.2. High V Steel. The optical micrograph of the longitudinal cross section of the fracture edge from slow cooling rate tests at temperatures of 750°C and 900°C is shown in Figure 15. The cross section of the fracture edge consists of voids near the fracture edge and the voids expand along the loading direction as shown in Figure 15(a). The voids are mainly concentrated close to the fracture edge. The deformation temperature at 900°C which exhibited the lowest % RA of 31.3% consists of micro voids closer to the fracture edge and cracks were observed on the sides as well as along the length of the fracture edge as shown in Figure 15 (b). The observed cracks were formed perpendicular to the loading direction and they were formed on the austenite grain boundaries lowering the ductility of steels. This confirms the brittle behavior of the steels with matches with the fracture surfaces of the steels observed in Figure 11(d). Similar cracking behavior was observed in the low V (0.04 wt.% V) steel after slow cooling and deformed at 900°C as shown in Figure 13(b).

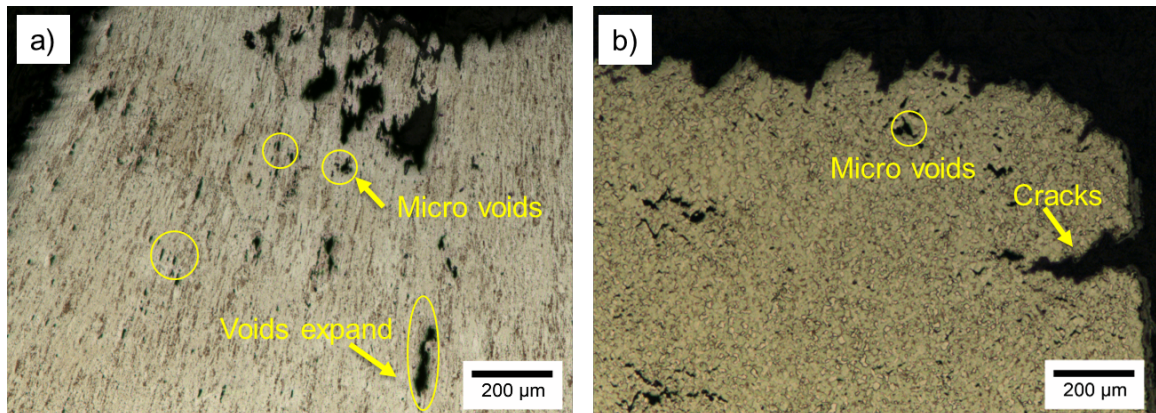


Figure 15: Optical micrographs of the longitudinal cross section of fracture edge of high V steel tested after slow cooling at (a) 750°C and (b) 900°C test temperatures.

The optical micrograph of the longitudinal cross section of the fracture edge of the high V steel tested after fast cooling at 700°C and 850°C is shown in Figure 16. The cross

section of the fracture edge at 700°C consists of micro voids and cracks close to the fracture edge as seen in Figure 16(a). The microstructure predominantly consists of ferrite as the samples was allowed to cool to room temperature after failure. The cross section of the fracture edge at 850°C consists of micro voids and cracks closer to the fracture edge as shown in Figure 16(b). The initial cracks form cavities that may extend along the loading direction leading to low ductility intergranular failure.

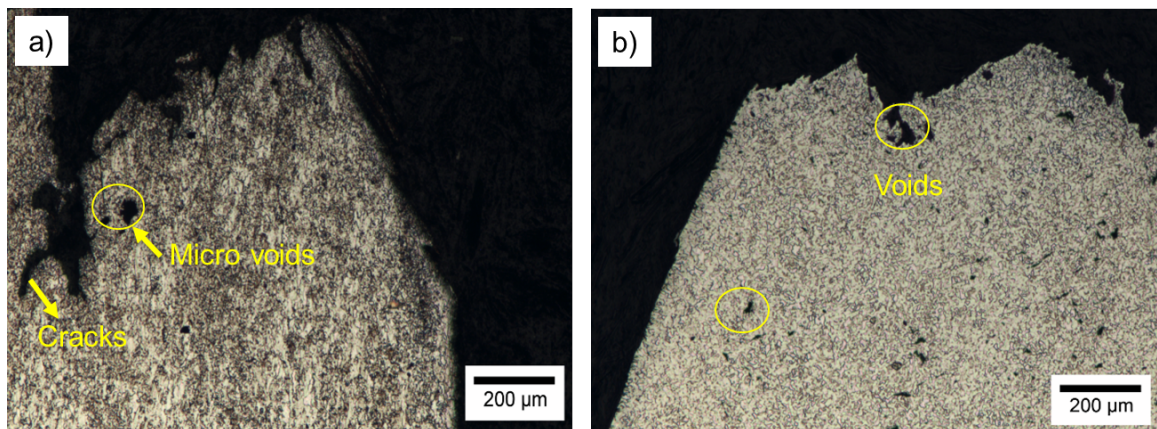


Figure 16: Optical micrographs of the longitudinal cross section of fracture edge of high V fast cooled steel at (a) 700°C and (b) 850°C test temperatures.

3.5. COMPARISON OF DUCTILITY TROUGH OF LOW AND HIGH V STEEL

The ductility trough of the two steels from the individual testing methods is shown in Figure 17. Figure 17(a) shows the hot ductility troughs for the high V and low V steels for the slow cooling tests, and Figure 17 (b) shows the hot ductility trough fast cooling test. Comparing the ductility trough of two steels, the low V steel had a better ductility than high V steel in both test methods. In low V steel, the trough from the fast cooling test is narrower than for the slow cooling test. The minimum ductility for the low V steel is below the A_{r3} transformation temperature of the alloy and may due to the formation of $V(C,N)$

and VN precipitates or liquation of MnS predicted by the thermodynamic modeling as shown in Figure 3. The difference in the shape of the ductility trough from the two test methods is likely caused by the difference in cooling rate of the test methods. The Joule heating was operated at a higher cooling rate than the servo-hydraulic load frame. For the high V steel, the lowest ductility is observed above the A_{r3} transformation temperature of the alloy in a complete austenitic region, while the ductility trough for the same steel from high cooling rate test method is lowest in the two phase region of ferrite and austenite and it is very close to the A_{r3} transformation temperature. The ductility troughs for high V steel from two testing methods appears to be deeper and broader. This may be due to the formation of more vanadium nitride precipitates above 830°C as predicted by the thermodynamic modeling as shown in Figure 4 or higher vanadium and nitrogen content of this steel. At low temperatures, typical recovery of ductility takes place as the ferrite volume fraction increased. It is important to note that the test methods involve reheating and solutioning of samples before cooling to test temperature. The thermomechanical cycle cannot redissolve all the expected precipitates such as MnS and TiN that form much above our soaking temperature capabilities. TEM and SEM-EDS analyses are planned in future work to investigate the observed differences in ductility.

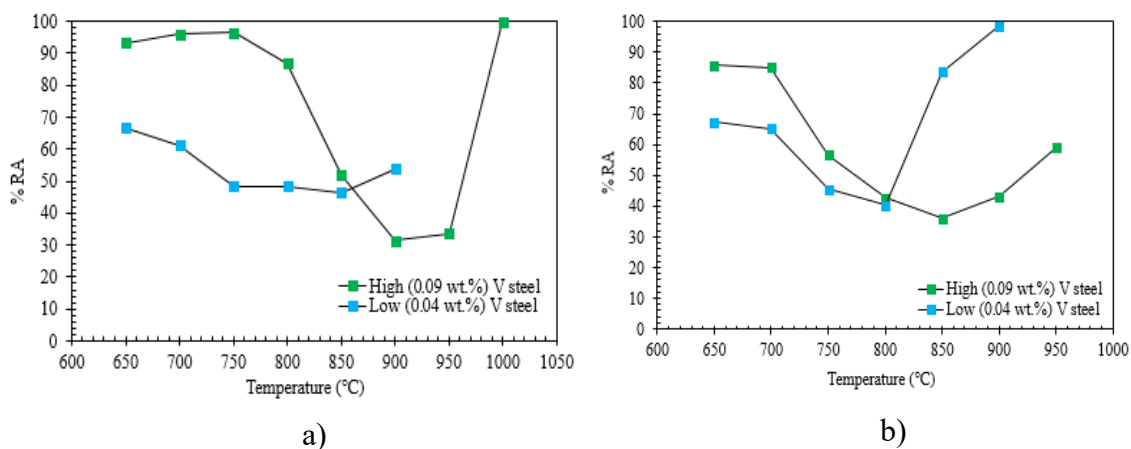


Figure 17: Hot ductility curves of high V and low V steel from a) servo-hydraulic MTS load frame with low heating/cooling rates and b) Joule resistive heating method with fast heating/cooling rates.

4. CONCLUSION

Hot ductility curves were obtained using two high temperature test methods namely i) a tensile test utilizing a servo-hydraulic load frame equipped with a resistance furnace and ii) thermomechanical testing apparatus using rapid Joule heating with an electro-mechanically controlled tensioning system. In the low (0.04 wt. %V) steel, the ductility decrease was observed from 700°C-850°C, below the A_{r3} transformation temperature. The loss in ductility may be mainly due to the combined precipitation of VN and V(C,N). The fracture mechanism changed from mixed mode intergranular with ductile voiding to highly ductile fracture with micro void coalescence at deformation temperature of 900°C. In comparison, the ductility decreases for the 0.09 wt.% V alloy occurred above the A_{r3} temperature in austenite for the low cooling rate test, while for the high cooling rate Joule heating test, the ductility loss was observed in a two-phase region of ferrite and austenite

with the lowest ductility occurring at 850°C close to the Ar₃ transformation temperature. Increasing vanadium and nitrogen levels increases the depth and width of ductility trough, likely due to the increased precipitation of VN. The precipitation in austenite for the 0.09 wt.% V is predicted to be mainly VN precipitates ranging from 1090°C - 840°C. The ductility of 0.09 wt.% V steel is lower than 0.04 wt.% V steel, is likely a result of the higher nitrogen level and strength of 116 ppm in the steel.

ACKNOWLEDGEMENT

The authors like to thank industrial partners of Peaslee Steel Manufacturing Research Center (PSMRC) for providing steel samples for the hot ductility studies. This project was funded by PSMRC at Missouri University of Science and Technology (Missouri S&T). The authors would like to thank the faculties, industry mentoring committee of PSMRC for their help and guidance.

REFERENCES

1. World steel production report, January 2021.
2. T. N. Baker, (2016) “Microalloyed steels”, *Ironmaking & Steelmaking*, Vol. 43, No.4, 2016, pp 264-307.
3. H. Xie, L. X. Du, J. Hu, R. D. K. Misra, “Microstructure and mechanical properties of a novel 1000 MPa grade TMCP low carbon microalloyed steel with combination of high strength and excellent toughness”, *Materials Science & Engineering A*, Vol. 612, 2014, pp 123–130.
4. T Gladman, *The Physical Metallurgy of Microalloyed Steels*, Maney, London, 2002.

5. B Mintz, "Hot Ductility of Steels and its Relationship to the Problem of Transverse cracking during continuous Casting", *International Materials Review*, Vol. 36, No.5, 1991, pp 187-217.
6. B Mintz, J M Arrowsmith, "Hot ductility behavior of C-Mn-Nb-Al steels and its relationship to crack propagation during the straightening of continuously cast strand", *Metals Technology*, Vol. 6, 1979, pp 24-32.
7. M. A. Matveev, "Causes of High Temperature Ductility Trough of Microalloyed Steels", *Trans Indian Inst Met*, Vol. 70, No.8, 2017, pp 2193-2204.
8. Sage A M., "Effect of Vanadium, Nitrogen and Aluminium on the Mechanical Properties of Reinforcing Bar Steels," *Metals Technology*, Vol.2,1976, pp 65-70.
9. Zajac S, Lagneborg R and Siwechi T., "The Role of Nitrogen in Microalloyed Steels", *Microalloying '95 Proceeding of International conference*, Pittsburgh, PA, 1995, pp 321-340.
10. B Patrick ,V Ludlow, "Development of Casting Practices to Minimise Transverse Cracking in Microalloyed Steels", *Revue de Metallurgie*, Vol. 91, 1994, pp 1081-1089.
11. B. Mintz, "Influence of Nitrogen on Hot Ductility of Steels and Its Relationship to Problem of Transverse Cracking", *Ironmaking & Steelmaking*, Vol. 27, No. 5, 2000, pp 343-347.
12. D N Crowther , B Mintz, "The influence of grain size and precipitation on hot ductility of microalloyed steels", *Materials Science and Technology*, Vol. 2 No. 11, 1986, pp 1099-1105.
13. B Patrick ,V Ludlow, "Development of Casting Practices to Minimize Transverse Cracking in Microalloyed Steels", *Revue de Metallurgie*, Vol. 91, 1994, pp 1081-1089.
14. B Mintz, "The Influence of Composition on the Hot Ductility of Steels and to the Problem of Transverse Cracking" *ISIJ International*, Vol.39, 1999, pp 833-855.
15. Bing-hua Chen, Hao Yu, " Hot ductility behavior of V-N and V-Nb microalloyed steels", *International Journal of Minerals, Metallurgy and Materials*, Vol. 19, No. 6, 2012, pp 525-529.

III. HOT DUCTILITY BEHAVIOR OF V-NB BEAM BLANK STEEL

Madhuri Varadarajan, Laura N. Bartlett, Ronald J. O'Malley, Simon N. Lekakh, M. F. Buchely

Peaslee Steel Manufacturing Research Center, Missouri University of Science and Technology,

1400 North Bishop Avenue, Missouri, United States 65409

ABSTRACT

Carbo-nitride forming microalloying elements, such as Nb and V are used to produce steels that exhibit high strength and toughness. Near-net-shape continuous cast beam blanks from these steels are subjected to significant deformation during straightening in the secondary cooling zone of the continuous caster and knowledge of the temperature dependence of the hot ductility of the steel is essential to prevent crack formation during casting. In this study, the hot ductility of a commercially cast beam blank from medium carbon (0.18 wt.% C) microalloyed 0.028 wt. %V and 0.02 wt. %Nb was investigated using two experimental methods that imposed different thermal histories prior to tensile loading. The first method employed a load frame equipped with resistance furnace heating, which provided slow cooling (1°C/s) to the test temperature after solution treatment at 1200°C. The second test method, which employed a thermomechanical simulator with direct Joule heating for temperature control, provided a faster cooling rate (4°C/s) from the solution treatment temperature to the test temperature. The tensile tests were performed at a 3×10^{-3} /s strain rate in a temperature window of 650°C - 950°C to mimic industrial unbending temperature conditions in the beam blank casting process. A ductility trough,

with a minimum reduction in area (%RA) at 800°C was observed, which was close to the A_{r3} transformation temperature of the alloy. Both test methods provided a similar minimum ductility temperature. However, the slow cooling rate test showed a wider low ductility temperature range than after faster cooling. The effects of thermal history on the ductility of this V-Nb micro-alloyed steel are discussed.

1. INTRODUCTION

In last few decades, the trend in steel processing has been to move towards near-net shape casting due to its many advantages, such as fewer rolling passes, lower capital cost, and higher rolling yields. Thin strip, thin slab and beam blank casting are typical examples of this trend. In particular, beam blank castings are used as a starting material for hot-rolling I-beams, which has advantages such as reduced energy consumption with lower CO₂ and NO_x emissions, lower roll costs due to reduced number of rolling strands, lower maintenance costs and increased productivity [1]. At the same time, near net shape beam blanks are more prone to form internal (porosity, solidification cracks) and surface defects (transverse, longitudinal cracks) than simple rectangular shaped sections because of their complex geometry [2,3]. It was reported that transverse cracks, perpendicular to the casting direction, are often located at the surface of flange and web region of the beam blank. These cracks often originate in the straightening area of the caster when unbending occurs at temperatures in the range of 700°C-1000°C, where the steel is known to exhibit lower ductility [4]. This “ductility trough” can be observed in hot tensile tests by measuring the % reduction in area (%RA) at specimen failure at various temperatures.

The extensive research was published to characterize the phenomena of ductility losses at high temperature with attempt to optimize the thermo-mechanical conditions to decrease the tendency for crack formation using various numerical methods. Kim et al. [5] developed a 2D transient coupled thermo elastic plastic model which simulated thermodynamic behavior of the solidified shell of a cast beam blank to analyze surface and internal cracks. Gaiyan Yang et al. [6] established a 2D microsegment model to study the distribution of temperature and stress using finite element method to understand the crack initiation mechanisms on beam blank surfaces during molding. Other researchers [3,7,8] have also used numerical methods to simulate the flow field, stress distribution, temperature field, and movement of inclusions to determine the factors that leads to defects and thereby optimize the casting process parameters. While the results from numerical simulations have benefitted the beam blank casting production, knowledge of the thermomechanical and ductility behavior of the as-cast steel is still needed. One of the significant problems related to the accuracy of FEM simulations is related to transient nature of high temperature material behavior and the property dependence of the steel on its thermal history before deformation. Unfortunately, little information is available in the literature concerning the effect of thermal history on hot ductility of commonly used micro-alloyed steels.

Optimal use of carbo-nitride forming microalloying elements, such as Ti, Nb, and V, can produce steels that exhibit high strength and toughness when appropriate thermomechanical processing is employed[9,10] . The hot ductility of steel is highly dependent on these microalloying elements and unfortunately their presence can sometimes lead to an increased susceptibility to transverse cracking[11].

Nb bearing precipitates, such as carbides, nitrides or carbonitrides have been shown to have a strong effect on the hot ductility of steels, deepening and widening the “ductility trough”, and extending the low ductility region to higher temperatures. Mintz et al. [12], and Srirachoenchai et al. [13], suggest that this is mainly due to the formation of Nb(C, N) precipitates which can retard recrystallization and form precipitates on austenite grain boundaries. Niobium levels as low as 0.017 % have been shown to have an adverse effect and the ductility continues to deteriorate as levels are increased up to 0.074% [14–16]. Vanadium behaves in a similar manner to niobium at high nitrogen levels (90-120 ppm) initiating transverse cracking; however, transverse cracking was not observed below 50 ppm nitrogen [17]. Also, vanadium levels below 0.07% have been reported to inhibit the drop in ductility [18].

The described changes in hot ductility are related to precipitation kinetics, therefore, it could be predicted that the thermal history of micro-alloyed steel before mechanical loading will influence the low ductility region. Therefore, it is important to understand the transient effects of cooling rate on hot ductility and the susceptibility of industrial beam blanks to transverse cracking. In this study, the hot ductility of a commercial as-cast beam blank (0.18 wt. % C) steel containing 0.028 wt. % V, 0.02 wt. % Nb and 90 ppm nitrogen was investigated using two experimental methods with different cooling rates before mechanical testing, mimicking the temperature condition and strain rate observed in an industrial continuous caster.

2. PROCEDURE

2.1. EXPERIMENTAL

Materials. The chemical compositions of commercially produced beam blank steel sample used in this study is listed in Table 1. Optical emission arc spectroscopy was used to determine the wt. % of elements present in the steel samples. Leco CS600 combustion analyzer and Leco TC500 inert gas fusion analysis was used to determine the composition of C, S, and N levels. The studied V-Nb micro-alloyed steel had 90 ppm N.

Table 1: Chemistry of the V-Nb micro alloyed steel (wt. %).

C	Mn	Si	P	S	Cr	Mo	Ni	V	Nb	N (ppm)
0.18	0.94	0.21	0.011	0.027	0.08	0.037	0.14	0.028	0.020	90

The samples for hot tensile testing were cut from a 285 mm long as cast beam blank from the locations shown in Figure 1. The hot ductility samples were prepared so that the tensile direction was perpendicular to the columnar grain structure to mimic strain direction observed in continuous casting process. The heat affected regions from the oxy-acetylene torch cuts were avoided during preparation of the tensile samples. Determination of Hot Ductility. The temperatures and strain rates applied in this research to measure the hot ductility were chosen based on known ranges for transverse crack formation during continuous casting [4]. Two experimental techniques with different preheating and cooling cycles were performed during the tests to detect the effect of thermal history on mechanical properties. Both methods involved reheating the specimens and holding them at 1200°C

for two minutes for re-dissolving the micro alloy precipitates [4,12], followed by cooling to the desired test temperature using two different cooling rates.

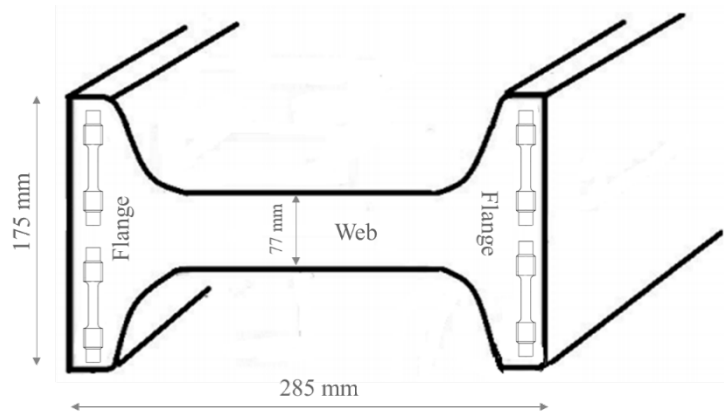


Figure 1: Position of hot ductility samples taken from a V-Nb micro alloyed beam blank.

After short stabilizing period, tensile testing was performed at a controlled strain rate. The two experimental procedures referred in this article as “slow” and “fast” cooling were utilized with different testing equipment. Slow cooling method was performed with an MTS servo-hydraulic load frame equipped with resistance furnace with SiC elements, which provided controlled cooling rate at 1°C/min. Subsize #3 round 6 mm diameter specimens with a gauge length of 25 mm were machined accordingly to the ASTM E8-16a standard. A custom-built thermomechanical testing apparatus that employs a rapid internal Joule heating system coupled with an electro-mechanically controlled tensioning system was used for controlled fast cooling at 4°C/min. A flat 97 mm long sample with a 5.55 x3 mm cross-section was used. A pyrometer (1 mm spot size, ± 1 °C) monitored the temperature of the sample.

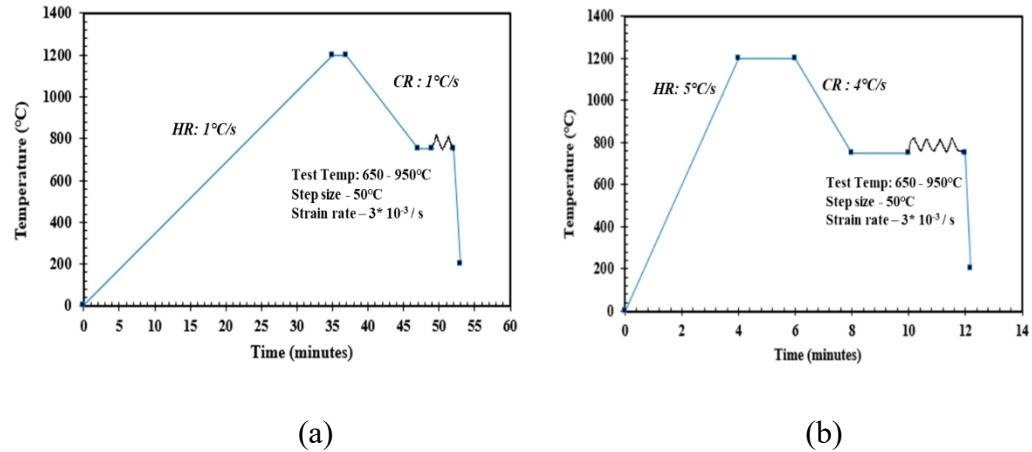


Figure 2: Shows a schematic of used temperature profile for both methods.

For slow cooling test, the thermomechanical cycle included heating at 1°C/s to 1200°C, holding 2 min, cooling to the test temperature in the range of 650°C-950°C at a cooling rate of 1°C/s, and 2 min holding at test temperature before applied force. For fast cooling schedule, 5 °C/s heating to 1200°C and 4°C/s cooling to test temperature were used with similar holding periods. In both schedules, strain to failure at a constant strain rate of $3 \times 10^{-3}/s$ which was selected to approximately match the strain rate during the straightening operation of the continuous casting process. For evaluating the ductility of the steels, the reduction in area was calculated using the following equation:

$$\% RA = \frac{A_0 - A_f}{A_0} \quad (6)$$

where: RA is the reduction in area, A_0 is the initial cross-sectional area (mm^2) and A_f is the fracture cross sectional area (mm^2).

Fractography and metallography analysis sections parallel to the tensile axis of one half of tested specimen were prepared for optical metallography using standard metallographic techniques to better understand microstructure/mechanical property

relationships and the origin of failure during testing. The second half of specimen, was used for fracture analysis with a scanning electron microscope (TESCAN-VEGA) and SEM-EDS.

2.2. THERMODYNAMIC SIMULATIONS

Thermodynamic modeling of the equilibrium phase precipitation was performed using ThermoCalc 2021b – TCS steel and Fe alloy database (TCFE 11). The continuous cooling transformation diagrams were simulated using JmatPro (v.11) for the experimentally used cooling rates.

3. RESULTS

3.1. STRESS-STRAIN BEHAVIOR OF V-NB MICRO ALLOYED STEEL

The engineering stress-strain curves obtained from the slow and fast cooling test schedules are shown in Figure 3.

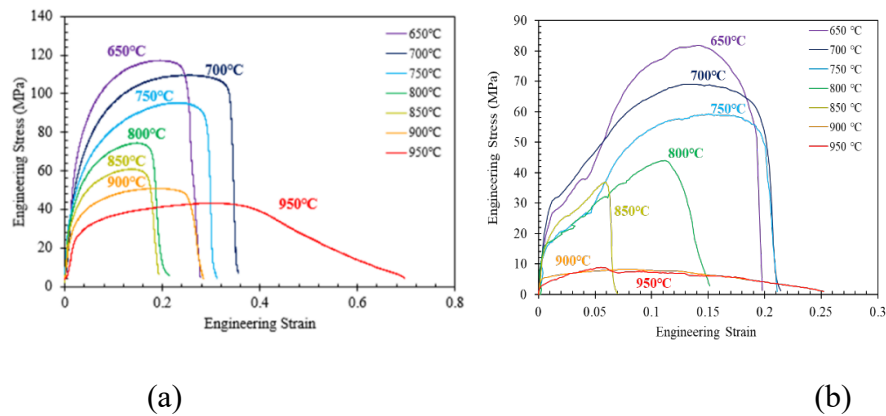


Figure 3: Engineering stress – strain curves at different deformation temperatures for: (a) slow and (b) fast cooling test schedules.

Both test schedulers showed monotonic change in tensile strength vs test temperature.

A typical downward trend in tensile strength as a function of increasing temperature from 650°C-950°C is shown in Figure 4. A difference in the strength levels obtained from the two testing methods could be attributed to different testing parameters as well as the specimen shape (round vs rectangular). In each test schedule, a high failure strain was observed at 950°C, and tensile curves exhibited a softening effect, indicating the onset of dynamic recrystallization (Figure 3).

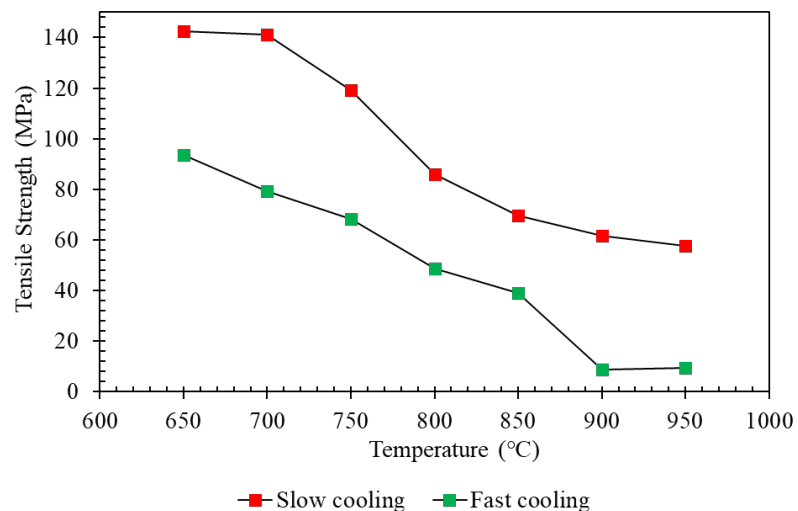


Figure 4: Relationship between tensile strength and temperature for the V-Nb micro-alloyed steel for two test schedules.

When compared to more or less monotonic trends of tensile strength, area reduction (RA) and strain to failure clear indicated intermediate brittleness region. For slow cooling, the RA varies between 6% - 98% and the ductility drop is observed from 900°C-750°C (Figure 5). Above this temperature, the RA has increased again from 14% at 900°C to 82%

at 950°C. With the fast-cooling method, the RA varies between 12%-94%, and the ductility drop is observed from 850°C - 750°C. Both testing methods produced a similar trend in the shape of the ductility trough and the ductility trough appears to be deeper and broader for the slow cooled condition. The lowest drop in ductility of steels observed at 800°C for both testing methods.

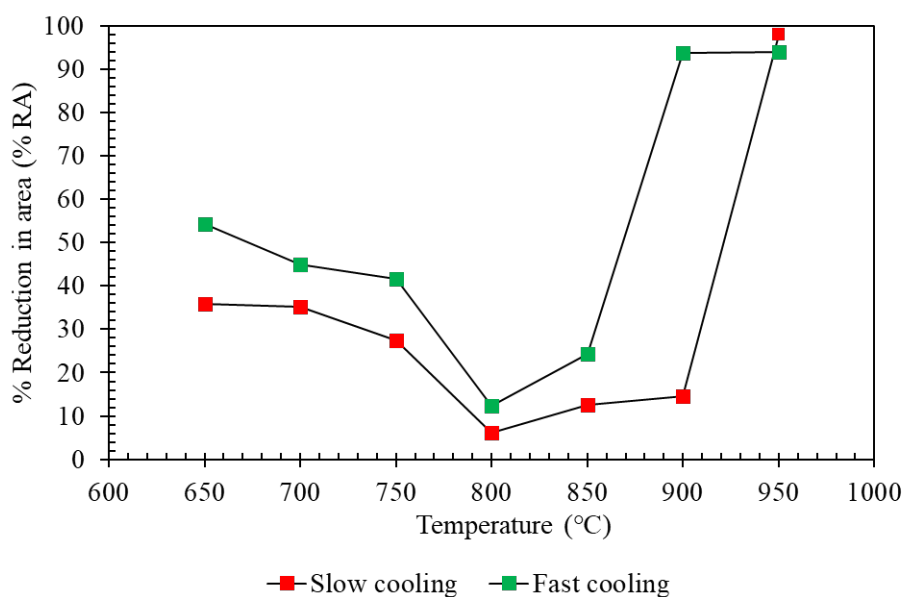


Figure 5: Hot ductility curves of V-Nb micro alloyed steel from two testing schedules.

3.2. EXAMINATION OF TESTED SPECIMENS

SEM fractography of the fractured surface for the fast-cooling test at deformation temperatures 800°C, when the specimen had the lowest ductility (12% RA) is shown at different magnifications in Figure 6 and Figure 7. The fractured surface exhibit brittle behavior with intergranular fracture surfaces, including intergranular decohesion, flat featureless facets, and the failure occurred along the ridges.

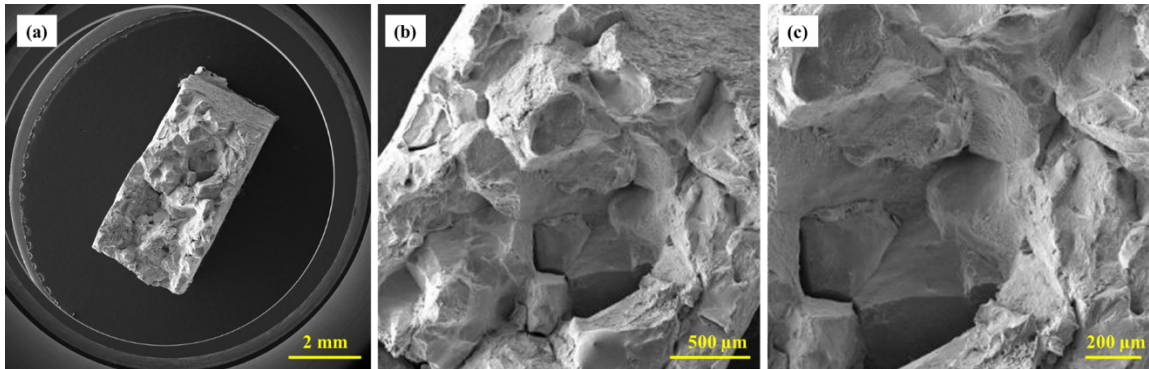


Figure 6: Fracture surfaces of V-Nb micro alloyed steel tested at at 800°C (fast test schedule).

The second lowest drop in ductility was observed at 850°C with 24% RA. The fracture surface at 850°C also exhibited a distinct brittle fracture with intergranular decohesion. The intergranular failure by micro void coalescence is characterized by small ductile dimples on the fracture surface (Figure 7).

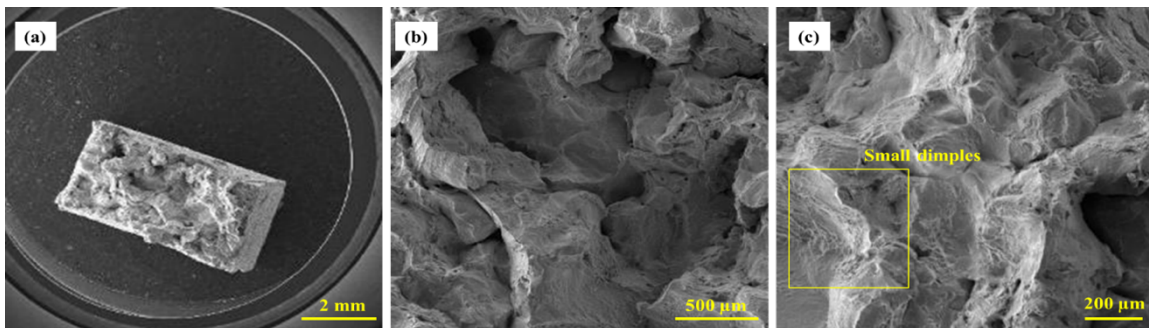


Figure 7: Fracture surfaces of V-Nb micro alloyed steel tested at 850°C test temperatures (fast test schedule).

In contrast, the fracture surface is entirely ductile, with micro void coalescence at lower (Figure 8) and higher (Figure 9) test temperatures. Small size dimples were found

on the fracture surface for the deformation temperature at 650°C. At 950°C, the fracture surface also was highly ductile and characterized by deep voids, large size dimples and absence of grain boundary facets.

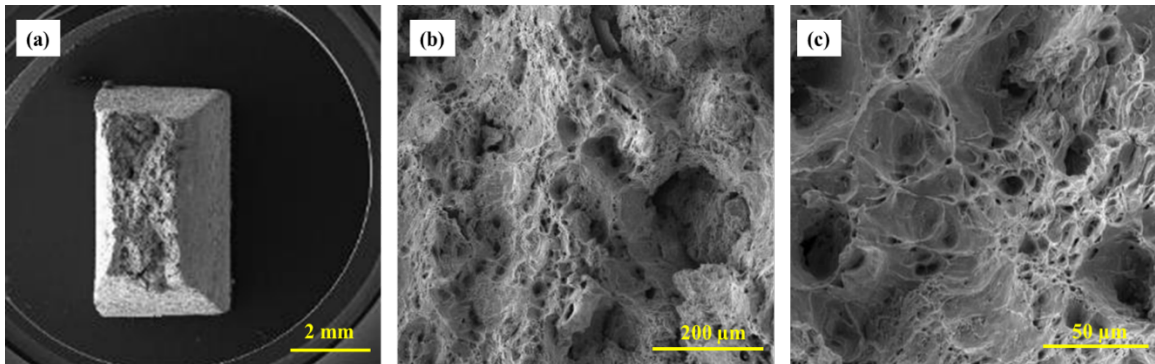


Figure 8: Fracture surfaces of V-Nb micro alloyed steel tested at 650°C (fast test schedule).

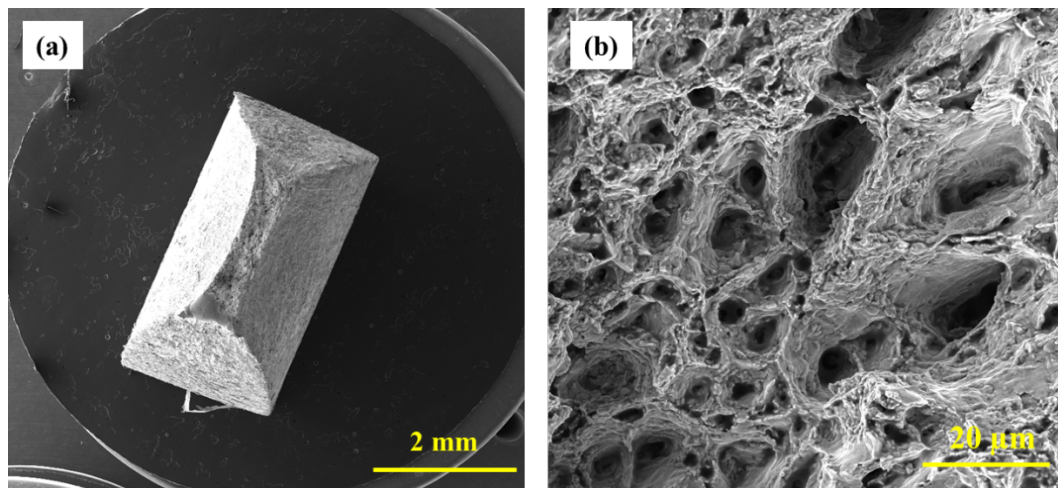


Figure 9: Fracture surfaces of V-Nb micro alloyed steel tested at 950°C (fast test schedule).

Fractured surfaces tested at slow test schedule were partially obscured by formed oxides after testing; therefore, some specific features were difficult to observe (Figure 10).

The fracture surface tested at 800°C and 850°C exhibited brittle behavior with intergranular fracture surfaces. At low deformation temperature 650°C, the fracture surface is entirely ductile with micro-void coalescence as shown and at 950°C, the fracture surface exhibited large deep voids typical of high ductility.

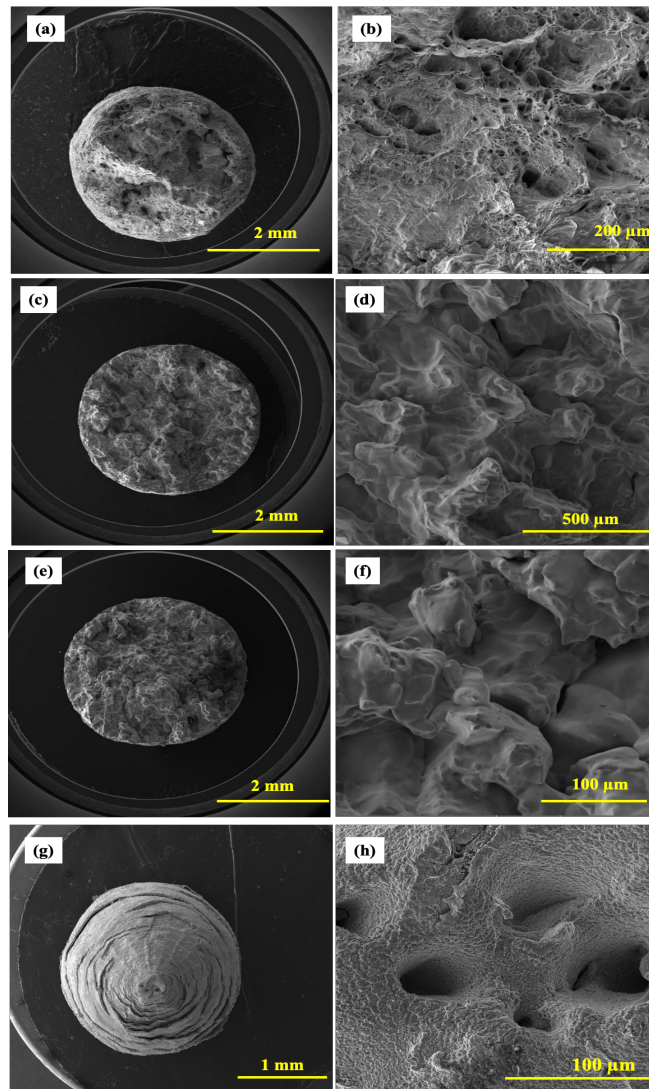


Figure 10: Fracture surfaces of V-Nb micro alloyed steel tested at a slow cooling rate: (a, b) at 650°C, (c, d) at 800°C, (e, f) 850°C and (g,h) 950°C test temperatures.

The optical micrograph taken at the longitudinal cross section of the fracture edge of the steel tested at 650°C, 800°C, 850°C applying fast cooling schedule is shown in Figure 11. The cross-section at 650°C consists of micro voids closer to the fracture edge. Thin films of ferrite were observed along the prior austenite grain boundaries at 800°C, which has the lowest 12% RA. When fast schedule was used, existed at test temperature austenite transformed to bainite and martensite during fast cooling at fracture allowing to observe mentioned ferrite films. These thin films of ferrite could be linked to intergranular cracking along the prior austenite boundaries as was observed in the fracture surface (Figure 6). At 850 °C, the intergranular cracks are seen propagating along the prior austenite grain boundaries.

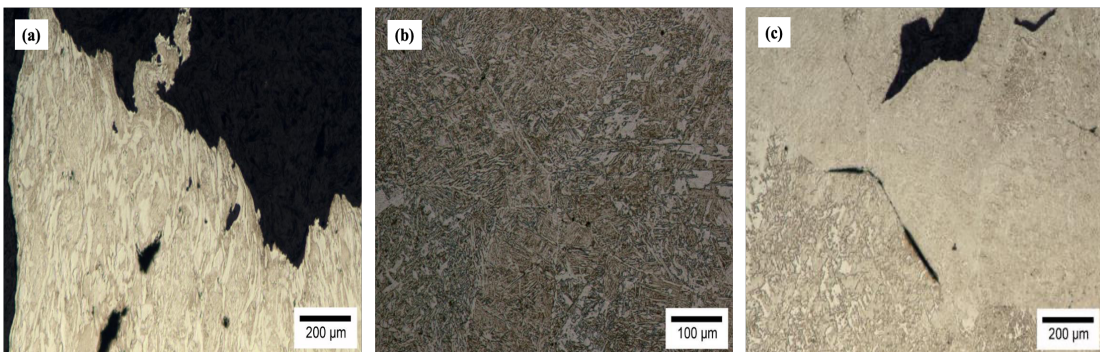


Figure 11: Optical micrographs of the longitudinal cross section of fracture edge of V-Nb micro alloyed steel tested at 650°C (a), 800°C (b,c) and 850°C (d) applying fast cooling schedule.

Because slow cooling test schedule restricted indication of phases existed during test, optical imaging in cross sections was used only for void and crack analysis (Fig. 12). The cross section of the fracture surface at a deformation temperature of 650°C contains micro voids closer to the fracture edge. The intergranular crack propagating along the prior

austenite boundaries at 800°C tests, which produced a low 6% RA. The same behavior was also observed at a deformation temperature at 850°C.

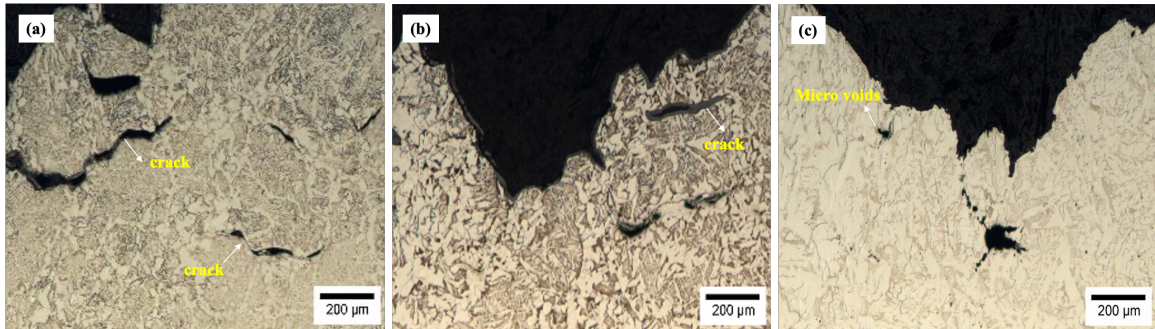


Figure 12: Optical micrographs of the longitudinal cross section of fracture edge of V-Nb micro alloyed steel after slow cooling at (a) 800°C, (b) 850°C and (c) 650°C test temperatures.

Representative samples from both test schedules, which exhibited the lowest drop in ductility at 800°C, were examined using SEM-EDS analysis and the analysis were performed on sections taken closer to the point of fracture (Figures 13, 14). At fast cooling schedule, MnS particles were predominantly present on the cracked region at the prior austenite grain boundaries. Further away from the cracked area, different shapes (globular, elongated) of MnS along with MnS with Nb-containing particles were observed.

The SEM micrographs, along with EDS analysis for the deformation temperature at 800°C from the slow schedule is shown in Figure 14. The EDS analysis at the cracked region consists of MnS-SiO₂ particles along with small spherical MnS inclusions.

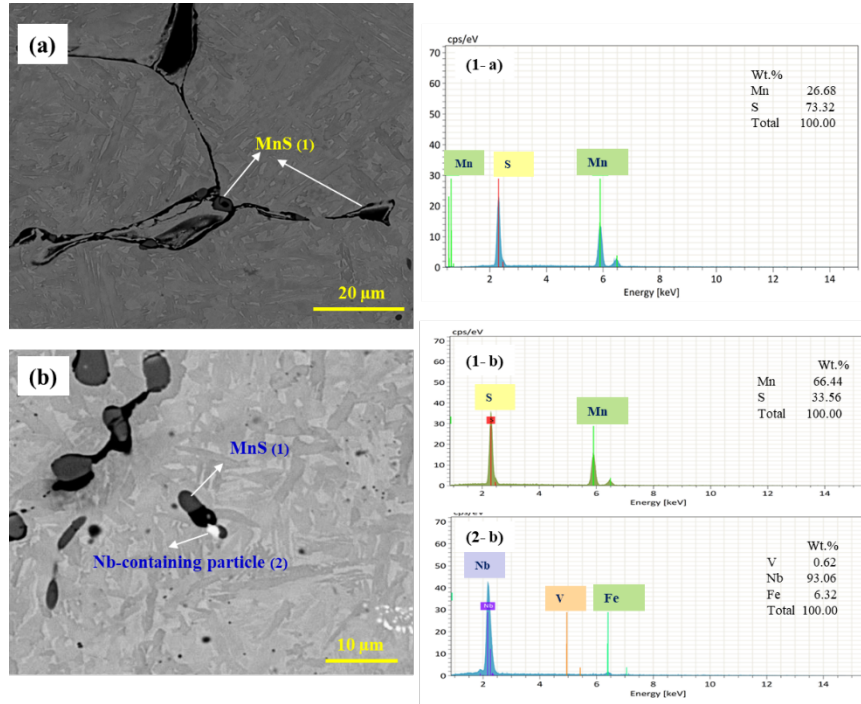


Figure 13: SEM – EDS analysis of the longitudinal cross section of fracture edge (800°C, fast schedule): (a) crack region showing the presence of MnS and (b) MnS with a Nb-containing particle in the matrix.

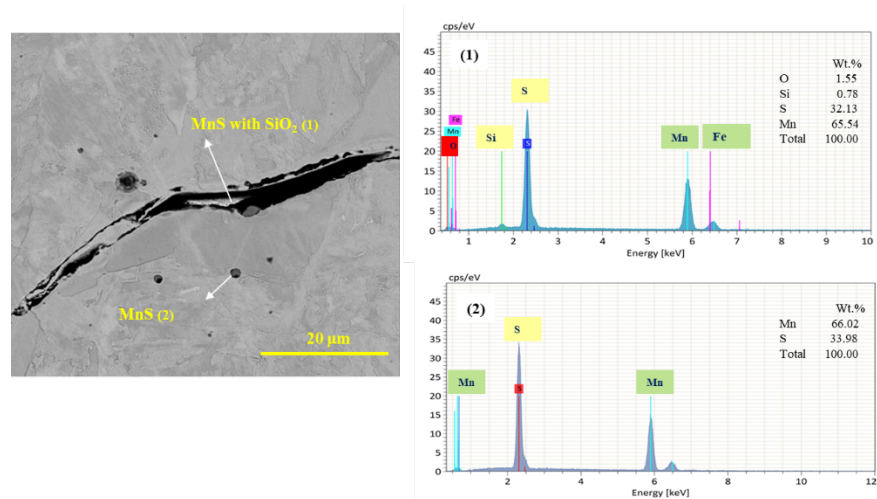


Figure 14. SEM – EDS analysis of the longitudinal cross section of fracture edge (800°C, slow schedule): at (1) crack region showing the presence of MnS-SiO₂ particles and (2) MnS inclusion.

4. DISCUSSION

The primary mechanism for transverse cracking in V-Nb micro alloyed steels is reported to be due to the precipitation of carbides, nitrides carbonitrides or sulfides, such as Nb(C,N), V(C,N) or complex (Nb,V)(C,N), AlN and MnS occurring at low strain rates in the temperature range of 1100°C-700°C [19]. The addition of V to the Nb-containing steel has been reported to decrease the activity of carbon and nitrogen, increase carbonitride stability and slow the kinetics of precipitation compared to Nb-microalloyed steel [20]. In V-Nb microalloy steels, vanadium and niobium precipitations usually exist as complex carbonitrides of (Nb,V)(C,N), the solubility of which is higher than that of NbC. Akben et al. [21] showed that the vanadium addition slows down the precipitation of Nb(C,N) and many researchers[4,17,20,22–24] have observed that V and Nb microalloyed steel had coarser and fewer precipitates than the Nb containing steel.

Therefore, thermodynamic calculations of studied steel were performed to establish possible link the drop in ductility to the precipitation and phase transformations. The calculated equilibrium phase stability plots for the V-Nb micro alloyed steel (Figure 14a) show the predicted temperature ranges for stability of liquid, austenite, ferrite, and various secondary phases. The temperature range of the start of austenite transformation to ferrite upon cooling (A_3) was around 817°C and the finish (A_1) was 709°C. The primary precipitates are MnS, which are stable below 1456°C, and niobium-vanadium carbonitrides, which are stable below 1150°C. The equilibrium composition of the complex carbonitride phase changed during cooling with increasing the vanadium and N in solid

solution with Nb and C (Figure 15b). The described thermodynamic calculations are in agreement with published experimental data.

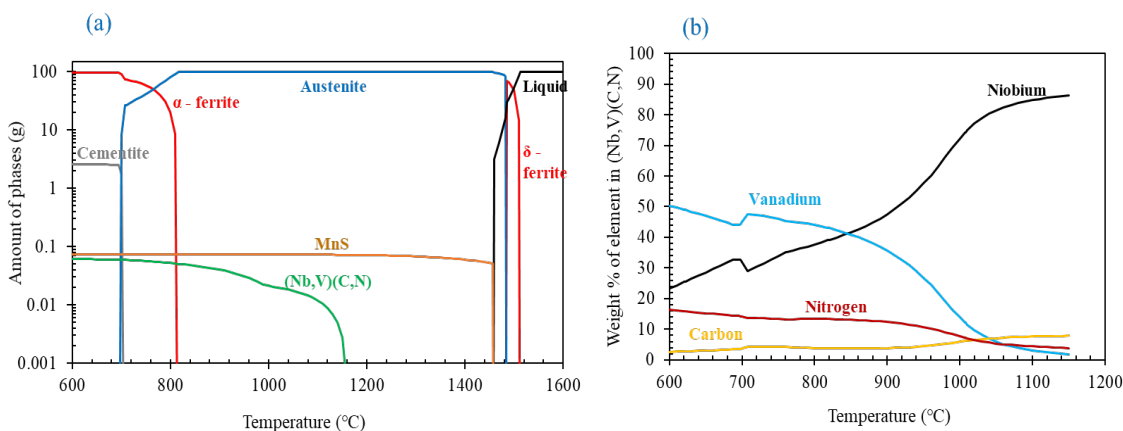


Figure 15: Equilibrium phase transformations during cooling of the studied V-Nb micro alloyed steel: (a) phase diagram and (b) distribution of elements in precipitated (Nb,V)(C,N).

The lowest reduction in area (RA) in the ductility trough was observed at 800°C, which is close to the austenite to ferrite transformation temperature (817°C) in the studied steel. Therefore, the ductility drop at this temperature is likely related to the formation of a thin layer of ferrite (Figure 11) along the austenite grain boundaries. Thin films of proeutectoid ferrite are formed along the prior austenite grain boundaries slightly below the A_{r3} Temperature. In a dual phase region of ferrite and austenite, the strain gets concentrated within the soft, thin ferrite films during deformation. The voids nucleate and coalesce at the grain boundary leading to separation of grains. This results in minimum ductility and intergranular failure as shown in Figure 6. The intergranular fracture also occurs when the predicted precipitates such as MnS or (Nb,V)(C,N) are present closer along the grain boundary, making it easier for the crack to propagate from one particle to

another. In addition, the lower solubility product of the precipitates in ferrite promotes precipitation in the ferrite film. Fine precipitates, such as $(\text{Nb},\text{V})(\text{C},\text{N})$ and MnS at the grain boundary, can also pin or delay grain boundary movement, encouraging grain boundary sliding [20].

In addition to effect of V-Nb carbonitride precipitation, it is essential to understand the role of sulphur on the ductility of the steels. Sulphur can reduce the hot ductility of steels by weakening the grain boundary area for the following reasons: (i) sulphur segregation to the boundary [25], (ii) formation of low melting Fe-S compounds at low Mn/S ratios, and the (iii) combined effect of Mn and sulphides on the formation of cavities, which links up to produce low ductility intergranular failure [26]. The effect of sulphur on the hot ductility usually depends on the test conditions. The amount of sulphur that redissolves depends on the Mn content. For a niobium containing steel with 1.4% Mn, the amount of sulphur redissolved is $>0.001\%$ S and it is this sulphur which controls the ductility of steels which precipitates in a fine spherical form at the austenite boundaries [27,28]. In current study, MnS starts precipitating just below the liquidus temperature of the alloy and during the reheat cycle sulphur will not go back into solution at 1200°C . These sulphides will continue to remain upon cooling to the test temperature and may influence the depth of the ductility trough. Furthermore, the thermodynamic simulation suggests that the amount of MnS formed is greater than the amount of complex $(\text{Nb},\text{V})(\text{C},\text{N})$ precipitates. The higher the volume fraction of MnS inclusions at the grain boundaries may be more closely spaced, making it is easier for voids to link together, resulting in intergranular failure. SEM-analysis also indicated that more MnS inclusions were present close to the fracture site and along the cracks propagating along prior austenite

grain boundaries, as shown in Figures 12 and 13. . In the fast-cooling test at, In this study, precipitates of MnS and (Nb,V)(C,N) were observed on the grain boundaries in the specimens tested at 850°C applying fast test schedule. Usually, these precipitate were accompanied with precipitate free zones (PFZ) on either side of the grain boundaries. During deformation, strain is concentrated in the weaker PFZ and micro voids form around the precipitate on grain boundary, leading to intergranular fracture by a micro void coalescence mechanism (Figure 7).

With decreasing temperatures to 650°C, a high-volume fraction of ferrite forms which resulting in a more uniform strain distribution between the austenite and ferrite phase, and ductility is recovered. The fracture surface at 650°C (Figure 8 and Figure 10(e,f)) is entirely ductile with micro void coalescence. These micro voids nucleate at strain discontinuity such as MnS inclusions or second phase particles such as (Nb,V)(C,N). Typical recovery of ductility takes place at a deformation temperature of 650°C.

From the other side, at higher temperatures, 950°C, the fracture surface has large deep voids and these voids are formed during deformation by grain boundary sliding and dynamic recrystallization [20,29,19] . The cracks that develop as a result of grain boundary slipping or stress concentration are prevented as a result of grain boundary movement away from the cracks. These isolated cracks grow into large deep voids as shown in Figure 9 and Figure 10(g,h).

In this study, the effect of thermal history on ductility drop was investigated by applying two type of test schedules. It was shown that the hot ductility behavior depended on applied cooling rates o(1°C/s vs 4°C/s) prior mechanical loading. There was clear indication of improvement in ductility when faster cooling was applied. One of the

possible mechanism could be related to phase transformation kinetics. To verify this statement, the continuous cooling transformation behavior of austenite during cooling at different cooling rates for V-Nb steel were simulated (Figure 16). At the lower temperature end of the ductility trough, the increased cooling rate used with the Joule heating experiment tended to measure 54% RA compared to the 35% RA in slower cooling rate at MTS frame test. This difference is likely due to the effect that cooling rate has on temperature that ferrite nucleates. For a slower studied 1°C/s cooling rate, the ferrite nucleation temperature is 788°C and at higher 4°C/s cooling rate the ferrite nucleation temperature is 767°C. This switch in ferrite nucleation kinetics explained experimentally observed extension of low ductility temperature window.

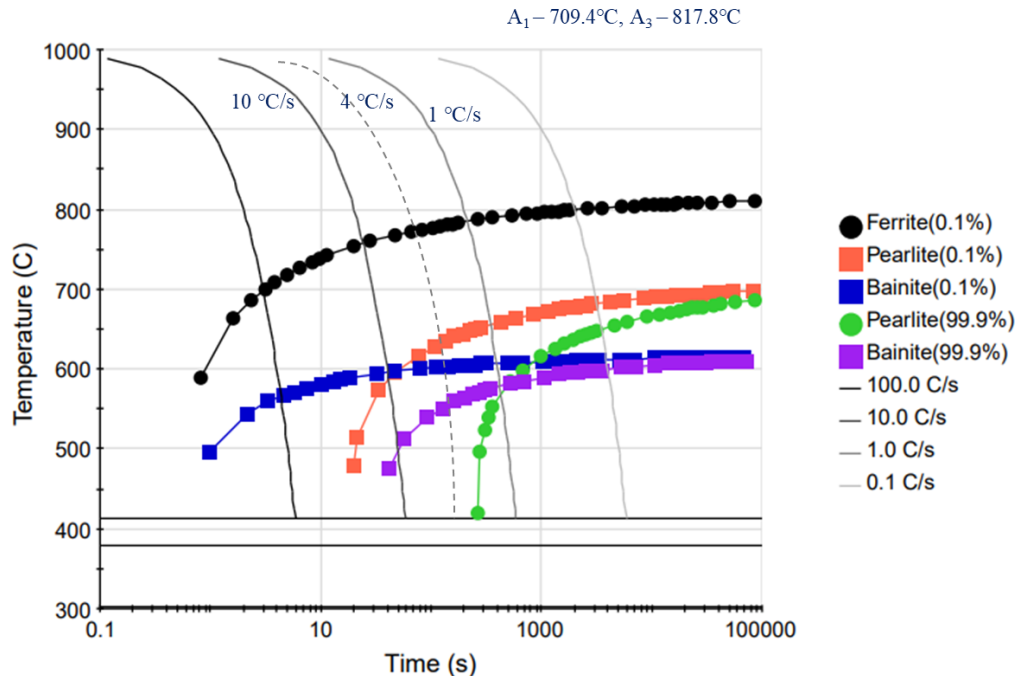


Figure 16: Continuous cooling transformation diagrams of studied V-Nb micro alloyed steel.

5. CONCLUSIONS

Hot ductility curves were obtained using two high temperature test methods: (1) a tensile test utilizing a servo hydraulic load frame with a resistance furnace (slow cooling test) and (2) a thermomechanical testing apparatus using rapid joule heating combined with an electro-mechanically controlled tensioning system (fast cooling test). Both test methods showed similar low ductility trends, but the upper and lower edges of the ductility trough temperature range differed between the two test methods. The differences are attributed to the differences in heating and cooling rate of the two test methods. The two testing methods displayed similar ductility minimums between 750°C-850°C from the fast-cooling test and between 750°C-900°C from the slow cooling test. Both test methods showed their lowest ductility at 800°C which was very close to the austenite to ferrite transformation temperature (817°C) of the alloy. The hot ductility loss at 800°C from the fast-cooling test method is due to the formation of thin films of ferrite on prior austenite grain boundaries, the strain gets concentrated at these thin films leading to intergranular cracks. The intergranular cracks were also found on the prior austenite grain boundaries at 800°C from the slow cooling test method. MnS inclusions was the predominant precipitate present close to the fracture site and along the cracks propagating along prior austenite grain boundaries as observed in slow cooling and fast cooling rate test. At high end of the trough, the ductility is recovered by dynamic recrystallization and at low temperatures, typical recovery of ductility takes place as the ferrite volume fraction increased.

REFERENCES

- [1] G. Yang, L. Zhu, W. Chen, X. Yu, G. Guo, Propagation of surface cracks on beam blank in the mould during continuous casting, *Ironmak. Steelmak.* 46 (2019) 809–818. <https://doi.org/10.1080/03019233.2018.1509475>.
- [2] G. Yang, L. Zhu, W. Chen, G. Guo, B. He, Simulation of crack initiation and propagation in the crystals of a beam blank, *Metals (Basel)*. 8 (2018). <https://doi.org/10.3390/met8110905>.
- [3] J.E. Lee, T.J. Yeo, O.H. Kyu Hwan, J.K. Yoon, U.S. Yoon, Prediction of cracks in continuously cast steel beam blank through fully coupled analysis of fluid flow, heat transfer, and deformation behavior of a solidifying shell, *Metall. Mater. Trans. A Phys. Metall. Mater. Sci.* 31 (2000) 225–237. <https://doi.org/10.1007/s11661-000-0067-5>.
- [4] B. Mintz, S. Yue, J.J. Jonas, Hot ductility of steels and its relationship to the problem of transverse cracking during continuous casting, *Int. Mater. Rev.* 36 (1991) 187–220. <https://doi.org/10.1179/imr.1991.36.1.187>.
- [5] K. Kim, H.N. Han, T. Yeo, Y. Lee, K.H. Oh, D.N. Lee, Analysis of surface and internal cracks in continuously cast beam blank, *Ironmak. Steelmak.* 24 (1997) 249–256.
- [6] G. Yang, L. Zhu, W. Chen, X. Yu, B. He, Initiation of surface cracks on beam blank in the mold during continuous casting, *Metals (Basel)*. 8 (2018). <https://doi.org/10.3390/met8090712>.
- [7] H.L. Xu, G.H. Wen, W. Sun, K.Z. Wang, B. Yan, Analysis of Thermal Behavior for Beam Blank Continuous Casting Mold, *J. Iron Steel Res. Int.* 17 (2010) 17–22. [https://doi.org/10.1016/S1006-706X\(10\)60191-4](https://doi.org/10.1016/S1006-706X(10)60191-4).
- [8] W. Chen, Y.Z. Zhang, C.J. Zhang, L.G. Zhu, S.M. Wang, B.X. Wang, J.H. Ma, W.G. Lu, Thermomechanical analysis and optimisation for beam blank continuous casting, *Ironmak. Steelmak.* 35 (2008) 129–136. <https://doi.org/10.1179/030192307X231865>.
- [9] M.P. Rao, V.S. Sarma, S. Sankaran, Development of high strength and ductile ultra fine grained dual phase steel with nano sized carbide precipitates in a V-Nb microalloyed steel, *Mater. Sci. Eng. A.* 568 (2013) 171–175. <https://doi.org/10.1016/j.msea.2012.12.084>.
- [10] E. V. Pereloma, I.B. Timokhina, K.F. Russell, M.K. Miller, Characterization of clusters and ultrafine precipitates in Nb-containing C-Mn-Si steels, *Scr. Mater.* 54 (2006) 471–476. <https://doi.org/10.1016/j.scriptamat.2005.10.008>.

- [11] K.R. Carpenter, R. Dippenaar, C.R. Killmore, Hot ductility of Nb- and Ti-bearing microalloyed steels and the influence of thermal history, *Metall. Mater. Trans. A Phys. Metall. Mater. Sci.* 40 (2009) 573–580. <https://doi.org/10.1007/s11661-008-9749-1>.
- [12] B. Mintz, J.M. Arrowsmith, Hot-ductility behaviour of C–Mn–Nb–Al steels and its relationship to crack propagation during the straightening of continuously cast strand, *Met. Technol.* 6 (1979) 24–32. <https://doi.org/10.1179/030716979803276471>.
- [13] K.J. Sricharoenchai C, Nagasaki C, Hot Ductility of High Purity Steels Containing Niobium, *ISIJ Int.* 32 (1992) 2–9.
- [14] J. R. Wilcox & R. W. K. Honeycombe, Hot ductility of Nb and Al microalloyed steels following high-temperature solution treatment, *Met. Technol.* (1984) 217–225.
- [15] C. Ouchi, K. Matsumoto, HOT DUCTILITY IN Nb-BEARING HIGH-STRENGTH LOW-ALLOY STEELS., *Trans. Iron Steel Inst. Japan.* 22 (1982) 181–189. <https://doi.org/10.2355/isijinternational1966.22.181>.
- [16] W. baorong Lu Zhen, Zhang hongtao, Effect of niobium on hot ductility of low C-Mn-steel under continuous casting simulation conditions, *Mater. Technol.* 61 (1967) 106–111.
- [17] B. Patrick, V. Ludlow, Development of casting practices to minimise transverse cracking in microalloyed steels, *Rev. Metall. Cah. D'Informations Tech.* 91 (1994) 1081–1089. <https://doi.org/10.1051/metal/199491071081>.
- [18] Y. Liu, L.X. Du, H.Y. Wu, R.D.K. Misra, Hot Ductility and Fracture Phenomena of Low-Carbon V–N–Cr Microalloyed Steels, *Steel Res. Int.* 91 (2020) 1–11. <https://doi.org/10.1002/srin.201900265>.
- [19] F.J. Ma, G.H. Wen, P. Tang, X. Yu, J.Y. Li, G.D. Xu, F. Mei, Causes of transverse corner cracks in microalloyed steel in vertical bending continuous slab casters, *Ironmak. Steelmak.* 37 (2010) 73–79. <https://doi.org/10.1179/030192309X12506804200465>.
- [20] B.H. Chen, H. Yu, Hot ductility behavior of V-N and V-Nb microalloyed steels, *Int. J. Miner. Metall. Mater.* 19 (2012) 525–529. <https://doi.org/10.1007/s12613-012-0590-6>.
- [21] M.G. Akben, B. Bacroix, J.J. Jonas, Effect of vanadium and molybdenum addition on high temperature recovery, recrystallization and precipitation behavior of niobium-based microalloyed steels, *Acta Metall.* 31 (1983) 161–174. [https://doi.org/10.1016/0001-6160\(83\)90076-7](https://doi.org/10.1016/0001-6160(83)90076-7).

- [22] D.N. Crowther, M.J.W. Green, P.S. Mitchell, The influence of composition on the hot cracking susceptibility during casting of microalloyed steels processed to simulate thin slab casting conditions, *Mater. Sci. Forum.* 284–286 (1998) 469–476. <https://doi.org/10.4028/www.scientific.net/msf.284-286.469>.
- [23] K. Banks, A. Koursaris, F. Verdoorn, A. Tuling, Precipitation and hot ductility of low C-V and low C-V-Nb microalloyed steels during thin slab casting, *Mater. Sci. Technol.* 17 (2001) 1596–1604. <https://doi.org/10.1179/026708301101509665>.
- [24] B. Mintz, R. Abushosha, The hot ductility of V, Nb/V and Nb containing steels, *Mater. Sci. Forum.* 284–286 (1998) 461–468. <https://doi.org/10.4028/www.scientific.net/msf.284-286.461>.
- [25] G.A. Osinkolu, M. Tacikowski, A. Kobylanski, Combined effect of AlN and sulphur on hot ductility of high purity iron-base alloys, *Mater. Sci. Technol. (United Kingdom)*. 1 (1985) 520–525. <https://doi.org/10.1179/mst.1985.1.7.520>.
- [26] T. H. Coleman & J. R. Wilcox, Transverse cracking in continuously cast HSLA slabs – influence of composition, *Mater. Sci. Eng. A*. 1 (1985) 80–83.
- [27] loyola de oliveria Mintz, B. abushoshsa, comineli, The influence of sulphides on the hot ductility of steels, in: *Int. Conf. Thermomechanical Process. Steels Other Mater.*, 1997.
- [28] O.Y. Yasumoto, Kunio, Y Maehara, Ura S, Effect of sulphur on hot ductility of low carbon steel austenite, *Mater. Sci. Technol.* 1 (1985) 111–116.
- [29] P.J. Wray, High Temperature Plastic-Flow Behavior of Mixtures of Austenite, Cementite, Ferrite, and Pearlite in Plain-Carbon Steels., *Metall. Trans. A, Phys. Metall. Mater. Sci.* 15 A (1984) 2041–2058. <https://doi.org/10.1007/BF02646839>.

SECTION

5. CONCLUSIONS AND RECOMMENDATIONS

5.1. CONCLUSIONS

Among all the laboratory testing methods, hot tensile tests have proven to be the most popular for the study of continuous cracking in continuously cast steels. Generally, the tests are carried out using a servo hydraulic load frame equipped with a resistance furnace or induction heater in a protective atmosphere. However, reproducing an as-cast structure similar to continuous cast product by reheating a sample remains challenging. This challenge has been overcome by the usage of Gleeble apparatus in which a specimen can be melted and resolidified in-situ, slowly cooled and tested representing a better simulation of the continuous casting conditions. However, the disadvantage is that only a small portion of the sample is tested so local non-uniformities play a remain role. The quantification of hot ductility of steels by measuring the % reduction in area of the steels from the hot tensile tests and the adjustment of seconding cooling zone to avoid the ductility trough has been the dominating tragedy to avoid transverse cracks.

In the present study, hot ductility curves were obtained using two high temperature test methods: (1) a tensile test utilizing a servo- hydraulic load frame with a resistance furnace and (2) a thermomechanical testing apparatus using rapid joule heating combined with an electro-mechanically controlled tensioning system. The test methods showed similar low ductility trends, but the upper and lower edges of the ductility trough differed

somewhat between the two test methods. The differences are attributed to the differences in heating and cooling rate of the two test methods.

But there exist some limitations. It should be noted that the fracture strains reported in the current hot tensile testing work and the strain levels that are reported to induce transverse cracking in continuous casting differ significantly. The fracture strains observed in a typical hot ductility tensile test ranges from 70% to 7%, while the surface strains observed during straightening in the continuous casting process usually are less than 2%. The significant difference in the reported strains results from differences in the failure criteria of the two test methods. In the former case, the reported strain is a strain to sample failure, while in the latter case, the reported strain is the strain to initiate a surface crack.

In the continuous casting process, the severity of transverse cracks depends on many other factors such as the depth of oscillation marks, which act as stress risers and also increases the segregation of P, S and Mn locally, providing a preferred site for the crack initiation, grain size and precipitate nucleation. All these factors must be carefully assessed while predicting the steels likelihood to transverse crack based on the information from hot tensile tests. Tensile test-based ductility measurements can only provide a relative indication of the low ductility temperature sensitivity range of an alloy.

More sophisticated testing procedures are ultimately required which test an in-situ solidified sample with controlled cooling to the test temperature to reproduce the complex precipitation process from the liquid state and its effect on hot ductility.

5.2. RECOMMENDATIONS

The above methods of MTS load frame and Joule resistive heating have one common shortcoming in that they do not allow for testing of the shell during solidification and subsequent cooling. High-temperature microalloy precipitants such as TiN can precipitate from the liquid or just below the solidus. Reheating of the specimen will not dissolve these nitrides. The only way to truly test what precipitation will be occurring in the as-cast slab and the subsequent effects on the ductility ranges during continuous casting is to design a test that involves solidification from the melt and then controlled cooling to the testing temperature. Our suggested solidification and testing approach are shown in Figure 5.1.

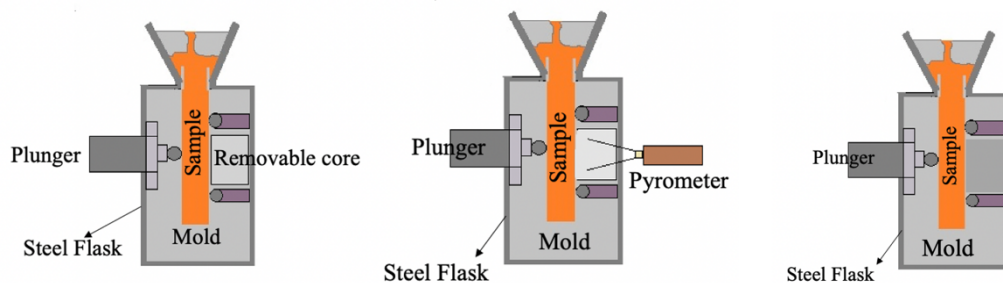


Figure 5.1: Solidification and testing approach of hot 3-pt bend tests.

Step (i): Melting and casting in a steel flask with the attached plunger and solid support

Step (ii): Cooling down to test temperature and temperature monitor by pyrometer and core window can be used to observe crack as well

Step (iii): 3 – point bending test

The experimental setup consists of an electric cylinder powered by a servo motor and controlled by an electric drive. A 20T compression load cell and a 25mm linear variable differential transformer (LVDT) were used to control and monitor force and displacement. A connector with the plunger attached penetrates inside the mold box shown in Figure 5.2. At the left side of the platform, the mold box with the attached solid supports, and a directly cast sample will be in contact with the plunger entering the mold box from the right side. The components such as the mold box, load cell, connectors etc., were placed on a custom-made platform, as shown in Figure 5.2. The electric cylinder, servo motor, and electrical drive were fixed to the platform. A protective steel plate was between the electric cylinder and the mold box to protect the device.

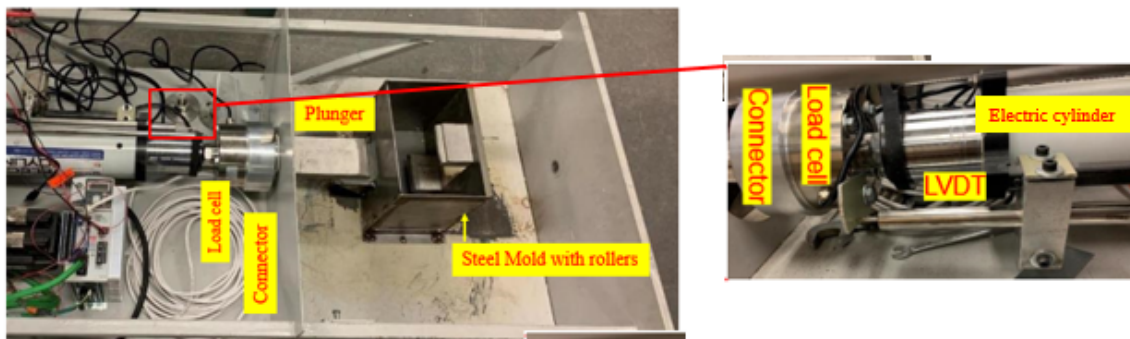


Figure 5.2: Controlled deformation test apparatus (a) Complete assembly of the experimental set up and (b) detail view of the LVDT moving along with the electric cylinder.

The hot 3-pt bend testing procedures can ultimately test an in-situ solidified sample with controlled cooling to the test temperature to reproduce the complex precipitation process from the liquid state and its effect on hot ductility.

BIBLIOGRAPHY

1. Yadong Wang, Qiang Ren, Lifeng Zhang, Xiaogang Yang, Wen Yang, Ying Ren, Haijie Zhang, "Formation and control of transverse corner cracks in the continuous casting slab of microalloy steel", *Steel Research International*, Vol 92, Issue 6, (2021), pp 1-11
2. B Mintz, "Hot Ductility of Steels and its Relationship to the Problem of Transverse cracking during continuous Casting", *International Materials Review*, Vol. 36, No.5, 1991, pp 187-217
3. B. G. Thomas et al, "Online dynamic control of cooling in continuous casting of thin steel slabs", *Proceedings of NSF Grant conference*, 2008, pp 1-16.
4. B Y R R Shephard, *Continuous casting produces high quality steel*, 2004, pp 33-35.
5. P J Wray, *Plastic flow and failure of plain carbon steels in ferrite and austenite region*, *Met. Technology*, Vol 8, No 1, 1981, pp 466-471.
6. D M Keene, C M Sellars, W J Tegart, *Deformation under hot working conditions*, 1968, The Iron and steel institute, London.
7. Lankford, W. T. (1972) "Considerations of Strength and Ductility in the Continuous-Casting Process", *Metall. Trans.*,3, 1331-1357.
8. B. G. Thomas, J.K. Brimacombe, and I. V. Samarasekera, *The Formation of Panel Cracks in Steel Ingots: A State-of-the-Art Review*, *ISS TRANSACTIONS*, Volume 7, 1986 – 7
9. Weinberg, F. (1979a), *The Ductility of Continuously-Cast Steel Near the Melting Point Hot Tearing* *Metall. Trans. B*, vol. 10B, June 1979, pp. 219-227.
10. Brimacombe, J.K., Sorimachi, K. *Crack formation in the continuous casting of steel. Metall Mater Trans B* **8**, 489–505 (1977).
11. JK Brimacombe, *The challenge of quality in the continuous casting process*, *Metallurgical and Materials Transactions B*, 1999
12. H G Suzuki, S Nishimura, and S Yamaguchi, "Embrittlement of Steels Occurring in the Temperature Range from 1000-600 °C", *Trans ISIJ*, Vol. 24, 1984, pp 169-174.
13. Hirowo G. S UZUKI, Satoshi NISHIMURA and Shigehiro YAMAGUCHI, *Characteristics of Hot Ductility in Steels Subjected to the Melting and Solidification*, *Trans. Iron Steel Inst. Jpn.*, vol. 22, 1982, pp. 48-56.

14. B Mintz, and J M Arrowsmith, "Hot ductility behavior of C-Mn-Nb-Al steels and its relationship to crack propagation during the straightening of continuously cast strand", *Metals Technology*, Vol. 6, 1979, pp 24- 32.
15. Ouchi, C. and Matsumoto, K. (1982). "Hot Ductility in Nb-bearing High Strength Low-alloy Steels", *Trans. ISIJ* 22 : 181-189.
16. Phase transformations in metals and alloys, by D A Porter and K E Easterling, 2nd edition, Chapman and Hall, 1992.
17. B Patrick and V Ludlow, "Development of Casting Practices to Minimise Transverse Cracking in Microalloyed Steels," *Revue de Metallurgie*, Vol. 91, 1994, pp 1081-1089
18. Crowther, D.N. and B. Mintz, Influence of carbon on hot ductility of steels, *Materials Science and Technology*, 1986. 2(7): p. 671-676.
19. B. Mintz, "The Influence of Composition on the Hot Ductility of Steels and to the Problem of Transverse Cracking,," *ISIJ Int.*, vol. 39, no. 9, pp. 833–855, 1999, doi: 10.2355/isijinternational.39.833
20. A Cowley, R Abushosha and B Mintz, "The influence of Ar₃ and Ae₃ temperatures on the hot ductility of steels", *Material Science and Technology*, Vol. 15, 1998, pp 1145-1153.
21. Mintz, B., Importance of Ar₃ temperature in controlling ductility and width of hot ductility trough in steels, and its relationship to transverse cracking, *Materials Science and Technology*, 1996. 12(2): p. 132-138.
22. Mintz B, Abushosha R, Cowley A, Preliminary analysis of hot ductility curve in simple C-Mn steels, *Materials Science and Technology*, 1998, 14(3), pp 222-226.
23. M. Wolf, "Initial solidification and strand surface quality of peritectic steels," vol. 9, pp. 8–9, 2018.
24. B. Mintz and R. Abushosha: CIMSymp, on Hot Workability of Steels and Light-composites, Ed, by McQueen, Koopl'va 'm' Ry'an, Met. Soc of CIM. Montreal, (1996), 399~10.
25. Takeuchi, E., Brimacombe, J.K. The formation of oscillation marks in the continuous casting of steel slabs. *Metall Mater Trans B* **15**, 493–509 (1984). <https://doi.org/10.1007/BF02657380>
26. Irving, W.R., Continuous casting of steel. 1993, London: The Institute of Materials.

27. Turkdogan, E.T., Causes and effects of nitride and carbonitride precipitation in HSLA steels in relation to continuous casting, AIME Steelmaking Conference proceedings, 1987. 70: p. 399-409.
28. Suzuki, M., H. Hayashi, H. Shibata, T. Emi, and I. Lee, Simulation of transverse crack formation on continuously cast peritectic medium carbon steel slabs, *Steel Research*, 1999. 70(10): p. 412-419.
29. Nozaki T (1978) A secondary cooling pattern for preventing surface cracks of continuous casting slab. *Trans ISIJ* 18:330–338.
30. K Soeyanto, “Improvement of surface quality of continuously cast steel control of cast structure and straightening temperature”, The University of Wollongong, 1995.
31. Y. Maehara, K. Yasumoto, Y. Sugitani, and K. Gunji, “Effect of carbon on hot ductility of as-cast low alloy steels,” *Trans. Iron Steel Inst. Japan*, vol. 25, pp. 1045–1052, 1985.
32. J. S. Rege, M. Hua, C. I. Garcia, and A. J. Deardo, “The Segregation Behavior of Phosphorus in Ti and Ti+Nb Stabilized Interstitial-Free Steels,” *ISIJ Int.*, vol. 40, no. 2, pp. 191–199, 2000, doi: 10.2355/isijinternational.40.191. [206].
33. H. Suzuki, S. Nishimura, and Y. Nakamura, “Improvement of hot ductility of continuously cast carbon steels,” *Trans. Iron Steel Inst. Japan*, vol. 24, no. 1, pp. 54–59, 1984.
34. B. Mintz, “Influence of Nitrogen on Hot Ductility of Steels and Its Relationship to Problem of Transverse Cracking,” *Ironmaking & Steelmaking*, Vol. 27, No. 5, 2000, pp 343–347.
35. Karjalainen, L.P., H. Kinnunen, and D. Porter, Hot ductility of certain microalloyed steels under simulated continuous casting conditions, *Materials Science Forum*, 1998. 284-286: p. 477-484. 203.
36. B Mintz and J M Arrowsmith, “Influence of Microalloying Additions on Hot Ductility of Steels,” in “Hot Working and Forming Processes,” The Metals Society, 1980, pp 99-103.
37. Sage A M., “Effect of Vanadium, Nitrogen and Aluminium on the Mechanical Properties of Reinforcing Bar Steels,” *Metals Technology*, Vol.2,1976, pp 65-70.
38. Zajac S, Lagneborg R and Siwechi T., “The Role of Nitrogen in Microalloyed Steels”, *Microalloying’95 Proceeding of International conference*, Pittsburgh, PA, 1995, pp 321-340.

39. D N Crowther, B Mintz, "The influence of grain size and precipitation on hot ductility of microalloyed steels," *Materials Science and Technology*, Vol. 2 No. 11, 1986, pp 1099-1105.
40. J R Wilcox and R W K Honeycombe, "Hot Ductility of Nb and Al Microalloyed Steels Following High Temperature Solution Treatment", *Metals Technology*, Vol. 11, 1984, pp 217-225.
41. C Ouchi and K Matsumoto, "Hot Ductility in Nb-bearing HighStrength Low-alloy Steels", *TransISIJ*, Vol. 22, 1982, pp 181-189.
42. L Zhen, Z Hongtao, W Baorong, "Effect of Niobium on Hot Ductility of LowC-Mn Steel Under continuous casting Simulation Conditions", *Steel Research*, Vol. 61, 1990, pp 620- 623.
43. P Sricharoenchai, C Nagasaki and J Kihara, "Hot Ductility of High Purity Steels Containing Niobium", *ISIJ International*, Vol. 32, 1992, pp 1102-1109.
44. Mintz B, D N Crowther, The influence of small additions of Ti on the hot ductility of steels, In Titanium technology in microalloyed steels, ed. T.N. Baker. 1997, London: The Institute of Materials, pp 98-113.
45. B. Mintz and R. Abushosha, "Effectiveness of hot tensile test in simulating straightening in continuous casting," *Mater. Sci. Technol.*, vol. 8, no. 2, pp. 171–178, Feb. 1992, doi: 10.1179/mst.1992.8.2.171.
46. R. Abushosha, S. Ayyad, and B. Mintz, "Influence of cooling rate and MnS inclusions on hot ductility of steels," *Mater. Sci. Technol.*, vol. 14, no. 3, pp. 227–235, Mar. 1998, doi: 10.1179/mst.1998.14.3.227
47. Turkdogan, E.T., Causes and effects of nitride and carbonitride precipitation in HSLA steels in relation to continuous casting, AIME Steelmaking Conference proceedings, 1987. 70: p. 399-409
48. E. T. Turkdogan, S. Ignatowicz, and J. Pearson, "The solubility of sulfur in iron and ironmanganese alloys," *J. Iron Steel Inst*, vol. 180, no. 8, pp. 349–354, 1955
49. Mintz, B., R. Abushosha, O.G. Comineli, and M.A. Loyola de Oliveira. The influence of sulfides on the hot ductility of steels, In THE'MEC' 97: International Conference on Thermomechanical Processing of Steels & Other Materials. 1997. Wollongong, Australia. p. 867-873
50. Abushosha, R., R. Vipond, and B. Mintz, Influence of sulfur and niobium on hot ductility of cast steels, *Materials Science and Technology*, 1991. 7(12): p. 1101-1107
51. T Gladman: *The Physical Metallurgy of Microalloyed Steels*, Maney, London, 2002

52. D. N. Crowther, Z. Mohamed, and B. Mintz, "The relative influence of dynamic and static precipitation on the hot ductility of microalloyed steels," *Metall. Trans. A* vol. 18, no. 11, pp. 1929–1939, 1987
53. Turkdogan, E.T. (1996), *Fundamentals of Steelmaking*, IOM, 1996, pp. 305-316.
54. M. M. Wolf, "Effects of tramp elements in continuous casting," *Ironmak. Steelmak.*, vol. 12, no. 6, pp. 299–301, 1985
55. T. Bloom, "The Influence of Phosphorus on the Properties of Sheet Steel Products and Methods Used to Control Steel Phosphorus Levels in Steel Product Manufacturing," *Iron Steelmak.*, vol. 17, no. 9, pp. 35–41, 1990.
56. N. E. Hannerz, "Critical hot plasticity and transverse cracking in the continuous slab casting with particular reference to composition," *Trans. Iron Steel Inst. Japan*, vol. 25, no. 2, pp. 149–158, 1985.
57. B. Mintz, A. Tuling, and A. Delgado, "Influence of silicon, aluminum, phosphorus, and boron on hot ductility of Transformation Induced Plasticity assisted steels," *Mater. Sci. Technol.*, vol. 19, no. 12, pp. 1721–1726, Dec. 2003, doi: 10.1179/174328413X13789824293948.
58. K. W. Andrews, "Empirical formulae for the calculation of some transformation temperatures," *J. Iron Steel Inst.*, vol. 203, pp. 721–727, 1965.
59. H. Kobayashi, "Hot-ductility Recovery by Manganese Sulphide Precipitation in Low Manganese Mild Steel," *ISIJ Int.*, vol. 31, no. 3, pp. 268–277, 1991, doi: 10.2355/isijinternational.31.268. [198].
60. C. Nagasaki, A. Aizawa, and J. Kihara, "Influence of Manganese and Sulfur on Hot Ductility of Carbon Steels at High Strain Rate," *Trans. Iron Steel Inst. Japan*, vol. 27, no. 6, pp. 506–217 512, 1987.
61. Y. Ohmori and Y. Maehara, "High-temperature ductility of AISI 310 austenitic stainless steels," *Mater. Sci. Technol.*, vol. 2, no. 6, pp. 595–602, Jun. 1986, doi: 10.1179/mst.1986.2.6.595.
62. G. A. de Toledo, O. Campo, and E. Lainez, "Influence of sulfur and Mn/S ratio on the hot ductility of steels during continuous casting," *Steel Res.*, vol. 64, no. 6, pp. 292–299, 1993.
63. B. Mintz and Z. Mohamed, "Influence of manganese and sulphur on hot ductility of steels heated directly to temperature," *Mater. Sci. Technol.*, vol. 5, no. 12, pp. 1212–1219, Dec. 1989, doi: 10.1179/mst.1989.5.12.1212.

64. H. Schrewe, "Strand Mechanics, Bending, Straightening and Bulging," *Contin. Cast. steel*, pp. 138–144, 1987.
65. K. Soeyanto, "Improvement of surface quality of continuously cast steel control of cast structure and straightening temperature," The University of Wollongong, 1995.
66. Irving, W.R. (1993), *Continuous casting of steel*, The Institute of Materials., 1993, pp. 1-120.
67. Deisinger, M. and Tacke, K.-H. (1997), *Ironmaking Steelmaking*, vol. 24, no. 4, 1997, pp. 321-328.
68. Maehara, Y., K. Yasumoto, H. Tomono, T. Nagamichi, and Y. Ohmori, Overview: Surface cracking mechanism of continuously cast low carbon low alloy steel slabs, *Materials Science and Technology*, 1990. 6(9): p. 793-806.
69. Manohar, P.A. and M. Ferry. The development of a technique for the determination of hot ductility of as-cast steel, In *Proceedings of Materials 98, The Biennial Conf. of the Institute of Materials engineering Australasia, Ltd.* ed. M. Ferry, 1998. p. 131-138
70. Crowther, D.N., M.J.W. Green, and P.S. Mitchell, The influence of composition on the hot cracking susceptibility during casting of microalloyed steels processed to simulate thin slab casting conditions, *Materials Science Forum*, 1998. 284-286: p. 469-476.
71. C. Ouchi and K. Matsumoto, "Hot Ductility in Nb-bearing High-strength Low-alloy Steels," *Trans. Iron Steel Inst. Japan*, vol. 22, no. 3, pp. 181–189, 1982, doi: 10.2355/isijinternational1966.22.181.
72. B. Mintz, J. Jonas, and S. Yue, "The influence of dynamic recrystallisation on the hot ductility of steels at low strain rates," in *The Minerals, Metals and Materials Society*, T. Chandra, Ed. *Recrystallisation '90*, 1990, pp. 553–8.
73. R. Bailey, R. Shiring, and H. Black, "Hot Tension Testing," *Work. Test. Tech.*, pp. 73–94, 1984
74. E. Kang, "Hot Ductility of TWIP steels," City University of London, 2014.
75. T. H. Coleman and J. R. Wilcox, "Transverse cracking in continuously cast HSLA slabs – influence of composition," *Mater. Sci. Technol.*, vol. 1, no. 1, pp. 80–83, Jan. 1985, doi: 10.1179/mst.1985.1.1.80
76. G. Cardoso, B. Mintz, and S. Yue, "Hot ductility of aluminium and titanium containing steels with and without cyclic temperature oscillations," *Ironmak. Steelmak.*, vol. 22, no. 5, pp. 365–377, 1995.

77. M. El-Waziri, F. Hassani, S. Yue, E. Es-Sadiqi, L. E. Collins, and K. Iqbal, "The Effect of Thermal History on the Hot Ductility of Microalloyed Steels," *ISIJ Int.*, vol. 39, no. 3, pp. 253–262, 1999, DOI: 10.2355/isijinternational.39.253.
78. K. Walker and R. Marshall, "Aluminium nitride precipitation and grain structure of continuously cast billet corners," *Mater. Sci. Technol.*, vol. 6, no. 9, pp. 867–71, 1990.
79. H. Luo, L. P. Karjalainen, D. A. Porter, H.-M. Liimatainen, and Y. Zhang, "The Influence of Ti on the Hot Ductility of Nb-bearing Steels in Simulated Continuous Casting Process," *ISIJ Int.*, vol. 42, no. 3, pp. 273–282, 2002, DOI: 10.2355/isijinternational.42.273
80. B. Mintz, J. M. Stewart, and D. N. Crowther, "The influence of cyclic temperature oscillations on precipitation and hot ductility of a C-Mn-Nb-Al steel," *Trans. Iron Steel Inst. Japan*, vol. 27, no. 12, pp. 959–964, 1987

VITA

Madhuri Varadarajan was born in Salem, Tamilnadu, India. She graduated with a Bachelor of Science in Metallurgical Engineering from PSG College of Technology in 2017. After her graduation, she worked as a Metallurgical Engineer at JSW Steel Limited from 2017-to 2018. In August 2018, she attended Missouri University of Science and Technology, studying low-temperature ductility behavior in micro-alloy steels. Madhuri received her master of science in Metallurgical Engineering from Missouri University of Science and Technology in May 2022 under the guidance of Dr. Laura Bartlett, Dr. Ronald O'Malley, and Dr. Simon Lekakh.